UNIVERSITY OF COPENHAGEN
FACULTY OF SCIENCE

PhD thesis

Tipping in the Greenland ice sheet

Noise, rate and chaos

Kolja Leon Kypke

Advisor: Peter Ditlevsen

Submitted: September 30, 2024

This thesis has been submitted to the PhD School of The Faculty of Science, University of Copenhagen

Abstract

The Greenland ice sheet is an important element of the Earth's climate system and is a central climate component for studying the phenomenon of abrupt changes in its overall state due to small changes in external forcing, commonly known as *tipping*. The focus on ice sheets is partly because of evidence of abrupt changes in the paleoclimate record of Greenland, and partly because the global consequences of tipping the ice sheet being easily understood. However, due to the vast complexity of the climate the conceptual understanding of tipping in simple low-dimensional systems requires some translation to be be applicable to any real-world system. This thesis analyzes three models along a hierarchy of dimension and number of processes to bridge that gap.

Firstly, the abrupt changes of the last glacial maximum, the Dansgaard-Oeschger events, are represented as noise-induced tipping in a one-dimensional conceptual model with multiplicative noise. This study discusses the different attributions to the deterministic and stochastic components in the Itô and Stratonovich interpretations of the stochastic integral. The discrepancy results in considerations with regards to the physical interpretation of the model, as well as the paradigms of bistability and monostability of the stadial and interstadial states.

Secondly, the contemporary Greenland ice sheet in a state-of-the-art model is demonstrated to exhibit a novel mode of variability, namely that of oscillating ice streams, under mild external atmospheric forcing. The result of increasing this external forcing at different rates is that the time before tipping occurs can vary by tens to hundreds of millennia. Using concepts from dynamical systems theory, specifically that of chaotic transients, it is determined that these long and seemingly random tipping times are due to crossing a bifurcation point rather than experiencing a non-monotonic *rate-induced tipping*. Furthermore, the delay of the tipping depends sensitively on the initial condition and the rate of forcing, implying chaotic variability.

Thirdly, a conceptual model of coupled oscillating ice streams is constructed and analyzed to validate the chaotic nature of the variability seen in the comprehensive model. This model displays various transitions to chaos, including period doubling, intermittency, and attractor crises, as well as chaotic transients similar to those that are proposed to delay the tipping in the comprehensive model.

Resumé

Indlandsisen på Grønland udgør en væsentlig komponent i Jordens klimasystem og er central for studiet af pludselige ændringer i dens samlede tilstand, ofte betegnet som *tipping*. Forskningens fokus på iskapper skyldes dels de observerede tegn på hurtige ændringer i Grønlands palæoklima, dels de globale konsekvenser af en tipping af indlandsisen, som er relativt let at forstå. Imidlertid kræver den komplekse natur af klimaet, at den konceptuelle forståelse af tipping i simple lavdimensionelle systemer oversættes for at kunne anvendes på virkelige systemer. Denne afhandling analyserer tre modeller langs et hierarki af dimensioner og processer for at udfylde dette videnshul.

For det første repræsenteres de bratte ændringer fra det sidste glaciale maksimum, kendt som Dansgaard-Oeschger-begivenhederne, som støjinduceret tipping i en endimensionel konceptuel model med multiplikativ støj. Undersøgelsen diskuterer de forskellige tilskrivninger til de deterministiske og stokastiske komponenter i Itô- og Stratonovich-fortolkningerne af det stokastiske integral. Uoverensstemmelserne rejser spørgsmål om den fysiske fortolkning af modellen samt paradigmerne for bistabilitet og monostabilitet af de stadiale og interstadiale tilstande.

For det andet demonstrerer en kompleks model af Grønlands indlandsis oscillerende isstrømme, under milde ydre atmosfæriske påvirkninger. Resultaterne viser, at tiden før en tipping kan variere fra ti til hundreder af årtusinder, afhængigt af hastigheden hvormed den ydre forcering ændres. Ved at anvende begreber fra dynamisk systemteori, specifikt kaotiske transienter, fastslås det, at disse lange og tilsyneladende tilfældige tipping-tider skyldes krydsning af et bifurkationspunkt snarere end en ikke-monotonisk *hastighedsinduceret tipping*. Desuden viser forsinkelsen af tipping en følsom afhængighed af starttilstanden og forceringshastigheden, hvilket indikerer kaotisk variation.

For det tredje er der konstrueret og analyseret en konceptuel model af koblede oscillerende isstrømme for at validere den kaotiske karakter af variabiliteten observeret i den komplekse model. Denne model viser forskellige overgange til kaos, herunder periode-dobling, intermittens og attractor-kriser samt kaotiske transienter, der svarer til dem, der forårsager forsinket tipping i den komplekse model.

Zusammenfassung

Der grönländische Eisschild ist ein wichtiger Bestandteil des Erd-Klimasystems, und ein zentraler Untersuchungsgegenstand des Phänomens von sogenannten *Kipppunkten*, das heißt abrupten Veränderungen des Gesamtzustandes eines Systems aufgrund kleiner Veränderungen externer Einflüsse. Der Schwerpunkt dieser Arbeit liegt auf Eisdecken, zum Einen weil es Hinweise auf abrupte Veränderungen in den Paläoklimaaufzeichnungen Grönlands gibt, und zum Anderen, weil die globalen Folgen des Überschreiten eines Kipppunktes der Eisschilde besonders klar sind. Allerdings erfordert unser konzeptionelles Verständnis von Kipppunkten, basierend auf niedrigdimensionalen dynamischen Systemen, eine gewisse Erweiterung um auf Systeme in der wirklichen Welt, wie zum Beispiel das enorm komplexe Klimasystem, anwendbar zu sein. Um diese Lücke zu schliessen, werden in dieser Arbeit drei Modelle analysiert, welche anhand ihrer Dimension und Anzahl von Prozessen eine Art Hierarchie bilden.

Zuerst werden abrupte Klimaveränderungen während letzten Glazials, die Dansgaard-Oeschger-Ereignisse, anhang eines eindimensionalen konzeptionellen Systems modelliert, welches als entscheidenden Mechanismus durch multiplikatives Rauschen induzierte Kipppunkte beinhaltet. Hier werden die verschiedenartigen Beiträge der deterministischen und stochastischen Komponenten in den Itô- und Stratonovich-Interpretationen des stochastischen Integrals diskutiert. Aus dieser Diskrepanz lassen sich Schlussfolgerungen zur physikalischen Interpretation des Modells, sowie der Paradigmen von Bi- und Monostabilität des stadialen und interstadialen Klimas, ableiten.

Zweitens wird in einem modernen und komplexen Gletschmodells eine neuartige Variabilität des grönlandischen Eisschilds in Form von oszillierenden Eisströmen festgestellt, welche bei einer mittleren Stärke der atmosphärischen Randbedingungen auftritt. Wird die Stärke der Randbedingung in unterschiedlichen Raten weiter erhöht, so kann der Zeitpunkt an dem der Kipppunkt de facto beobachtet wird um Hunderte von Jahrtausenden variieren. Unter Verwendung von Konzepten aus der Theorie der dynamischen Systeme, insbesondere der chaotischen Transienten, wird festgestellt, dass diese langen und scheinbar zufälligen Zeitpunkte des Eisschild-Kollapses nach dem Überqueren eines Bifurkationspunkts eintreten, und nicht etwa auf ein nicht-monotones, *ratenbedingtes Kippen* zurückzuführen sind. Darüber hinaus hängt der Zeitpunkt des Kollapses stark von den Anfangsbedingungen sowie der Änderungsrate der Anfangsbedingungen ab, was eine chaotische Variabilität des Eisschilds impliziert.

Zuletzt wird ein neues konzeptionelles Modell oszillierender, gekoppelter Eisströme vorgeschlagen und analysiert, um die chaotische Natur der im komplexen Gletschermodell beobachteten Variabilität zu bestätigen. Dieses Modell zeigt verschiedene Übergänge zum Chaos, darunter Periodenverdopplung, Intermittenz und Attraktorkrisen. Desweiteren beinhaltet es chaotische Transienten welche denen ähneln, die im komplexen Modell als Mechanismus des verzögerten Eisschild-Kollapses vorgeschlagen wurden.

Acknowledgments

I'm extremely grateful to my advisor, Peter Ditlevsen, without whom none of this would have been possible. His breadth of knowledge and support was the perfect combination to allow me to develop my own research ideas and mature as a scientist. I am also indebted to Marisa Montoya at the Universidad Complutese de Madrid and Peter Ashwin at the University of Exeter for giving me the opportunity to experience the research environment at different institutions. Similarly, I thank Shuting Yang at the Danmarks Meteorologiske Institut for the chance to work with an Earth Systems Model. A huge debt of gratitude goes to my previous advisors the the University of Guelph, William Langford and Allan Willms, for their role in starting my scientific career and encouraging me to undertake the journey to Copenhagen.

A large thanks goes to the European Union's Horizon 2020 grant, the source of the Marie Skłodowska-Curie international training network CriticalEarth which funded my PhD program. More importantly, it equipped me with an invaluable cohort of fellow PhD scholars whom I always looked forward to seeing during our bi-annual workshops. Special thanks goes to my academic sibling Jade Ajagun-Brauns, along with Jan Swierczeck-Jereczeck, Raphael Römer and Ignacio del Amo for helping me during my stays abroad as well as Reyk Börner, Oliver Mehling, and Paolo Bernuzzi for helping me develop my scientific understanding. I am also thankful to Johannes Lohmann for his mentorship and being a source of inspiration, as well as Eliza Cook and Maria Caso Bramsen for all their help.

A big thank you goes to my fellow PhD students at PICE for sharing this journey with me: Mikkel, Niels, Marta, Dina, Meg, Reuben and Andrea. In the same vein I would like to thank Julian, Eliot, Natalie, Jen and Lars for their friendship. Thanks also to the rest of the group at UCM: Jorge and Alex for answering any questions I had or didn't know I had yet about ice sheet modelling, and Sergio, Dani, Antonio, Fèlix and the rest for making me feel at home in Madrid. Thanks as well as my family who always believed in me no matter what, along with my friends in Canada - Peter, Lucas, David and Rowan, plus Harry in France, who were always there for me and gave me the extra motivation to finish in a timely manner. Finally, thank you to Addie for just about everything.

List of articles and manuscripts

1. K. Kypke and P. Ditlevsen. On the representation of multiplicative noise in modeling Dansgaard–Oeschger events. *Physica D: Nonlinear Phenomena*, 466:134215, 2024

2. K. Kypke, M. Montoya, A. Robinson, J. Alvarez-Solas, and P. Ditlevsen. Delay of collapse of the Greenland ice sheet due to ice stream oscillations. Prepared for submission

3. K. Kypke, P. Ashwin, and P. Ditlevsen. Chaotic variability in a model of coupled ice streams. Prepared for submission

Contents

Chapter 1

Introduction

1.1 Tipping in the climate system

The study of the climate in recent decades has a particular focus on the consequences of anthropogenic forcing of the climate system. With the increasing magnitude and rate of warming experienced by the global climate, special interest is being paid to researching how it has reacted or may yet react to such forcing. A primary concept in this field of research is that of *tipping events* and their associated thresholds, known as *tipping points*, in the climate [3]. Tipping events and their associated tipping points are a loosely defined phenomenon, indicating an abrupt change in the state of system. This can mean changes in the state occur very quickly relative to its intrinsic timescale, or that the state can change by a large amount when a relatively small change in external forcing is applied to it. In the climate context, tipping phenomena can be global [105], but more focus is put on *tipping elements* which generally refers to subsystems or a combination of coupled subsystems of the climate that may experience a tipping event with drastic consequences. For example, the loss of a large percentage of the West Antarctic ice sheet [28] or the Greenland ice sheet [10], the weakening of the northward ocean circulation in the Atlantic [7, 23], or the dieback of the Amazon rain forest [11] are all commonly studied tipping elements. Tipping points are a result of very strong nonlinear interactions between components of the climate system, meaning studying them is similarly complex. In an ever-changing climate, understanding tipping points is vital to be able to establish *safe operating space* of anthropogenic climate forcing from which tipping events can be avoided.

1.2 Mathematical framework of tipping

As mathematics is the primary tool used to study physical systems, it is useful to be able to describe these tipping points mathematically as well. There is a rich history in the literature of mathematical tools and frameworks that

are able to describe, both qualitatively and quantitatively, the mechanism by which abrupt changes in systems can occur. Coarsely, tipping is investigated as being one of three types: bifurcation-induced, noise-induced, and rate-induced [4].

Bifurcation-induced tipping

Bifurcation-induced tipping (b-tipping) is an application of the bifurcations studied in dynamical systems theory to a system that experiences a tipping event. These describe the qualitative change in the topological nature of a system under continuous parameter variations [55]. The simplest examples are that of the codimension one (meaning only one parameter is varied) *saddle-node* or *fold* and Hopf bifurcations. An example of the saddle-node bifurcation in one dimension, where a stable fixed point and an unstable fixed point (which is generally a saddle in dimensions larger than one, hence the name) collide and annihilate each other, is given in Fig. 1.1. In a system that is initially bistable, a continuous parameter variation brings the left stable and middle unstable fixed points closer together, until they meet in a saddle-node bifurcation and cease to exist, causing the system to jump to the only remaining fixed point on the right.

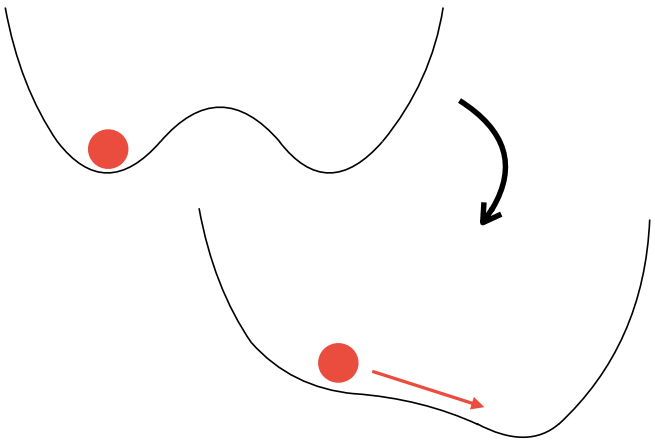

Figure 1.1: B-tipping in a 1D system. Under continuous parameter variation, the bistable potential becomes monostable (a bifurcation) and the system jumps to a new state.

There are many different types of bifurcations, becoming more complicated as the codimension increases. A bifurcation need not necessarily equate to a tipping point – the qualitative change of a system does not always mean a given equilibrium state changes by a significant amount. For example, stable node transforming into a small limit cycle after undergoing a supercritical Hopf

bifurcation results a topologically different phase space, but a solution will occupy the same region of phase space. Often appended to the description of a tipping point is some notion of *irreversibility* of the tipping: once a parameter variation causes a tipping event, reversing this change in parameter does not return you to the state before the tipping. A particularly relevant bifurcation that supplies this is the *double-fold bifurcation* structure shown in Fig. 1.2 that exhibits bistability and is ubiquitous to the study of b-tipping in the climate science.

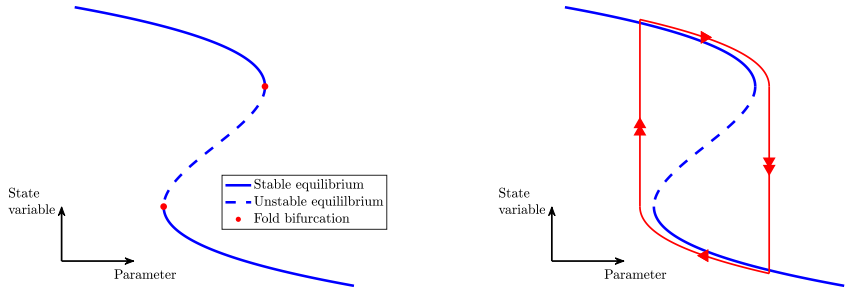

Figure 1.2: Left: Bifurcation diagram of the double-fold bifurcation. Right: Hysteresis (red curve) of the double-fold bifurcation.

This bistability also results in the phenomenon of *hysteresis*, which is the dependence of the state of a system on its history. Navigating the double fold via continuous parameter variation, a distinct *hysteresis loop* is created: for a system on the lower branch to reach the upper branch, it must first cross the return fold bifurcation. This lends an irreversibility to the tipping: after a system tips, returning the parameter to its value fore the tipping point will not return the system to where it was, as it is now stuck on the lower branch. This irreversibility is particularly relevant to studies of the climate system in terms of motivating parameter ranges from which tipping can be avoided, as the tipping cannot be trivially undone.

The weakness of bifurcation theory is that it deals, at least in the classical theorem, with asymptotic states of autonomous systems. Some obvious issues arise: although centre manifold theorems exist to be able to reduce the dimensionality of a system to one low codimension bifurcations can be investigated, the climate and its subsystems are neither in an asymptotic state nor autonomous. Such methods are better suited to *conceptual models* of the climate, whereby many assumptions are made to simplify the dynamics and represent the most significant interactions in low dimensional systems, preferably using systems of ordinary differential equations. Such conceptual models are safest when describing processes that vary over very long time scale, which allows some notion of a quasi-steady state being achieved and asymptotic dy-

namics being valid. Additionally, processes that occur over very long time scales typically act on very large spatial scales [117] and thus b-tipping can be seen in models of systems on the global scale [15, 104].

Noise-induced tipping

Noise-induced tipping (n-tipping) might occur in cases where very fast processes on a much smaller spatial scale than the dynamics of interest do indeed have a significant effect on the overall variability and cannot be averaged out. By representing the fast (and often chaotic) dynamics as a sequence of random impulses on the evolution in the slow dynamics, the tools of stochastic differential equations can be used. The prototypical example of n-tipping is that of a bistable potential in one dimension, with stochastic perturbation of a trajectory allowing it to overcome the potential barrier caused by the unstable fixed point, which is shown in Fig. 1.3. In this simple example using the same bistable potential as in the b-tipping example without any parameter variation, random perturbations of small magnitude on the system have a probabilistic chance of being successively in the same direction, allowing the system to overcome the strongly stabilizing gradient and crossing over the unstable fixed point. Over time, these perturbations might cause the system to tip back to the left fixed point, then back to the right and so on. That means that neither fixed point is asymptotically stable but rather *metastable*. As no parameters are being varied, irreversibility in the sense mentioned previously is not a consideration, and indeed the system may find itself in its original state, albeit at an indeterminate time due to the probabilistic nature of stochastic dynamics.

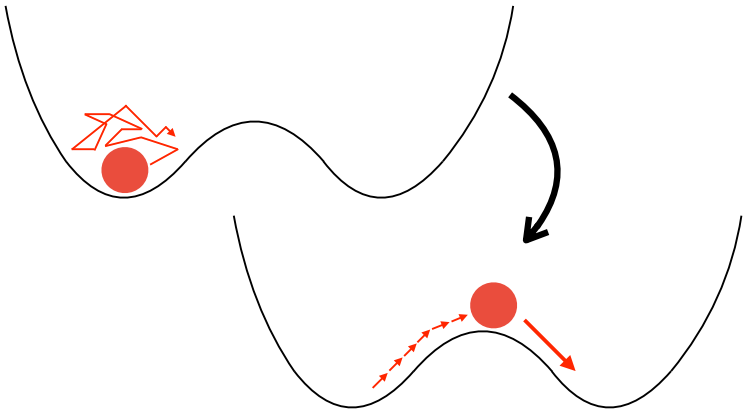

Figure 1.3: N-tipping in a 1D system. Under continuous stochastic perturbation (noise), a system may overcome a potential barrier and jump to a new start.

Rate-induced tipping

Rate-induced tipping may occur in scenarios where the forcing parameter varies in time. Since the problem is now inherently non-autonomous, the tools of bifurcation theory are not entirely applicable. While it is meaningful to still consider the *frozen* system for a fixed (in time) parameter value to determine asymptotic equilibrium states and even bifurcations of these, the basins of attraction can be impacted in the non-autonomous scenario. A schematic example is shown in Fig. 1.4. A bistable potential experiences a continuous parameter shift that changes the location of the potential, but not its stability landscape. If the shift occurs slowly such that the system can continually equilibrate towards the fixed point (known as *tracking* the fixed point), tipping will not occur. For a rapid enough shift where the system cannot track the fixed point, it will tip to the other stable state. Although a

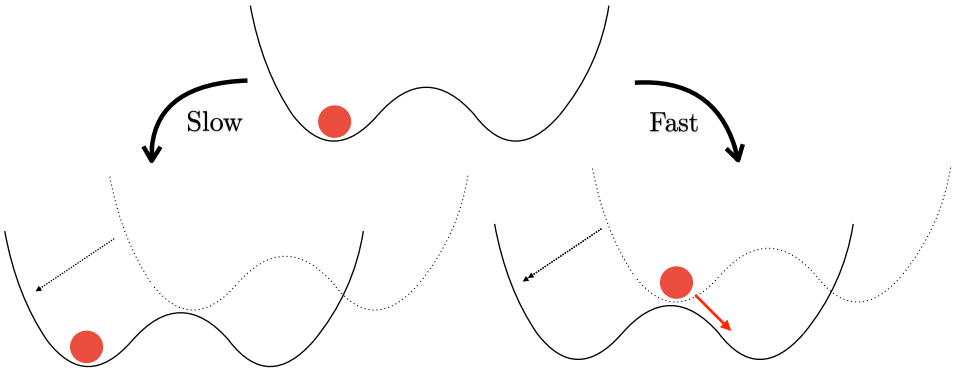

Figure 1.4: R-tipping in a 1D system. Under non-autonomous parameter variations that change the location of the potential in phase space, the rate of change might allow the system to track the change (left) or not, causing it to tip to a different state (right).

cartoon, this example illustrates the concept of basin instability, a prerequisite for r-tipping in low dimensions [94]. For this 1D system, the basin boundary lies at the unstable fixed point between the two minima. Consider the *infinite rate*, where the parameter shift occurs instantly. If the initial condition of the system, in this case the left stable fixed point, is such that is is past the basin boundary after the infinite-rate shift, then that (fixed point) is said to be basin unstable and r-tipping is possible. More important however is the critical rate, which is the slowest rate at which r-tipping happens. Of the three types of tipping, r-tipping is perhaps the most important in regards to studies of climate systems due to their non-autonomous nature. A large factor is that simulations done with climate models are performed in a transient way, so rate-induced effects should always be under consideration.

1.3 Hierarchy of models

The tipping scenarios described above are quite simple to understand, especially in their one-dimensional, conceptual formulation. The issue is that the climate and its subsystems are not even close to being simple or low-dimensional. The question then is: how *can* these concepts of tipping be understood in real systems? It is important to consider these along a ranking of climate models. Climate models exist along a scale of dimensionality, as well as quantity of processes that the model, and this organization is called the *hierarchy of models* [22]. Low order models that include only a few interactions between relatively little components of the climate system or one of its subsets may be useful at replicating very clear tipping behaviour and allowing one to identify exactly the tipping elements, but not so helpful when seeking any sort of quantitative diagnosis of tipping probabilities that might be useful for future predictions. On the other end are comprehensive models, which are better suited for properly simulating the real climate system, but are computationally very expensive and struggle in making pellucid what components of a system are most relevant to the tipping. Most importantly, physical and experimental observations are required to be able to strengthen or falsify the theories that the models are based on. The end goal is a synthesis, using results from models higher on the hierarchy along with understanding from models on the lower end, to arrive at a theory that properly represents the observational data.

1.4 Chaos

Another important aspect of the climate system that is not always present in low-order conceptual models is that of chaotic variability. Chaos will play a primary role in chapter 3 and 4, warranting brief mention here. The definition of chaos used in this work is that of a deterministic system that displays exponential divergence of nearby trajectories after a certain amount of time. Chaos is ubiquitous when describing real-world climate systems - indeed, the most famous example of a chaotic system is that of Lorenz [71], used to describe atmospheric convection. The impact of chaos on tipping is a degree of non-monotonicity of the relationship between the varying parameters with tipping and subsequently an uncertainty of parameter ranges from which tipping may occur. Things that are taken for granted in these frameworks, such that bifurcations occur past some critical point or that r-tipping occurs beyond some critical rate, no longer hold in cases where attractors are strange and basin boundaries are fractal. This adds additional complication to the low-order conceptualization of the complex systems.

1.5 Objectives of this thesis

This thesis looks at models along a hierarchy: a purely conceptual model derived from real data, a conceptual model derived from physical equations, and a high-dimensional comprehensive model. All three deal in some way with the Greenland ice sheet and its modes of variability, with the latter two being explicitly related and distinct from the first. What is explored are the concepts of the three types of tipping and how they may be represented along the hierarchy. Chapter 2 deals with the manifestation of multiplicative noise and its consequences on modelling abrupt changes captured in the paleoclimate record of the Greenland ice sheet as n-tipping. It deals with how the high level of abstraction of conceptual models can lead to issues when seeking to use them to understand real-world processes underlying observational data. Chapter 3 involves a comprehensive b- and r-tipping modelling study of the Greenland ice sheet under future warming, where the loss of the ice sheet can be delayed by up to hundreds of thousands of years due to regional internal variability. In this case, the scale of the modelling is such that complete comprehension of the observed tipping behaviour is obscured, but a full inclusion of all relevant physical processes allows for incredibly interesting phenomena. Chapter 4 deals with a model that exhibits a much less drastic form of tipping compared to the first two, investigating the change of the behaviour of a system from periodic to chaotic. It is a companion to the study of chapter 3, seeking to isolate the most relevant dynamics and explore how these behave to strengthen the hypothesis made for the comprehensive model. Simultaneously, it demonstrates the rich behaviour exhibited by chaotic systems and how it is possible to still comprehend them despite the apparent randomness.

Chapter 2

N-tipping in a conceptual model derived from data

2.1 Introduction

The model study of this chapter, Kypke and Ditlevsen (2024) [60], hereafter KD24, centres around the most direct evidence of abrupt changes in the paleoclimate: that of the ice-core record extracted from the Greenland ice sheet. This project originated from the simple observation that the paleoclimate record displays different amplitudes of fast variations depending on the mean state [25]. Under the paradigm of a stochastic differential equations, this is termed *multiplicative* noise as the stochastic term is in some way multiplied with the state variable, in contrast to additive noise which has a constant amplitude and as such the noise is simply added to the deterministic part. The inclusion of multiplicative noise when modelling this paleoclimate record is the topic of KD24 and thus this chapter begins with an overview of the nuances of the simple stochastic differential equations that are the mathematical framework of this project. What follows is an overview of the paleoclimate record that is the subject of this study, as well as a brief description of some studies that follow a similar methodology to complement their mention in the article KD24, which is presented in its entirety in the final section of this chapter.

2.2 Stochastic differential equations

It is desirable to consider some dynamical process that includes some amount of randomness. In the context of a climate system, this randomness is due to chaotic dynamics that resolve over a much shorter time scale than that of the evolution of the mean climate state – this is the Hasselman paradigm [40] Consider a one-dimensional differential equation for a process that has some

slow, deterministic dynamics and much faster stochastic dynamics,

$$\frac{dx}{dt} = f(x) + g(x)\xi_t \tag{2.1}$$

This equation is known as the Langevin equation [64]. The function $f(x)$ describes the slow dynamics, with $g(x)$ representing the strength of the fast dynamics ξ_t. This term ξ_t is denoted the *noise* term. A desired property for the solution x of the system (2.1) is for the future evolution of the state to depend only on the current state and the stationary probability density. This is roughly speaking the Markov property, and a system endowed with this is known as a Markov process [32]. In some respects, a Markov process is stochastic analogue of differential equation for deterministic systems. For the deterministic dynamics, the Markov property is satisfied if the initial value $x(0)$ and the time t is known. However, the stochastic dynamics represent the combined effects of many shorter steps which are not directly resolvable.

For the solution x to be a Markov process, it is required for the noise to be Gaussian and white [43]. The Gaussian statistics can be achieved by recognizing that on the timescale of the deterministic dynamics, dt, the stochastic process acts as a sequence of short, independent events such that the Central Limit Theorem [32] may be applied. A white noise process is defined by its first and second moment,

$$\begin{aligned} \mathbb{E}(\xi_t) &= 0 \\ \mathbb{E}(\xi_t \xi_s) &= \delta(t-s). \end{aligned} \tag{2.2}$$

The second condition supplies the most desired quality of a white noise process, namely that it has a correlation time of zero. While no physical process can have a zero correlation time, this assumption is made without too many issues by considering the timescale separation inherent to the system at hand. As the timescale of the slow dynamics dt is much larger than that of the fast stochastic dynamics, the stochastic impulses measured at each t are effectively independent from those measured at $t + dt$. This is the *white noise approximation* and allows the application of the results of stochastic dynamics.

An issue arises in that the white noise process as defined does not represent a function in the ordinary sense. For instance, it does not take in some time t and return a value of the function at that point. In this way it is similar to the Dirac-delta function $\delta(t-s)$ which defines its correlation time. The Dirac-delta is also not an ordinary function but rather a *generalized function* (also called a distribution, but this verbiage is avoided so as to not cause confusion with probability distribution) which takes as an input a test function rather than a point. Using the Dirac-delta as an example, a generalized function can be defined only by integration with some other function $f(t)$,

$$\int_{-\infty}^{\infty} f(t)\delta(t-s)dt = f(s), \tag{2.3}$$

which gives the definition of the Dirac-delta function as a corresponding to a generalized function $\phi_\delta(\varphi)$ with the property

$$\phi_\delta(\varphi) = \varphi(s). \tag{2.4}$$

This notion can be extended to the stochastic case, leading to *generalized stochastic processes* (GSP) which are a class of generalized functions. Specifically, a GSP $\phi(\varphi)$ takes in a function φ and assigns to it a random variable, and has the condition of being linear and converging in probability distribution. GSP have the properties of being infinitely differentiable, with these derivatives are also generalized functions, and

$$\dot{\phi}(\varphi) = -\phi(\dot{\varphi}). \tag{2.5}$$

If a GSP is Gaussian, then it may be defined by the mean and covariance,

$$\begin{aligned} &\mathbb{E}(\phi(\varphi)) = m(\varphi) \\ &\mathbb{E}([\phi(\varphi) - m(\varphi)][\phi(\psi) - m(\psi)] = C(\varphi, \psi) \end{aligned} \tag{2.6}$$

where $m(\varphi)$ is the mean function, and the Gaussian property survives the derivation,

$$\begin{aligned} &\mathbb{E}(\dot{\phi}(\varphi)) = -m(\dot{\varphi}) \\ &\mathbb{E}([\dot{\phi}(\varphi) - m(\varphi)][\dot{\phi}(\psi) - m(\psi)]) = C(\dot{\varphi}, \dot{\psi}). \end{aligned} \tag{2.7}$$

As an example, the GSP associated with white noise has mean and covariance

$$\begin{aligned} &\mathbb{E}(\phi(\varphi)) = 0 \\ &\mathbb{E}(\phi(\varphi)\phi(\psi)) = \int_0^\infty \int_0^\infty \delta(t-s)\varphi(t)\psi(s)dtds. \end{aligned} \tag{2.8}$$

As a GSP in this case is only useful when associated with a stochastic process, we consider the GSP $\phi_W(\varphi)$ corresponding to the stochastic process W_t, which has the properties

$$\begin{aligned} &\mathbb{E}(W_t) = 0 \\ &\mathbb{E}(W_t W_s) = \min(t, s). \end{aligned} \tag{2.9}$$

Using the differentiation properties of the GSP, the mean and covariance of the derivative of $\phi_W(\varphi)$ can be calculated,

$$\begin{aligned} &\mathbb{E}(\dot{\phi}_W(\varphi)) = 0 \\ &\mathbb{E}(\dot{\phi}_W(\varphi)\dot{\phi}_W(\psi)) = \int_0^\infty \int_0^\infty \delta(t-s)\varphi(t)\psi(s)dtds. \end{aligned} \tag{2.10}$$

This is exactly equal to the mean and covariance of the white noise GSP, thus giving the result that the white noise process is a GSP which is the derivative

of a GSP corresponding to the stochastic process W_t. The process W_t is named the Wiener process and has the properties

$$\begin{aligned} \mathbb{E}(W_t) &= 0 \\ \mathbb{E}(W_t W_s) &= \min(t, s). \end{aligned} \tag{2.11}$$

The Wiener process has the property that its increments are independent - the probability density of an increment in time, $W_t - W_s$, depends only on $t-s$ and not on previous values of W_t. This gives that the white noise process can be thought of, in a sense, as the derivative of a stochastic process that has stationary independent increments. Using this Wiener process, the Langevin equation 2.1 is given in the form

$$dx = f(x)dt + g(x)dW_t \tag{2.12}$$

which is termed a stochastic differential equation (SDE). This form is preferred due to the irregularities of the white noise process ξ_t. Technically, this equation is still incomplete due to the issues that arise when taking the integral of the stochastic term, which is the focus of KD24.

Further than a Markov process, it is desired for the solution of an SDE to have continuous sample paths so as to represent a continuous physical system. In that case, the system is known as a Markov diffusion process. Fundamentally, Markov diffusion processes, which are written as SDEs (2.12), are general processes with stationary independent increments. They can be derived as such: Locally in t, such that x is close to constant, $f(x) = -a$ and $g(x) = b$ by linearization. Therefore, Markov diffusion processes are locally an SDE of the form $dx = -adt + bdW_t$. Since dW_t is Gaussian the resulting x is Gaussian and can be defined by the first two moments. These are termed the *drift* and the *diffusion* and correspond to the functions $f(x)$ and $g^2(x)$ in equation (2.12). This is the reason why it is possible to define the system by only two terms: Since the primary condition that a system is a Markov diffusion process is tied to that which guarantees continuous sample paths, it is the result that a continuous Markov process can be represented fully by the drift and diffusion, which is linear in dW_t. This linear dependence on dW_t is vital – if the process were any smoother, it would not retain the Markov property. On the other hand, if the process were any more irregular the property of continuous sample paths would be lost [43].

As a Markov diffusion process is defined by its first two moments, it has associated with it a Fokker Planck equation (FPE) [31, 51, 87],

$$\frac{\partial p(x,t)}{\partial t} = -\frac{\partial}{\partial x}\big[f(x)p(x,t)\big] + \frac{1}{2}\frac{\partial^2}{\partial x^2}\big[g(x)^2 p(x,t)\big], \tag{2.13}$$

which describes the temporal evolution of the probability density of the process and is the basis for the analysis carried out in KD24. To precisely summarize, a stochastic process that is pathwise continuous and has the Markov property

is the solution $x(t)$ of equation (2.12) furnished with a stochastic integral such as that of Itô or Stratonovich.

It is possible to describe a stochastic process with nonwhite noise that retains the Markov property. As mentioned previously, any noise representing some physical process will have a nonzero correlation time and will thus not be white. Additionally, the Wiener process has a variance that increases with time, meaning it is not a stationary process. This is not an issue in the stochastic modelling of the climate, as the negative feedback of the climate drift guarantees the solutions do not increase without bound. However, if noise is to represent some physical process in and of itself, it would be strange for it have variance increasing with time. Hence, a good representation would be a stochastic process which is both stationary and Gaussian. There is only one such process, namely the Ornstein-Uhlenbeck (O-U) process,

$$dy = -\gamma y dt + \sigma dW_t, \tag{2.14}$$

which has the correlation function

$$\langle y(t)y(s)\rangle = \frac{\sigma^2}{2\gamma}\exp[-\gamma|t-s|]. \tag{2.15}$$

This gives a correlation time $\tau_{\text{corr}} = \gamma^{-1}$ for the O-U process. This is also commonly called a *red* or *Brownian* noise process.

Augmenting an SDE with a second equation 2.14 that describes the fast fluctuations, as is done in equation (13) in KD24, results in a solution which is still a Markov process. The reason this is not immediately applicable in the scope of non-parametric modelling of D-O events, and in general why both the white noise assumption and zero-inertia case is made, is that the paleorecord consists of a time series of a single variable and thus the model should be similarly one-dimensional. To properly model a red noise process to retain the Markov property in this scheme requires a paleorecord on the timescale of the fast dynamics. As the ice-core record is one of the highest resolution paleoclimate proxies available, it would be difficult to imagine some new marker that would represent the fast dynamics. It only appears in the ice record as some noise on the mean climatic state, which can only be interpreted in the Gaussian white noise sense. Thus the white noise approximation is not only necessary from the mathematical analysis side, but also from the data side.

The visualization of a low order SDE as a particle in a potential well is useful because it gives an idea of what parts of the dynamics belong to the deterministic (slow) drift, with the stochastic (fast) diffusion modulating the behaviour within this potential. This analogy extends to the representation of the climate system where the potential describes some underlying climate dynamics and the noise is the effect of chaotic processes on much shorter time scales, i.e. weather, as in the Hasselmann paradigm. For multiplicative

noise the delineation between drift and diffusion, in this case climate and weather, is not so clear. This is because for additive noise a single separation of time scales is sufficient to make the approximation that weather acts as a white noise process on the climate time scale. With inertial systems, a third timescale is involved, which complicates the multiplicative noise case. Just as any real-world stochastic process should be assumed to be the white noise limit of a coloured noise process, so too should it be expected that a climate system has some inertial effects on some timescale. As is described in the paper, the relative size of this third timescale can have a profound effect on how the stability of the climate system is understood. Physically, the intuition behind the different Itô and Stratonovich interpretations depending on the relative relaxation and noise correlation time scales is thus: In the view of the Itô integral representing a more 'discontinuous' process (which it is natural to do as a result of its non-anticipating nature) then the idea that the noise acts on a faster time scale than the inertia means that the variable, imagined as a particle in a potantial well, experiences a more 'rough' noise. In contrast, if the Stratonovich integral is thought of to represent a limit of a continuous process – which is how it was derived, and that it follows the regular chain rule supports this – the fact that the noise acts slower than the inertial relaxation means the variable has the noise somehow smoothed by the inertia.

2.3 Dansgaard-Oeschger events

During the last glacial period, paleoclimate proxies show clear abrupt transitions in the mean climate state [21]. Ice core records extracted from the Greenland ice sheet display sudden jump in the ratio of two isotopes of oxygen, ^{16}O and ^{18}O. The heavier isotope ^{18}O is associated with precipitation at lower temperatures [20], and thus the ratio of ^{18}O to ^{16}O, known as δ^{18}O, is an indicator of atmospheric temperature. Multiple ice core records from various locations in Greenland all show these jumps in δ^{18}O, signifying that it is not some regional temperature variations but rather a climatic phenomenon on a larger spatial scale. The ice core record displays two distinct states in the δ^{18}O time series. Lower values of δ^{18}O correspond to the colder *stadial* climate interspersed by the warmer *interstadial* climate with larger (less negative) δ^{18}O values. The magnitude of δ^{18}O is such that the difference in temperature between these states is 5 to 15 degrees Celsius [50, 120]. Most notable is the timescale of the shift from the stadial to the interstadial, which occurs over only decades. These changes from stadial to interstadial climate are known as the Dansgaard-Oeschger (D-O) events, and are the premier example of evidence for abrupt climate change.

The climate signal in Greenland in invariably linked to the north Atlantic ocean. Since the precipitation that occurs over Greenland originates from evaporation over the north Atlantic, the δ^{18}O signal is linked to the tem-

perature of the precipitation source as well. Additionally, temperatures of Greenland are influenced by the nearby large heat reservoir that is the Atlantic ocean. The north Atlantic is evidenced to show a strong meridional (south to north) circulation pattern which brings warm, high salinity water from the tropics to the higher latitudes, where it then sinks to become bottom water and travels back to the tropics. This mode of circulation is known as the Atlantic Meridional Overturning Circulation (AMOC) and is driven by differences in temperature and salinity between the tropics and the mid- to high-latitudes. This thermohaline circulation (THC) has been suggested to display different states corresponding to different strengths of the circulation, i.e different magnitudes of volume flux across latitude bands [107].

Furthermore, these different modes of circulation have been replicated in ocean models [106]. The circulation can be vigorous, with a large pole-to-equator salinity gradient that transports large amounts of heat from the equator northwards. Alternatively, the circulation can be weak or even stagnant with reduced northward heat transport. In this way, the two states seen in the ice core record might represent modes of circulation for the AMOC, namely stagnant in the stadial and stronger in the interstadial. The circulation might even travel in reverse in the glacial climate [12], corresponding to states of the THC where temperature differences dominate the flow as opposed to salinity differences. This is in contrast to the AMOC of the present day, which is in a strong circulatory mode. The hypothesis that it might weaken due to increased freshwater flux in the mid-to-high latitudes, correspondingly decreasing the salinity gradient and weakening the circulation, would result in decreased heat transport to the north Atlantic. Still, the mechanism by which these abrupt changes happen could be the same, encouraging continual study of the D-O events.

Other physical processes may be involved the inception or progression of D-O events. Sea ice, which would serve to insulate the ocean-atmosphere boundary in the north Atlantic and thereby reduce the heat transfer, might explain the asymmetry between the transition from the stadial to the interstadial and vice versa [27, 86]. Atmospheric carbon dioxide levels have been suggested to modulate the duration and frequency of the D-O events, explaining the longer interstadials earlier in the LGP compared to the shorter ones that occurred more recently [116]. The D-O events themselves might be triggered by large atmospheric forcing due to volcanic eruptions [70], which clashes with the paradigm of bifurcation- or noise-induced tipping, where a large shift in state is due to a small, non-abrupt change in forcing.

The changes in mean climate of the D-O events are also reflected in paleoclimate proxies in other parts of the world, implying the change in climate state goes beyond Greenland or even the northern hemisphere. Most prominent is the ice core record of Antarctica, which shows a more gradual shift in temperature in the time periods corresponding to D-O events. This coupling has been explained as a *bi-polar see-saw* between temperatures in the northern

Atlantic and southern ocean [84, 106]. Since the northern Atlantic is connected to the southern ocean which in turn influences the precipitation over and and thus the ice-core record in Antarctica, there is an anti-phase relationship between warming in Greenland and warming in Antarctica. Moreover, due to the much larger mass of the southern Atlantic compared to the northern Atlantic, any changes are smoothed by the larger thermal inertia, explaining the more gradual increase and decrease of δ^{18}O in Antarctic ice cores. Other paleoclimate proxies displaying signals related to D-O events are also mentioned in KD24.

Modelling of D-O events

The literature is rife with attempts to replicate D-O events to explain their cause and/or underlying mechanisms. This is done along the hierarchy of models, meaning both low-order dynamical systems as well as large comprehensive models have been employed by different studies. The work done in KD24 is of the former type, so specific attention is paid to models of this class. While comprehensive models [66, 74, 101, 116] are much more representative of real-world processes, their major weakness in replicating D-O events is that most are oscillatory in nature and not spontaneously occurring , as is suggested by the data [26].

Two broad approaches to conceptual modelling of D-O events are seen in the literature. Firstly are phenomenological models built from physical principles which seek to replicate the behaviour of the D-O events without mimicking them exactly. These may include a stochastic element whereby the abrupt transitions are triggered randomly, or are purely deterministic models which rely on an oscillatory mechanism to replicate the cycles. Similar to the comprehensive models, non-stochastic low-order models rely on a purely oscillatory mechanism to replicate the D-O cycles [90] and will not be discussed. For stochastic models, in addition to the model of Vettoretti et al. [116] mentioned previously, the model of Monahan, Timmermann and Lohmann [76, 110] models the overturning circulation rather than the D-O events themselves. This model explicitly includes multiplicative noise, but as described in KD24 it is clear which stochastic interpretation is applicable. The 2018 study of Boers et al. [9] and the 2023 study of Riechers et al. [91] include a sea ice component along with a model of the ocean circulation, with the latter also including non-Gaussian noise, namely an α-stable process that describes sudden, large of sea ice removal events.

The other approach is that of the models derived directly from the data. These studies all assume the same Langevin form of a slow deterministic drift, the *climate potential*, plus a stochastic component representing fast processes as seen in equation 2.1. These are again subdivided into two classes, namely parametric models which assume the precise functional form of the potential and estimate the parameters of this function, and non-parametric models.

Parametric models generally take the from of either a one-dimensional polynomial bistable potential model or a two-dimensional relaxation-oscillator of the form of a Van der Pol or FitzHugh model [30, 115]. Non-parametric models, by construction, can only derive a model with dimension equal to the number of observational time series included. For those studies that do use multiple time series [8, 92], a gradient system is assumed.

Two-dimensional relaxation-oscillation models of D-O events arose primarily to represent some other qualities of the signal beyond the abrupt changes, specifically the asymmetry in the transitions. While the jump from stadial to interstadial occurs very rapidly and in accordance with an abrupt transition due to noise-induced tipping, the transition from interstadial to stadial is generally more gradual. A one-dimensional stochastic differential equation with a bistable potential implies a time-reversal symmetry of the stochastic process, which does not match the reality of the time series of the LGP. What two-dimensional models offer is two different paths in phase space that can represent the different state transitions. Since these two paths are implied to be unidirectional, this creates some manner of periodic orbit and hence a relaxation-oscillation.

Some models that exhibit relaxation-oscillations, such as the FitzHugh model, also have parameter regimes that show excitability. An excitable system is one with a single stable equilibrium, but the phase space is such that any large enough perturbation from this equilibrium will embark on an *excursion* to a different part of phase space before returning to the equilibrium. These systems are generally the result of some fast-slow dynamics where the slow dynamics has a cubic structure typical of bistable systems [54, 119]. This means in the fast dynamics, the solution will move to one of the two branches of the cubic manifold, appearing as a bistable system. However, on the slow manifold, the flow serves to push the solution towards the equilibrium. This combinations means that a trajectory perturbed far enough from the equilibrium will rapidly jump to the unstable branch of the cubic, where it will then move along until it reaches a fold bifurcation, whereafter it will jump the the stable branch and approach the equilibrium. This equilibrium would represent the stadial in the case of the D-O events, while the unstable cubic branch is the interstadial.

The 1999 study of Ditlevsen [24], the first to perform an inverse SDE modelling of D-O events, considered the noise term to be a combination of an α-stable process and a O-U red noise process with correlation time of less than a year. While the Markov property can be supplied by the α-stable noise and the red noise process considered as a separate equation, the system will not have continuous sample paths. The recent study of Riechers et al. [92] employs the Kramer-Moyal expansion of the master equation to derive the first-order (drift) coefficients for an SDE of a system where the isotope and a second Greenlandic paleoclimate record – that of atmospheric calcium dust – are coupled.

The studies described in the following paragraphs all derive stochastic differential equations in some parametric way. The 2010 study of Livina et al. [67] study assumes stationary of the stochastic process only in a sliding window of time, allowing for the climate potential to to also vary in time. The potential varies in polynomial order such that here are between one and four stable states at a given time. The size of the sliding window also affects the amount of stable states: since the noise is assumed additive, the number of peaks in the probability density function determines the number of stable states.

The 2009 study of Kwasniok and Lohmann [57] describes the use of non-linear Kalman filtration techniques for estimating parameters of stochastic models. This technique has the advantage of being able to estimate observational (i.e. non-dynamic) noise. In this case, it would be the noise that occurs due to the deposition of the isotope and its vertical diffusion through the ice sheet, along with noise introduced through the extracting of the ice core and measuring the isotope signal. The 2012 study of Kwasniok and Lohmann[58] describes a damped oscillator with additive stochastic forcing on both the position and velocity. Using a Kalman filter to estimate the parameters of the model, they find that the strong dissipation regime so that the relaxation time of the inertia (γ^{-1} in KD24) is very small. This suggests that inertial effects do not play a major role in the physical processes underlying the D-O events. The 2013 study of Kwasniok [56] again uses a Kalman filter to estimate the parameters of a bistable potential and a 2D relaxation-oscillating FitzHugh-type model. It also studies a Gaussian mixture model, where the process is assumed to be switching between multiple processes with Gaussian probability densities. In this way, the stadial and interstadial are modelled as different processes, with some transition probability between the two.

The 2015 study of Krumscheid et al. [53] introduces a framework to model stochastic processes using maximum likelihood estimation of parameters for a bistable potential. The 2016 study of Mitsui and Cruxifix [75] study also describes two models, one being a bistable potential and the other of the relaxation oscillator. A nonlinear Kalman filter is utilized along with Bayesian estimation. What sets this study apart is the inclusion of the variation of both insolation and global ice volume, which acts a time-dependent eternal forcing. The 2017 study of Boers et al. [8] study uses Bayesian inference to estimate the parameters of *generalized Langevin equation*, which is a Langevin equation that describes a non-Markovian processes. The 2019 study of Lohmann and Ditlevsen [68] investigates three paradigms of dynamical models used to represent D-O events: the bistable potential and the FitzHugh and Van der Pol oscillators. To do so, Bayesian statistics are employed to estimate the parameters of the three types of models, to see which form best represents D-O events. In this study, not just the stationary probability density of the process is used to derive the model, but other statistical properties, such as the distribution of the waiting times between subsequent D-O events as well

as their duration, are considered.

The conceptual models described in the section above generally exhibit either monostability or bistability in their deterministic dynamics. This is an important distinction as well as a primary result of KD24, namely that stochastic interpretation due to modelling assumptions can lead to the data being interpreted in one way or the other. The primary difference is the return from the stadial to the interstadial being path dependent, that is the physical mechanism responsible for the transition from the stadial to the interstadial is not the same as the other direction. Not only is this a reason for the asymmetry of the transitions, but could also explain why the length of the interstadial is related to the rate of temperature decrease therein [69]. Secondly, a change in the amplitude of the stochastic forcing for a constant climate potential would result in very different trajectories whether the system has a bistable potential or a monostable one. In the case of bistability where both the stadial as well as the interstadial are stable, any reduction in the stochastic forcing will have the effect of decreasing the transition rate between the states. This would increase the metastability, in terms of residence time, for both states. On the other hand, in the monostable setting, a decrease in stochastic forcing would serve to not only decrease the transition probability from the stadial to the interstadial, but also increase the rate of the return to the stadial, since the relative contribution deterministic dynamics to the flow is larger. The residence time in the stadial would be greatly increased, and greatly reduced for the interstadial.

2.4 The paper

Physica D 466 (2024) 134215

Contents lists available at ScienceDirect

Physica D

journal homepage: www.elsevier.com/locate/physd

On the representation of multiplicative noise in modeling Dansgaard–Oeschger events

Kolja Kypke *, Peter Ditlevsen

Physics of Ice, Climate and Earth, Niels Bohr Institute, University of Copenhagen, Tagensvej 16, 2200, Copenhagen, Denmark

ARTICLE INFO

Dataset link: https://www.iceandclimate.nbi.ku.dk/data/

Keywords:
Stochastic dynamical system
Dansgaard–Oeschger events
Multiplicative noise

ABSTRACT

The interpretation of multiplicative noise in a stochastic differential equation in the context of data-driven inverse modeling is discussed. Application to the well-known paleoclimate phenomenon of Dansgaard–Oeschger events leads to qualitatively different 'climate potentials' in the case of the Itô or the Stratonovich interpretation of the stochastic integral. While a physical model is endowed with an interpretation from construction, whether implicitly or explicitly, inverse models derived from data do not afford such a luxury. In this case, a physical model must accompany the mathematical model equation in order to be able to choose a stochastic interpretation. This case study illustrates the differences between the two representations of stochastic noise and demonstrates the need for input from physical constraints when constructing conceptual stochastic models of the observed climate records.

1. Introduction

One of the most famous examples of abrupt climate changes observed in the paleoclimatic record are the Dansgaard–Oeschger (D–O) events. The climate record of the Last Glacial Period (LGP), which spanned approximately 120 to 11 kiloyears before year 2000 (kyr b2k), is measured in the ice-cores of the Greenland ice sheet and marked by distinct and abrupt transitions between colder stadial and warmer interstadial periods [1]. These climatic changes are known as D–O events, and occurred about 24 times in the LGP. The D–O events correspond to approximately 10–15 Kelvin of warming in Greenland over the course of a few decades, with subsequently incremental cooling to the fully glacial conditions of the stadial [2]. While there is only direct evidence of D–O events in the LGP because the ice-core record of Greenland only extends to the end of the last interglacial period, they may not be unique to this time period. Coupling with Antarctic ice-cores [3], evidence in marine sediment cores [4] and speleothems [5] (see also references therein) suggest they may have occurred in previous glacial periods as well.

D–O events are interesting in the context of the present climate primarily because of their temporal scale. They are an example that the climate can change on time scales that could be of consequence in the near future, namely of decades to centuries. They are additionally intriguing because there is no universal agreement on their cause and transition mechanism. The transitions between stadial and interstadial states themselves may be externally forced [6–11], stochastic [12–17] or even both [18]. Possible important physical drivers for the transitions include change in sea ice [19,20], atmospheric carbon dioxide levels [21,22] or volcanic events [23]. Comprehensive models generally exhibit D–O events as oscillations [24,25] and transitions are not spontaneous. See also the review articles [26–28].

D–O events are difficult to simulate in complex models, thus a full understanding of their causes is still lacking. For this reason it is desirable to investigate them using low order dynamical systems models where the dynamics are in full view. Without a full understanding, a modeling strategy is to construct simplified models, optimizing parameters to best fit to observational data. This is an inverse modeling approach. Such conceptual models may be either data-derived [29–31] or constructed from physical principles [32,33]. Generally the data-derived inverse models of D–O events do not propose a physical mechanism whereas conceptual models developed from physical principles tautologically do.

1.1. Stochastic differential equation models of D–O events

This study derives a conceptual model from the data in an inverse modeling scheme. The model paradigm this study follows is to describe the climate proxy as the variable x of a stochastic differential equation

* Corresponding author.
E-mail address: kolja.kypke@nbi.ku.dk (K. Kypke).

https://doi.org/10.1016/j.physd.2024.134215
Received 25 September 2023; Received in revised form 15 February 2024; Accepted 16 May 2024
Available online 20 May 2024

(SDE):

$$dx = F(x)dt + \sigma(x)dW_t, \tag{1}$$

where the Wiener process $W_t = \int_0^t \xi_s ds$ has the properties $\langle \xi_t \rangle = 0$, $\langle \xi_{t_1} \xi_{t_2} \rangle = \delta(t_1 - t_2)$ and ξ_t is Gaussian distributed, i.e. ξ_t is a white noise Gaussian process. The crux of this methodology is to model the climate as being driven by some long timescale climate dynamics described by a function $F(x)$ along with a stochastic component that represents processes that occur on much faster time scales.

Observing the record showing two distinct climate states, the stadial and the interstadial (see Fig. 1), it is natural to consider the abrupt changes as being a transition from one stable state to the other stable state. The measured quantity in the ice core is δ^{18}O, a ratio of heavier ^{18}O isotopes to lighter ^{16}O, and is a proxy for local temperature. Correlation of ocean sediment records with the ice-core record [34] suggest that the Atlantic ocean is the source of the transitions. In this sense, the paleoclimate temperature variations are themselves a proxy of north Atlantic ocean circulation strength. A mechanism of bistablity in the north Atlantic is that of the thermohaline circulation with multiple modes of circulation [35]. Two regimes of flow, one with strong equator-to-pole meridional overturning circulation and one with weak circulation, correspond to warmer and colder Greenland temperatures respectively.

This bistability is seen in both conceptual models [36,37] as well as general circulation models [38], with more recent earth system models being able to reproduce spontaneous 'D–O-like' events [39]. A proposed mechanism for D–O events is such a bistable climate system, i.e. the ocean circulation, with a stochastic term, i.e. freshwater fluxes from atmospheric forcing via wind stress, surface heating, and precipitation, that causes transitions between the two states. Examples of studies that follow a similar framework involve methods such as models with non-Gaussian noise [12], Kalman filters [29], Gaussian mixture models or relaxation-oscillation models [15], Bayesian parameter inference [17, 30], and non-stationary potentials [16].

1.2. Additive noise

The majority of previous studies assume the intensity of the noise is constant or *additive* [12,16,17,29]. The Fokker–Planck equation associated with the additive noise SDE

$$dx = F(x)dt + \sigma dW_t \tag{2}$$

is

$$\partial_t P(x,t) = -\partial_x \big[F(x)P(x,t)\big] + \frac{\sigma^2}{2}\partial_x^2 \big[P(x,t)\big]. \tag{3}$$

When the stationary probability distribution is obtained from the observed time series record, the potential that drives the dynamics of the additive noise SDE is obtained from the Fokker–Planck equation by having $\partial_t P = 0$:

$$U(x) = -\frac{\sigma^2}{2}\log[P(x)] \tag{4}$$

where $\frac{\partial U}{\partial x} = -F(x)$. The potential can be uniquely determined from the stationary probability density $P(x)$ up to a constant factor of the noise strength. Due to the monotonicity of the logarithm the maxima of the probability density function $P(x)$ coincide with the minima of the potential $U(x)$ and thus with the stable equilibria of the deterministic dynamics. Therefore the number of equilibria will always be identical to the number of maxima in probability density.

1.3. Multiplicative noise

From the paleoclimatic record it is observed that the intensity of the fast fluctuations constituting the noise as indicated in Eq. (1) depends on the climate state [40]. State dependent noise is termed *multiplicative* noise. In this case deriving the resulting potential is not completely straightforward. This is due to the fact that when integrating the noise term by way of generalized functions, the resulting Riemann–Stieltjes integral

$$\int_a^b G(t)dW(t) = \lim_{n\to\infty} \sum_{i=1}^{n} G(\tau_i)[W(t_i) - W(t_{i-1})], \tag{5}$$

where $\tau_i \in [t_{i-1}, t_i]$, has a different expected value depending on where in the interval τ_i is chosen. The two most common choices are the left endpoint, named the *Itô interpretation* [41], and the midpoint, named the *Stratonovich interpretation* [42]. Often the *α-convention* is used to designate the different interpretations, where the value of α in the interval $\tau_i = (1-\alpha)t_{i-1} + \alpha t_i$ is 0 for Itô and 1/2 for Stratonovich. In theory, any value of $\alpha \in [0,1]$ is a valid choice for the stochastic integral, but these are by far the two most common. For a more general function $G\big(x(t)\big)$, the definition of the integral is

$$\int_a^b G\big(x(t)\big)dW(t) = \lim_{n\to\infty} \sum_{i=1}^{n} G\big(x^*(\tau_i)\big)[W(t_i) - W(t_{i-1})], \tag{6}$$

and the α-convention is $x^*(\tau_i) = (1-\alpha)x(t_{i-1}) + \alpha x(t_i)$.

Due to the difference of the stochastic integrals, Eq. (1) is incomplete and an interpretation of the noise term must be specified [43]. As a consequence the same SDE can result in different stochastic processes depending on whether the Itô or Stratonovich interpretation is applied. A corollary is that two different SDEs, one interpreted as Itô and the other as Stratonovich, can result in the same stochastic process. Thus solving the inverse problem of deriving the SDE, and especially the potential, from a stochastic realization requires a specification of the noise. Here we perform the derivation of the SDE from the data for both the Itô and Stratonovich integrals.

As SDEs they are distinguished by the notation $dx = F_I(x)dt + \sigma(x)\cdot dW_t$ for Itô and $dx = F_S(x)dt + \sigma(x)\circ dW_t$ for Stratonovich, where F_I and F_S are different potential functions. The associated Fokker–Planck equation using the α convention is

$$\partial_t P(x,t) = -\partial_x \left[\Big(F(x) + (1-\alpha)\sigma(x)\sigma'(x)\Big)P(x,t)\right] + \frac{1}{2}\partial_x^2\big[\sigma(x)^2 P(x,t)\big]. \tag{7}$$

As can be seen from this equation, a simple relation exists between the drift terms of the two interpretations,

$$F_S(x)dt + \sigma(x)\circ dW_t = \left[F_I(x) + \frac{1}{2}\sigma(x)\sigma'(x)\right]dt + \sigma(x)\cdot dW_t, \tag{8}$$

so any Stratonovich integral may be converted to an Itô integral and vice versa. This relation is especially useful when numerically integrating an SDE since the commonly used Euler–Maruyama method is only applicable to Itô SDEs. A Stratonovich SDE can be converted to one of the Itô type and integrated using the Euler–Maruyama method, or alternatively integrated with a predictor–corrector scheme such as a Heun method. Itô and Stratonovich integrals have some other differences as well, the most notable being that differentiation under the Itô interpretation requires the Itô lemma [41],

$$f\big(x(t)\big) = f\big(x(0)\big) + \int_0^t f'\big(x(s)\big)dx(s) + \frac{1}{2}\int_0^t f''\big(x(s)\big)ds. \tag{9}$$

On the other hand the Stratonovich interpretation uses the chain rule of regular calculus.

One previous study includes state-dependent noise in the form of a piecewise constant noise term, where the amplitude is a lower constant value in the interstadials than in the stadials [44]. However their state dependent noise function $\sigma(x)$ still has a derivative that is zero except for a single point, so there is no difference between the stochastic interpretations.

2. Data

The paleoclimate data studied is a time series of the δ^{18}O in permille as measured in the Greenlandic ice-core extracted as part of the North GReenland Ice-core Project (NGRIP) [45]. The 20-year average values

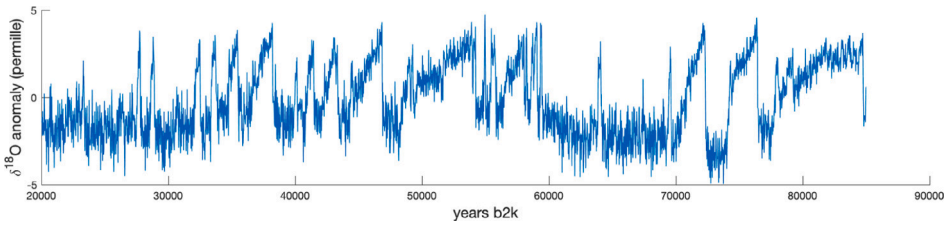

Fig. 1. Detrended δ^{18}O signal from NGRIP from years 20 to 85 kyr b2k (note that time runs from right to left).

on the GICC05modeltext time scale are used [46]. The time series is also truncated at 85 kyr b2k as the resolution decreases further back in time due to the thinning of layers of ice in the ice core. For a further distinction of the two states, the data is detrended. Insolation trends due to orbital variations are removed through subtracting a 25 kyr running mean [17] and the resulting δ^{18}O anomaly is analyzed. This 25 kyr running mean corresponds to the highest frequency of orbital variations, namely precession, which has a period of approximately 20 kyr. This method is effectively a rectangular kernel, which has the important property of not filtering out impulses, i.e. the D–O events themselves. Fig. 1 shows the time series that is the starting point of this study.

3. Methods

3.1. Derivation of multiplicative noise $\sigma(x)$

A heuristic method is used to derive the multiplicative noise term $\sigma(x)$ from the data. Since the fluctuations are larger in the stadials than in the interstadials [40] we prescribe a linearly decreasing function of $\sigma(x)$ with respect to the $\delta^{18}O$ anomaly. Physically, if the noise term is to represent the influence of the atmosphere, an increase in Greenlandic temperatures corresponds to a decrease in the meridional temperature gradient which in turn decreases atmospheric forcing. Following the definition of the stadial and interstadial periods [47], the data is separated into the two states. The values of $\langle x\rangle$ and σ in each of these two states is derived, and the linear function is constructed from these values. To measure σ it is assumed that the signal in either of the two states follows an Ornstein–Uhlenbeck (O–U) process, following [40]

$$dx = -\theta x + \sigma dW_t. \tag{10}$$

For a stationary O–U process the variance is given by the fluctuation–dissipation relation

$$\mathrm{Var}(x) = \frac{\sigma^2}{2\theta}, \tag{11}$$

and the term θ may be recovered from the autocorrelation

$$\langle x(t)x(s)\rangle = \mathrm{Var}(x)\exp[-\theta|t-s|]. \tag{12}$$

3.2. Derivation of the non-linear potentials F(x)

Once the function $\sigma(x)$ is determined the multiplicative Fokker–Planck Eq. (7) is solved for $F(x)$ for the two stochastic calculi. Fig. 2 shows the two potentials $U(x) = \int F(x)dx$ in the Itô and Stratonovich interpretations, along with the potential for the additive noise case (2). When comparing the drift in the multiplicative noise cases to that of the additive noise case, the stability of the interstadial is much reduced. Further, for the Itô case, the interstadial has in fact lost stability such that the resulting climate potential is mono stable.

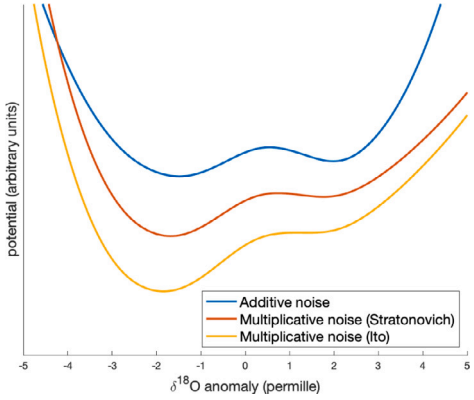

Fig. 2. Derived potentials.

4. Discussion

Due to the qualitative difference of the potential obtained by the two different stochastic interpretations, careful consideration is required when deriving physical properties of the system from observations. The question to be answered is whether the climate potential that underlies the D–O events is monostable, as in the Itô calculus, or bistable, as in the Stratonovich calculus. How is a choice of a stochastic integral made? The data itself is agnostic to interpretation, and mathematically the problem is inconsequential: either interpretation works, as long as they are applied consistently. The choice is ultimately a modeling problem. In this case the SDE inversely modeled by the data requires a conceptual physical model of the phenomenon by which to interpret the results. Conventional understanding is that a physical system is better suited to Stratonovich interpretation. The Wong–Zakai theorem [48] gives that the limit of a sequence of stochastic processes with finite autocorrelation that goes to zero is interpreted as Stratonovich. In this sense it is derived from a continuous process. For a fully discrete system, for example in financial analysis, the Itô interpretation is more appropriate.

However, the one dimensional SDE is generally the result of simplification of dynamics that occur on multiple time scales. Through this reduction, multiplicative noise of the Itô type can be seen in physical systems as well. The most prominent example are inertial systems with colored noise,

$$\begin{aligned}\ddot{x} &= -\gamma(x)\dot{x} + F(x) + \sigma(x)\eta \\ \dot{\eta} &= -\frac{a}{\tau_n}\eta + \frac{\lambda}{\tau_n}\xi_t\end{aligned} \tag{13}$$

where for convenience, we use the notation, $\dot{x} \equiv dx/dt$ and $dW_t = \xi_t dt$.

To reduce the complexity of Eq. (13), two limits are taken: one is an adiabatic elimination of fast inertia ($\tau_r = \gamma(x)^{-1} \to 0$) into the overdamped regime (also known as the strong dissipation or Smoluchowski regime) and the second is the white-noise approximation of the unresolved dynamics ($\tau_n \to 0$). If the time scale of the inertial relaxation is greater than that of the noise autocorrelation ($\tau_r \gg \tau_n$), then the

multiplicative noise is Itô in the limit as both go to zero. If the noise autocorrelation in greater than the relaxation time scale of the inertia ($\tau_r \ll \tau_n$), the Stratonovich interpretation for the multiplicative noise is used [49–54].

The system of Eq. (13) in the white noise limit is

$$\ddot{x} = -\gamma(x)\dot{x} + F(x) + \sigma(x)\xi_t. \tag{14}$$

For additive noise $\sigma(x) = \sigma$, adiabatic elimination is equivalent to setting the left hand side of Eq. (14) equal to zero [55,56]. This is not the case for multiplicative noise, where the limits must be taken carefully. Eq. (13) in the white noise and adiabatic limit is

$$\dot{x} = \frac{F(x)}{\gamma(x)} + \frac{1}{2}\frac{\sigma(x)^2}{\gamma(x)}\frac{\partial\gamma(x)^{-1}}{\partial x} - \frac{\alpha}{2}\frac{\partial\sigma(x)^2\gamma(x)^{-2}}{\partial x} + \frac{\sigma(x^*)}{\gamma(x^*)}\xi_t, \tag{15}$$

where $x^* = \alpha x(t+dt) + (1-\alpha)x(t)$ [56]. In the case where the fluctuation–dissipation theorem applies,

$$\frac{\sigma(x)^2}{2\gamma(x)} = \text{constant} \tag{16}$$

the system obtained by setting the left hand side of Eq. (13) to zero

$$\dot{x} = \frac{F(x)}{\gamma(x)} + \frac{\sigma(x^*)}{\gamma(x^*)}\xi_t, \tag{17}$$

is equivalent to the system interpreted in the *anti-Itô* ($\alpha = 1$) sense. This is the result of Volpe et al. [57] and Lançon et al. [58], see also [56,59].

Another example where we see Itô multiplicative noise is in an SDE with noise feedback delay [60]. This is a circuit system which has been designed to effectively act in an Itô manner by implementing an explicit dependence of the multiplicative noise on the previous time step through introducing a delay of the feedback of the state on the noise term, i.e. the x in the $\sigma(x)$ term. One dimensional systems can also be either Itô or Stratonovich in the case where multiple times scales are involved [61,62].

Now understanding the situation, we return to the case of the δ^{18}O anomaly time series. To accompany the SDE derived directly from the data, a conceptual physical model is required, which will not only provide an idea of the underlying mechanisms but also provide a stochastic interpretation. The stochastic bistable Stommel-type model [36] has been extended to include multiplicative noise by Timmermann, Lohmann and Monahan [63,64]. Their multiplicative noise term arises due to a stochastically parameterized eddy transport in salinity and temperature. As in Cessi [36], the temperature relaxes quickly to some mean value, and a white noise approximation may be made. In this case the white-noise limit is taken via the Wong–Zakai theorem, so that the resulting SDE uses Stratonovich calculus. Then the thermohaline circulation remains bistable based on the model derived from the data.

In another study, Kwasniok and Lohmann [65] fit the D–O event time series data to a stochastic oscillator

$$\ddot{x} = -\gamma\dot{x} + F(x) + \sigma\xi_t \tag{18}$$

which is Eq. (14) with constant damping and additive noise. The variable x represents a temperature proxy and its derivative is the change in temperature, but otherwise the system is not physically defined. They find it is in the strongly dissipative regime and can be reduced to a first-order equation by adiabatic elimination of the second derivative. By augmenting the system with multiplicative noise, a reduction to first order would result in an SDE

$$dx = \frac{F(x)}{\gamma}dt + \frac{\sigma(x)}{\gamma}dW_t, \tag{19}$$

with the Itô interpretation. However, this interpretation still relies on the fact that the autocorrelation of the noise is assumed to be decaying faster than the relaxation of the fast variable, i.e $\tau_r \gg \tau_n$. This could be understood as a temporal scale of the thermal relaxation time of the surface temperature of Greenland and the autocorrelation time of the atmospheric variability. The stochastic interpretation is still a result of modeling choices.

Various studies model the D–O events using a two-dimensional model generally assume the form of a van der Pol or FitzHugh–Nagumo type model [15,17,22]. These have a form similar to Eq. (14), but the variable of interest is on the fast timescale. This means the system is in the underdamped regime and cannot be adiabatically reduced to one dimension. While the models in these studies include only additive noise, we again consider their stochastic interpretation in the possible case of multiplicative noise. In the underdamped regime of Eq. (14) the difference between the Itô and Stratonovich integrals is smaller than dt, so they are equivalent. First, the second order SDE is split into a system of first-order equations

$$\begin{aligned} dx &= v\,dt \\ dv &= \big(-\gamma v + F(x)\big)dt + \sigma(x)dW_t. \end{aligned} \tag{20}$$

Using the α-convention, $x^* = (1-\alpha)x(t) + \alpha x(t+dt)$. Expanding the term $\sigma(x^*)dW_t$,

$$\begin{aligned} \sigma(x^*)dW_t &\approx \sigma(x(t))dW_t + \sigma'(x(t))\big(\alpha x(t+dt) + (1-\alpha)x(t) - x(t)\big) \\ &\quad \times dW_t + \mathcal{O}(dt^2) \\ &\approx \sigma(x(t))dW_t + \alpha\sigma'(x(t))dx\,dW_t + \mathcal{O}(dt^2) \\ &\approx \sigma(x(t))dW_t + \alpha\sigma'(x(t))v(t)dt\,dW_t + \mathcal{O}(dt^2), \end{aligned} \tag{21}$$

and the difference between the interpretations given in the α term is of the order $(dt)^{3/2} < dt$ and thus vanishes faster than the time scale of the dynamics. If instead there is a stochastic component to both variables,

$$\begin{aligned} dx &= v\,dt + \sigma_x dW_t \\ dv &= \big(-\gamma v + F(x)\big)dt + \sigma_v(x)dW_t. \end{aligned} \tag{22}$$

Then the stochastic term is in the fast variable is instead

$$\sigma_v(x^*)dW_t \approx \sigma_v\big(x(t)\big)dW_t + \alpha\sigma_v'\big(x(t)\big)v(t)dt\,dW_t + \alpha\sigma_v'(x(t))\sigma_x dt + \mathcal{O}(dt^2), \tag{23}$$

and the difference between the Itô and Stratonovich interpretations is now of the order dt and must be taken into account.

The previously mentioned study of Krumscheid et al. [44] has state-dependent noise in a data-driven model derivation and assumes Itô calculus. Their multiplicative noise term takes the form of a piecewise constant function, and as such has zero derivative except at the jump. Due to this, the difference between the Itô and Stratonovich interpretations vanishes except at a single point, which can be safely disregarded. Their study does include continuous functions as candidate noise terms but find the additive noise model outperforms them with regard to their parameter fitting routine.

5. Conclusions

In this study, we have derived a data-driven conceptual model of the D–O events including multiplicative noise and seen the reduced stability of the interstadial state when compared to the stadial. We also describe the need to specify a stochastic calculus to be able to interpret the climate potential of the model. We have outlined models which may be interpreted as either Itô or Stratonovich in limiting cases and suggest that the interpretation depends on a physical understanding of the system. For example, if the system derived from the data were meant to represent the stability of the thermohaline circulation but the stochastic integral interpreted as Itô, one would arrive to the erroneous conclusion that the data shows the overturning circulation was monostable, when there is evidence beyond the ice-core record that it is bistable.

The result that the Itô interpretation leads to monostable dynamics is one that is echoed by other conceptual models [17,33,65]. These monostable excitable models with fast–slow dynamics, which require at least 2 dimensions, mirrors the scenario in which the Itô interpretation is applicable. That is, the Itô interpretation comes about due to reduction of a strongly dissipative inertial system, which can be represented as a 2D system with different timescales, to a system in 1D.

Ultimately, this work shows that when deriving stochastic models, the stochastic interpretation can fundamentally affect the results. Interpreting whether the underlying nature of the climate that gave rise to D–O events is a mono- or bi-stable system is vital step to understanding the phenomenon. This is affected by the noise interpretation, which seems to be a completely non-physical, mathematical formalism but is in fact determined by the timescales of the dynamics of the system.

CRediT authorship contribution statement

Kolja Kypke: Investigation, Writing – original draft, Conceptualization. **Peter Ditlevsen:** Conceptualization, Supervision, Writing – review & editing.

Declaration of competing interest

The authors declare that they have no known competing financial interests or personal relationships that could have appeared to influence the work reported in this paper.

Data availability

The ice-core record from the NGRIP project is available at https://www.iceandclimate.nbi.ku.dk/data/.

Acknowledgments

K.K. is supported by the European Union's Horizon 2020 project under the Marie Skłodowska-Curie Innovative Training Network CriticalEarth, grant agreement no. 956170. This is a contribution to the European Union's Horizon 2020 research and innovation programme Tipping Points in the Earth System (TiPES), grant agreement no. 820970.

References

[1] W. Dansgaard, S.J. Johnsen, H.B. Clausen, D. Dahl-Jensen, N.S. Gundestrup, C.U. Hammer, C.S. Hvidberg, J.P. Steffensen, A.E. Sveinbjörnsdottir, J. Jouzel, G. Bond, Evidence for general instability of past climate from a 250-kyr ice-core record, Nature 364 (6434) (1993) 218–220, http://dx.doi.org/10.1038/364218a0.

[2] P. Kindler, M. Guillevic, M. Baumgartner, J. Schwander, A. Landais, M. Leuenberger, Temperature reconstruction from 10 to 120 kyr b2k from the NGRIP ice core, Clim. Past 10 (2) (2014) 887–902, http://dx.doi.org/10.5194/cp-10-887-2014.

[3] S. Barker, G. Knorr, R.L. Edwards, F. Parrenin, A.E. Putnam, L.C. Skinner, E. Wolff, M. Ziegler, 800,000 Years of abrupt climate variability, Science 334 (2011) 347, http://dx.doi.org/10.1126/science.1203580.

[4] B. Martrat, J.O. Grimalt, N.J. Shackleton, L. De Abreu, M.A. Hutterli, T.F. Stocker, Four climate cycles of recurring deep and surface water destabilizations on the Iberian margin, Science 317 (5837) (2007) 502–507, http://dx.doi.org/10.1126/science.1139994.

[5] F. Held, H. Cheng, R.L. Edwards, O. Tüysüz, K. Koç, D. Fleitmann, Dansgaard-Oeschger cycles of the penultimate and last glacial period recorded in stalagmites from Türkiye, Nature Commun. 15 (1) (2024) 1183, http://dx.doi.org/10.1038/s41467-024-45507-5.

[6] T. Mitsui, M. Crucifix, Influence of external forcings on abrupt millennial-scale climate changes: a statistical modelling study, Clim. Dyn. 48 (7) (2017) 2729–2749, http://dx.doi.org/10.1007/s00382-016-3235-z.

[7] J.A. Rial, R. Saha, Modeling abrupt climate change as the interaction between sea ice extent and mean ocean temperature under orbital insolation forcing, in: Abrupt Climate Change: Mechanisms, Patterns, and Impacts, American Geophysical Union (AGU), 2011, pp. 57–74, http://dx.doi.org/10.1029/2010GM001027.

[8] K. Riechers, T. Mitsui, N. Boers, M. Ghil, Orbital insolation variations, intrinsic climate variability, and Quaternary glaciations, Clim. Past 18 (4) (2022) 863–893, http://dx.doi.org/10.5194/cp-18-863-2022.

[9] M. Crucifix, Oscillators and relaxation phenomena in Pleistocene climate theory, Phil. Trans. R. Soc. A 370 (1962) (2012) 1140–1165, http://dx.doi.org/10.1098/rsta.2011.0315.

[10] M. Schulz, A. Paul, A. Timmermann, Relaxation oscillators in concert: A framework for climate change at millennial timescales during the late Pleistocene, Geophys. Res. Lett. 29 (24) (2002) 46–1–46–4, http://dx.doi.org/10.1029/2002GL016144.

[11] A. Ganopolski, S. Rahmstorf, Rapid changes of glacial climate simulated in a coupled climate model, Nature 409 (6817) (2001) 153–158, http://dx.doi.org/10.1038/35051500.

[12] P.D. Ditlevsen, Observation of α-stable noise induced millennial climate changes from an ice-core record, Geophys. Res. Lett. 26 (10) (1999) 1441–1444, http://dx.doi.org/10.1029/1999GL900252.

[13] P.D. Ditlevsen, M.S. Kristensen, K.K. Andersen, The recurrence time of Dansgaard–Oeschger events and limits on the possible periodic component, J. Clim. 18 (14) (2005) 2594–2603, http://dx.doi.org/10.1175/JCLI3437.1.

[14] P.D. Ditlevsen, K.K. Andersen, A. Svensson, The DO-climate events are probably noise induced: statistical investigation of the claimed 1470 years cycle, Clim. Past 3 (1) (2007) 129–134, http://dx.doi.org/10.5194/cp-3-129-2007.

[15] F. Kwasniok, Analysis and modelling of glacial climate transitions using simple dynamical systems, Philos. Trans. R. Soc. Lond. Ser. A: Math. Phys. Eng. Sci. 371 (1991) (2013) 20110472, http://dx.doi.org/10.1098/rsta.2011.0472.

[16] V.N. Livina, F. Kwasniok, T.M. Lenton, Potential analysis reveals changing number of climate states during the last 60 kyr, Clim. Past 6 (1) (2010) 77–82, http://dx.doi.org/10.5194/cp-6-77-2010.

[17] J. Lohmann, P.D. Ditlevsen, A consistent statistical model selection for abrupt glacial climate changes, Clim. Dyn. 52 (11) (2019) 6411–6426, http://dx.doi.org/10.1007/s00382-018-4519-2.

[18] A. Ganopolski, S. Rahmstorf, Abrupt glacial climate changes due to stochastic resonance, Phys. Rev. Lett. 88 (3) (2002) 038501, http://dx.doi.org/10.1103/PhysRevLett.88.038501.

[19] T.M. Dokken, K.H. Nisancioglu, C. Li, D.S. Battisti, C. Kissel, Dansgaard-Oeschger cycles: Interactions between ocean and sea ice intrinsic to the Nordic seas, Paleoceanography 28 (3) (2013) 491–502, http://dx.doi.org/10.1002/palo.20042.

[20] S.V. Petersen, D.P. Schrag, P.U. Clark, A new mechanism for Dansgaard-Oeschger cycles, Paleoceanography 28 (1) (2013) 24–30, http://dx.doi.org/10.1029/2012PA002364.

[21] R. Banderas, J. Álvarez-Solas, M. Montoya, Role of CO_2 and Southern Ocean winds in glacial abrupt climate change, Clim. Past 8 (3) (2012) 1011–1021, http://dx.doi.org/10.5194/cp-8-1011-2012.

[22] G. Vettoretti, P. Ditlevsen, M. Jochum, S.O. Rasmussen, Atmospheric CO2 control of spontaneous millennial-scale ice age climate oscillations, Nat. Geosci. 15 (4) (2022) 300–306, http://dx.doi.org/10.1038/s41561-022-00920-7.

[23] J. Lohmann, A. Svensson, Ice core evidence for major volcanic eruptions at the onset of Dansgaard–Oeschger warming events, Clim. Past 18 (9) (2022) 2021–2043, http://dx.doi.org/10.5194/cp-18-2021-2022.

[24] K. Sakai, W.R. Peltier, Dansgaard–Oeschger oscillations in a coupled atmosphere–ocean climate model, J. Clim. 10 (5) (1997) 949–970, http://dx.doi.org/10.1175/1520-0442(1997)010<0949:DOOIAC>2.0.CO;2.

[25] G. Vettoretti, W.R. Peltier, Fast physics and slow physics in the nonlinear Dansgaard–Oeschger relaxation oscillation, J. Clim. 31 (9) (2018) 3423–3449, http://dx.doi.org/10.1175/JCLI-D-17-0559.1.

[26] P.U. Clark, N.G. Pisias, T.F. Stocker, A.J. Weaver, The role of the thermohaline circulation in abrupt climate change, Nature 415 (6874) (2002) 863–869, http://dx.doi.org/10.1038/415863a.

[27] A.C. Clement, L.C. Peterson, Mechanisms of abrupt climate change of the last glacial period, Rev. Geophys. 46 (4) (2008) http://dx.doi.org/10.1029/2006RG000204.

[28] C. Li, A. Born, Coupled atmosphere-ice-ocean dynamics in Dansgaard-Oeschger events, Quat. Sci. Rev. 203 (2019) 1–20, http://dx.doi.org/10.1016/j.quascirev.2018.10.031.

[29] F. Kwasniok, G. Lohmann, Deriving dynamical models from paleoclimatic records: Application to glacial millennial-scale climate variability, Phys. Rev. E 80 (6) (2009) 066104, http://dx.doi.org/10.1103/PhysRevE.80.066104.

[30] N. Boers, M.D. Chekroun, H. Liu, D. Kondrashov, D.-D. Rousseau, A. Svensson, M. Bigler, M. Ghil, Inverse stochastic–dynamic models for high-resolution Greenland ice core records, Earth Syst. Dyn. 8 (4) (2017) 1171–1190, http://dx.doi.org/10.5194/esd-8-1171-2017.

[31] K. Riechers, L. Rydin Gorjão, F. Hassanibesheli, P.G. Lind, D. Witthaut, N. Boers, Stable stadial and interstadial states of the last glacial's climate identified in a combined stable water isotope and dust record from Greenland, Earth Syst. Dyn. 14 (3) (2023) 593–607, http://dx.doi.org/10.5194/esd-14-593-2023.

[32] N. Boers, M. Ghil, D.-D. Rousseau, Ocean circulation, ice shelf, and sea ice interactions explain Dansgaard-Oeschger cycles, Proc. Natl. Acad. Sci. USA 115 (47) (2018) E11005–E11014, http://dx.doi.org/10.1073/pnas.1802573115.

[33] K. Riechers, G. Gottwald, N. Boers, Glacial abrupt climate change as a multi-scale phenomenon resulting from monostable excitable dynamics, J. Clim. (2024) http://dx.doi.org/10.1175/JCLI-D-23-0308.1.

[34] G. Bond, W. Broecker, S. Johnsen, J. McManus, L. Labeyrie, J. Jouzel, G. Bonani, Correlations between climate records from North Atlantic sediments and Greenland ice, Nature 365 (6442) (1993) 143–147, http://dx.doi.org/10.1038/365143a0.

[35] W.S. Broecker, D.M. Peteet, D. Rind, Does the ocean-atmosphere system have more than one stable mode of operation? Nature 315 (6014) (1985) 21–26, http://dx.doi.org/10.1038/315021a0.

[36] P. Cessi, A simple box model of stochastically forced thermohaline flow, J. Phys. Oceanogr. 24 (9) (1994) 1911–1920, http://dx.doi.org/10.1175/1520-0485(1994)024<1911:ASBMOS>2.0.CO;2.
[37] H. Stommel, Thermohaline convection with two stable regimes of flow, Tellus 13 (2) (1961) 224–230, http://dx.doi.org/10.3402/tellusa.v13i2.9491.
[38] S. Rahmstorf, Bifurcations of the Atlantic thermohaline circulation in response to changes in the hydrological cycle, Nature 378 (6553) (1995) 145–149, http://dx.doi.org/10.1038/378145a0.
[39] I. Malmierca-Vallet, L.C. Sime, the D–O community members, Dansgaard–Oeschger events in climate models: review and baseline Marine Isotope Stage 3 (MIS3) protocol, Clim. Past 19 (5) (2023) 915–942, http://dx.doi.org/10.5194/cp-19-915-2023.
[40] P.D. Ditlevsen, S. Ditlevsen, K.K. Andersen, The fast climate fluctuations during the stadial and interstadial climate states, Ann. Glaciol. 35 (1) (2002) 457–462, http://dx.doi.org/10.3189/172756402781816870.
[41] K. Itô, Stochastic integral, Proc. Imp. Acad. 20 (8) (1944) 519–524, http://dx.doi.org/10.3792/pia/1195572786.
[42] R.L. Stratonovich, A new representation for stochastic integrals and equations, SIAM J. Control 4 (2) (1966) 362–371, http://dx.doi.org/10.1137/0304028.
[43] N.G. van Kampen, Itô versus Stratonovich, J. Stat. Phys. 24 (1) (1981) 175–187, http://dx.doi.org/10.1007/BF01007642.
[44] S. Krumscheid, M. Pradas, G.A. Pavliotis, S. Kalliadasis, Data-driven coarse graining in action: Modeling and prediction of complex systems, Phys. Rev. E 92 (4) (2015) 042139, http://dx.doi.org/10.1103/PhysRevE.92.042139.
[45] North Greenland Ice Core Project members, High-resolution record of Northern Hemisphere climate extending into the last interglacial period, Nature 431 (7005) (2004) 147–151, http://dx.doi.org/10.1038/nature02805.
[46] S.O. Rasmussen, M. Bigler, S.P. Blockley, T. Blunier, S.L. Buchardt, H.B. Clausen, I. Cvijanovic, D. Dahl-Jensen, S.J. Johnsen, H. Fischer, V. Gkinis, M. Guillevic, W.Z. Hoek, J.J. Lowe, J.B. Pedro, T. Popp, I.K. Seierstad, J.P. Steffensen, A.M. Svensson, P. Vallelonga, B.M. Vinther, M.J. Walker, J.J. Wheatley, M. Winstrup, A stratigraphic framework for abrupt climatic changes during the Last Glacial period based on three synchronized Greenland ice-core records: refining and extending the INTIMATE event stratigraphy, Quat. Sci. Rev. 106 (2014) 14–28, http://dx.doi.org/10.1016/j.quascirev.2014.09.007.
[47] J. Lohmann, P.D. Ditlevsen, Objective extraction and analysis of statistical features of Dansgaard–Oeschger events, Clim. Past 15 (5) (2019) 1771–1792, http://dx.doi.org/10.5194/cp-15-1771-2019.
[48] E. Wong, M. Zakai, On the convergence of ordinary integrals to stochastic integrals, Ann. Math. Stat. 36 (5) (1965) 1560–1564, http://dx.doi.org/10.1214/aoms/1177699916.
[49] S. Faetti, C. Festa, L. Fronzoni, P. Grigolini, P. Martano, Multiplicative stochastic processes in nonlinear systems: Noise-induced transition from the overdamped to the inertial regime, Phys. Rev. A 30 (6) (1984) 3252–3263, http://dx.doi.org/10.1103/PhysRevA.30.3252.
[50] R. Graham, A. Schenzle, Stabilization by multiplicative noise, Phys. Rev. A 26 (3) (1982) 1676–1685, http://dx.doi.org/10.1103/PhysRevA.26.1676.
[51] S. Hottovy, A. McDaniel, G. Volpe, J. Wehr, The Smoluchowski-Kramers limit of stochastic differential equations with arbitrary state-dependent friction, Comm. Math. Phys. 336 (3) (2015) 1259–1283, http://dx.doi.org/10.1007/s00220-014-2233-4.
[52] R. Kupferman, G.A. Pavliotis, A.M. Stuart, Itô versus Stratonovich white-noise limits for systems with inertia and colored multiplicative noise, Phys. Rev. E 70 (3) (2004) 036120, http://dx.doi.org/10.1103/PhysRevE.70.036120.
[53] G.A. Pavliotis, A.M. Stuart, Analysis of white noise limits for stochastic systems with two fast relaxation times, Multiscale Model. Simul. 4 (1) (2005) 1–35, http://dx.doi.org/10.1137/040610507.
[54] K. Sekimoto, Temporal coarse graining for systems of Brownian particles with non-constant temperature, J. Phys. Soc. Japan 68 (4) (1999) 1448–1449, http://dx.doi.org/10.1143/JPSJ.68.1448.
[55] C.W. Gardiner, Handbook of Stochastic Methods: For Physics, Chemistry and Natural Sciences, second ed., in: Springer Series in Synergetics, vol. 13, Springer, Berlin, 1997.
[56] T. Kuroiwa, K. Miyazaki, Brownian motion with multiplicative noises revisited, J. Phys. A 47 (1) (2014) 012001, http://dx.doi.org/10.1088/1751-8113/47/1/012001.
[57] G. Volpe, L. Helden, T. Brettschneider, J. Wehr, C. Bechinger, Influence of noise on force measurements, Phys. Rev. Lett. 104 (17) (2010) 170602, http://dx.doi.org/10.1103/PhysRevLett.104.170602.
[58] P. Lançon, G. Batrouni, L. Lobry, N. Ostrowsky, Drift without flux: Brownian walker with a space-dependent diffusion coefficient, Europhys. Lett. (EPL) 54 (1) (2001) 28–34, http://dx.doi.org/10.1209/epl/i2001-00103-6.
[59] R. Mannella, P.V.E. McClintock, Itô versus Stratonovich: 30 years later, Fluct. Noise Lett. 11 (1) (2012) 1240010, http://dx.doi.org/10.1142/S021947751240010X.
[60] G. Pesce, A. McDaniel, S. Hottovy, J. Wehr, G. Volpe, Stratonovich-to-Itô transition in noisy systems with multiplicative feedback, Nature Commun. 4 (1) (2013) 2733, http://dx.doi.org/10.1038/ncomms3733.
[61] W. Moon, J.S. Wettlaufer, On the interpretation of Stratonovich calculus, New J. Phys. 16 (5) (2014) 055017, http://dx.doi.org/10.1088/1367-2630/16/5/055017.
[62] T. Morita, On the interpretation of multiplicative white noise, Phys. Lett. A 82 (5) (1981) 215–217, http://dx.doi.org/10.1016/0375-9601(81)90187-0.
[63] A. Timmermann, G. Lohmann, Noise-induced transitions in a simplified model of the thermohaline circulation, J. Phys. Oceanogr. 30 (8) (2000) 1891–1900, http://dx.doi.org/10.1175/1520-0485(2000)030<1891:NITIAS>2.0.CO;2.
[64] A.H. Monahan, A. Timmermann, G. Lohmann, Comments on “Noise-induced transitions in a simplified model of the thermohaline circulation”, J. Phys. Oceanogr. 32 (3) (2002) 1112–1116, http://dx.doi.org/10.1175/1520-0485(2002)032<1112:CONITI>2.0.CO;2.
[65] F. Kwasniok, G. Lohmann, A stochastic nonlinear oscillator model for glacial millennial-scale climate transitions derived from ice-core data, Nonlinear Process. Geophys. 19 (6) (2012) 595–603, http://dx.doi.org/10.5194/npg-19-595-2012.

Chapter 3

B- and r-tipping in a comprehensive ice sheet model

3.1 Introduction

This project and article of this chapter deals with the interplay of rate-induced tipping within a chaotic system. Similarly to noise-induced tipping, r-tipping in the setting of a double-fold bifurcation occurs through a saddle manifold in between stable states. Due to climate systems being spatially extended, it should be expected for them to display chaotic variability. This chaotic nature can cause complications when trying to comprehend the tipping behaviour, as it introduces unpredictability. There are two types of unpredictability related to tipping in chaotic systems that manifest. Firstly, for a given parameter value, what is the final attractor? Secondly, under a parameter shift that causes a system to tip, at what time will the tipping occur?

The former issue arises primarily due to uncertainties in the basins of attraction for different states of a system. For chaotic attractors or chaotic non-attracting sets between attractors such as chaotic saddles, basin boundaries can be fractal [37] or even riddled [80]. For this reason, two very nearby initial conditions may actually belong to two different basins of attraction, and there is no guarantee that increasing the confidence in the initial state will result in an increase in the confidence of the resulting asymptotic state. This can be similar to the non-chaotic phenomenon of partial tipping [1], where nearby initial conditions under a parameter shift can diverge to separate attractors.

The latter issue comes about due to *lifetimes* associated with non-attracting chaotic sets. These lifetimes are the mean time a trajectory spends near a chaotic non-attracting set due to following along its stable manifolds before eventually being repelled. The chaotic non-attracting set can be the previously mentioned chaotic saddle in between the stable attractors or a *ghost attrac-*

tor that lingers after a boundary crisis causes the annihilation of a previously stable chaotic attractor [38]. In the case of a chaotic saddle, a trajectory that experiences r-tipping may remain about this state for a while before reaching the other asymptotic state. For a ghost attractor, a system that experiences a b-tipping from a chaotic attractor will also have transients that remain in the phase space of this attractor that no longer exists before eventually tipping to the only remaining stable attractor. Both cases result in chaotic transients, which are long-lived transients that remain near the stable manifolds of a chaotic non-attracting set. The escape time from these transients depends sensitively on the initial condition of the system, but for an ensemble they are exponentially distributed which creates the unpredictability. Furthermore, in complex systems where only transient forcing is possible and the true bifurcation values are not known, the scenarios might appear similar, and it is not trivial to determine whether b-tipping or r-tipping has occurred. This is the case of the system that is the subject of the article of this chapter: a study on how a regional phenomenon – that of an oscillating ice stream – can seemingly affect the large scale tipping of the entire ice sheet, along with the investigation of whether it is indeed possible to diagnose the displayed chaotic transients as being a result of b- or r-tipping.

The project described in this chapter began as a straightforward project of r-tipping of the Greenland ice sheet. R-tipping generally occurs in systems with multiple feedback timescales [29]. A simple understanding is such: in simple bistable tipping systems, it is positive feedbacks that establish the two states and negative feedbacks that keep them stable. If there are positive feedbacks that act on a very fast timescale compared to some negative feedbacks, a parameter forcing at a large rate can induce these positive feedbacks before the negative ones can kick in. On the other hand, of the forcing rate is slow, the negative feedbacks are able to keep up with the positive ones, and the system tracks the changing equilibrium and does not tip.

Ice sheets are components of the climate that generally evolve on very long time scales. The bulk of their dynamics occurs as creep flow in response to changes in the amount of mass flux at their surface. Mass at the surface is added in the form of precipitation, also called accumulation, and lost due to melting or sublimation, also called ablation. This process depends largely on surface air temperature. Accumulation also depends heavily on the moisture content in the air, giving both a positive and negative feedback associated with the elevation of the ice sheet surface. Since moisture reduces with elevation, so too will the accumulation decrease until the ice sheet reaches steady state. On the other hand, due to the negative lapse rate of temperature in the atmosphere a thicker ice sheet will experience more accumulation due to the lower temperature – this is the melt elevation feedback. There is an equilibrium altitude, above which accumulation occur and below which ablation occurs. For the example of an ice sheet above this equilibrium line, if suddenly there is some atmospheric forcing that increases the altitude of the line, the

resulting melt will still take thousands of years [65]. Thus the melt-elevation feedback is relatively insensitive to rate-induced tipping. Another positive feedback prevalent is the ice-albedo feedback, where more ice cover reflects more incoming solar radiation and thereby decreasing the absorbed energy from the sun, promoting lower temperatures and ice sheet growth. Similarly to accumulation and ablation, this is also not expected to experience r-tipping due to the slow speed of the ice sheet flow.

Where ice sheets do experience fast flow velocities is in ice shelves, which are sections of ice sheets that are floating in the ocean. Due to this, they do not experience as much friction at their base and are able to advance more easily. Ice shelves can be grounded underwater, and this portion that is underwater can experience additional melting due to increasing ocean temperatures, causing the grounding line to retreat. If this grounding line is on a retrograde slope, the retreat will expose more of the ice sheet base to the warmer ocean, further increasing melt in a positive feedback. This is dubbed the marine ice sheet instability [103, 118]. Due to the the increased flow velocities, as well as the possibility of calving of large sections of the ice sheet, the mass loss can be much quicker than for atmospheric sources of climate forcing. This may be the situation in the west Antarctic ice sheet (WAIS), where large sections are ice shelves grounded on a retrograde slope, and suggests there may be the possibility of r-tipping the WAIS.

In contrast to the WAIS, Greenland does not have a large amount of floating ice shelves. While it does contain many marine-terminating outlet glaciers, many of which are accelerating in mass loss [42, 44, 48, 52, 63, 73, 93, 111], these are most limited to the southern and western coasts of Greenland. Anthropogenic temperature forcing is strongest in those areas, which somewhat explains their increasing melting rates. Ultimately, the fact that are largely constrained to mountainous regions near the coast suggest that they have a limited impact on the mas loss of the GrIS as a whole [45]. Thus, the relatively slow evolution of the GrIS suggest that r-tipping due to anthropogenic temperature forcing is not expected to occur.

Indeed, that is also (somewhat) the conclusion of the project of this chapter. Firstly, the qualities of the chaotic transients and their scaling laws suggest, though not with overwhelming confidence due to the low sample size, that the tipping was due to a bifurcation (or boundary crisis) rather than rate-induced effects. Perhaps more pertinently, the timescales of the tipping trajectories exceeded 100 kyrs, even for warming rates of 0.1 Kelvin/yr. Not only does this exceed the timescale of Milankovitch cycles [5], which have a much greater effect on global climate than 1 Kelvin of warming, but it is also impossible to consider the climate that forces the ice sheet as being constant for such a length of time. The results of this article are not so relevant to any ideas of anthropogenic climate change, but rather they demonstrate the issues that the complexity of a system can impart on the tipping behaviour. The remainder of this chapter is dedicated to the background on how ice sheets are

modelled, along with a brief introduction of the concept of chaotic transients before the manuscript of a paper that reports on the findings of this project.

3.2 Ice Sheet Dynamics

An ice sheet behaves as a very viscous fluid. It can thus be mathematically described by the equation for Stokes flow,

$$\nabla \cdot \mathbf{u} = 0 \tag{3.1}$$

$$\rho \mathbf{g} - \nabla \cdot \boldsymbol{t} = 0, \tag{3.2}$$

where $\boldsymbol{u}$ is the velocity vector, ρ is the density of ice, $\boldsymbol{g}$ is the gravitational force vector and $\boldsymbol{t}$ is the Cauchy stress tensor. The diagonal elements of $\boldsymbol{t}$ are the normal stresses and the off-diagonal elements are the shear stresses. The deviatoric stress tensor $\boldsymbol{\tau}$ is the total stress $\boldsymbol{t}$ minus the hydrostatic pressure,

$$\boldsymbol{t} = -p\boldsymbol{I} + \boldsymbol{\tau}. \tag{3.3}$$

The deviatoric stress tensor determines the deformation of the ice and is related to the strain rate tensor $\dot{\boldsymbol{\varepsilon}}$ by the viscosity,

$$\boldsymbol{\tau} = 2\eta\dot{\boldsymbol{\varepsilon}}, \tag{3.4}$$

where the strain depends on the velocity,

$$\dot{\boldsymbol{\varepsilon}} = \frac{1}{2}\Big(\nabla\mathbf{u} + \nabla\mathbf{u}^T\Big). \tag{3.5}$$

Generally, an effective stress and strain is used. This is calculated as

$$\tau = \sqrt{\frac{1}{2}I_2(\boldsymbol{\tau})}, \tag{3.6}$$

where $I_2(\boldsymbol{\tau})$ is the second invariant of the tensor,

$$I_2(\boldsymbol{\tau}) = \frac{1}{2}\big[\,\mathrm{tr}\,(\boldsymbol{\tau}^2) - (\mathrm{tr}\,\boldsymbol{\tau})^2\big]. \tag{3.7}$$

Since the deviatoric stress tensor is traceless, the effective stress can be written in index notation as

$$\tau = \sqrt{\frac{1}{2}\tau_{ij}\tau_{ij}}. \tag{3.8}$$

The same is done for the effective strain,

$$\dot{\varepsilon} = \sqrt{\frac{1}{2}\dot{\varepsilon}_{ij}\dot{\varepsilon}_{ij}} \tag{3.9}$$

where the components can be given explicitly as

$$\dot{\varepsilon}_{ij} = \frac{1}{2}\left(\frac{\partial u_i}{\partial x_j} + \frac{\partial u_j}{\partial x_i}\right). \tag{3.10}$$

From experimental observation [33, 78], the effective viscosity η that now governs the relationship

$$\tau_{ij} = 2\eta\dot{\varepsilon}_{ij} \tag{3.11}$$

depends on the temperature and pressure as well as the strain,

$$\eta(T, p, \tau) = \frac{1}{2A(T, p)\tau^{n-1}}. \tag{3.12}$$

This may be arranged to be written in terms of the effective strain rate as

$$\eta(T, p, \dot{\varepsilon}) = \frac{1}{2}\big(A(T, p)\big)^{-1/n}\dot{\varepsilon}^{(1-n)/n}. \tag{3.13}$$

This equation is know as Glen's Flow law, and underpins the deformational creep flow of ice sheets. The *rate factor* $A(T, p)$ is given as an Arrhenius law,

$$A(T, p) = A_0 \exp\big[-(Q + pV)/RT\big], \tag{3.14}$$

and represents the softness of the ice: the warmer the ice, the softer it is and the faster it will deform. Equations 3.1, 3.2 and 3.11 describe the fundamental equations of ice sheet flow.

Since the rate factor depends on the temperature, the system now must be thermomechanically coupled. The thermodynamics of the system are described by an equation for the balance of the internal energy U,

$$\rho\frac{DU}{Dt} = -\nabla\cdot\boldsymbol{q} + \operatorname{tr}(\boldsymbol{t}\cdot\dot{\boldsymbol{\varepsilon}}) + \rho r, \tag{3.15}$$

where $\frac{D\bullet}{Dt} = \frac{\partial\bullet}{\partial t} + (\nabla\bullet)\cdot\mathbf{u}$ is the material or Lagrangian derivative. The internal energy is assumed to depend linearly on temperature, such that $\frac{DU}{Dt} = c\frac{DT}{Dt}$ where c is the specific heat capacity of ice. The heat flux $\boldsymbol{q}$ can be described as due to conduction, where for $\boldsymbol{q} = -\kappa\nabla T$, κ is the thermal conductivity of ice. The dissipation $\operatorname{tr}(\boldsymbol{t}\cdot\dot{\boldsymbol{\varepsilon}})$ transforms kinetic energy into internal energy. Expanding

$$\boldsymbol{t} = -p\boldsymbol{I} + \boldsymbol{\tau} = -p\boldsymbol{I} + 2\eta\dot{\boldsymbol{\varepsilon}}, \tag{3.16}$$

gives $\operatorname{tr}(\boldsymbol{t}\cdot\dot{\boldsymbol{\varepsilon}}) = 2\eta\operatorname{tr}(\dot{\boldsymbol{\varepsilon}}^2) = 4\eta\dot{\varepsilon}^2$. The radiation flux r is negligible in an ice sheet. Thus the thermodynamic equation simplifies to

$$\rho c\frac{DT}{Dt} = \kappa\Delta T + 4\eta\dot{\varepsilon}^2. \tag{3.17}$$

Boundary conditions that set the equilibrium state that the ice sheet evolves to must be described. The boundary is free at the surface and interacting with bedrock or ocean at its base. A kinematic and dynamic boundary

condition is described for a free boundary as follows. At the interface with the atmosphere, the stresses are negligible and the dynamic boundary condition is the *stress-free* condition. There is a volume flux driven by the surface mass balance a_s, which is the difference between the accumulation of ice through densification of snowfall and the ablation of surface ice. Defining the free surface as $z = h(x, y, t)$, its material derivative is equal to the vertical surface mass balance, giving

$$\frac{\partial h}{\partial t} + u_x \frac{\partial h}{\partial x} + u_y \frac{\partial h}{\partial y} - u_z = a_s. \tag{3.18}$$

The sign of a_s is chosen such that positive corresponds to mass gain. A temperature boundary condition is required to solve the equation 3.17 and is simply that the ice temperature at the surface is equal to the atmospheric temperature at the surface. In this way, the surface boundary is entirely determined by external conditions: the accumulation rate and the surface temperature.

At the base of the ice sheet, the ice may either be grounded on bedrock or floating on the ocean. There is a basal mass balance a_b which describes the mass lost due to melting and the mass gained due to refreezing. For grounded ice, the interface is no longer stress-free due to friction. This friction stress can produce melting in the case of sliding at the bedrock. Heat also enters the base of the ice sheet though a geothermal heat flux. Finally, since the melting temperature of ice decreases as pressure increases, the ice is at its warmest at the base of the ice sheet and there is a heat flux from the basal ice into the ice sheet above. Similar to the free surface, the boundary condition for the base $z = b(x, y, t)$ is given by

$$\frac{\partial b}{\partial t} + u_x \frac{\partial b}{\partial x} + u_y \frac{\partial b}{\partial y} = a_b, \tag{3.19}$$

where $u_z = 0$ since the ice cannot penetrate into the bedrock and a_b is the vertical basal mass balance determined by the thermodynamic balance and the input geothermal heat flux. The sign of a_b is chosen such that positive corresponds to mass loss (melting).

A floating ice sheet over the ocean is called an ice shelf. Since the interface between ocean and ice is a free boundary, the dynamic and kinematic boundary conditions are described as follows. Boundary stresses are those of the hydrostatic pressure of the water column along with shear stresses due to ocean circulation, although this latter stress is generally negligible. The thermodynamic boundary condition is such that the basal ice is the same temperature as the water. There is a heat flux from the water into the basal ice as well as a frictional heating from the current, which describes the basal mass balance. However, since the ice temperature is prescribed by the ocean temperature, it is more typical to derive the basal mass balance or basal heat fluxes from measured quantities. There are also lateral stresses on ice shelves.

Due to the differences in the lateral pressures on the ice shelf portion that is above versus below the sea level, the ice shelf thins at it advances. Eventually, crevasses form that extend though the thickness of an ice shelf, causing it to break off in an event known as calving. This effects a mass flux given as a calving rate a_c.

Similarly to floating ice shelves, grounded ice sheets have areas where there is water under the ice sheet. If the basal ice reaches the pressure melting point, water under the ice sheet serves to decrease the basal friction. This can occur over areas of hard bedrock where a layer of water lubricates the ice sheet, or else in areas with weak till which becomes saturated with water and can deform very easily. These areas are known as ice streams because they have a very large streaming velocity at their base which extends to the entire ice column. These basal velocities depend on the basal shear stress τ_b and have different functional forms depending on the conditions at the base. Crucial to all is the effective pressure a the base of the ice, which is the difference between the overburden pressure and the pressure of the water layer. For sliding over hard bedrock, the topography is typically rough. The pressure of the subglacial water layer serves to reduce basal stress by filling cavities in the lee side of undulations in the bedrock as well as uplifting the ice sheet through buoyancy. In the case of a soft deformable till at the base of the ice sheet, the basal stress depends on the till rheology, which turn directly depends on the quantity subglacial water that can permeate the till and reduce internal friction. Overall, the boundary condition for grounded ice must be different based on whether there is basal sliding or not. In the former case, the horizontal velocities at the base in equation 3.19 are zero and the base simply loses or gains mass as given by the basal mass balance. In the case of nonzero basal velocity, it is determined by the basal shear stress. Since the streaming velocity dominates over deformational creep it is easier to measure the velocity than the basal shear stress and empirical sliding laws can be derived in this way.

Using the continuity equation and the boundary conditions, the thickness of an ice sheet can be determined. Integrating equation 3.1 from the base to the surface and using the Leibniz integration rule, then substituting equations 3.18 and 3.19, gives

$$\frac{\partial}{\partial x}\int_b^h u_x dz + \frac{\partial}{\partial y}\int_b^h u_y dz + \frac{\partial h}{\partial t} - \frac{\partial b}{\partial t} = a_s + a_b - a_c. \tag{3.20}$$

Finally, defining the ice thickness $H = h - b$ and depth-averaged horizontal velocities $\bar{u}_x = 1/H \int_b^h u_x dz$ and $\bar{u}_y = 1/H \int_b^h u_y dz$, the equation for the change in ice thickness is

$$\frac{\partial H}{\partial t} = -\nabla \cdot H\bar{\mathbf{u}} + a_s + a_b - a_c. \tag{3.21}$$

Ice sheet model Yelmo

The numerical ice sheet model Yelmo [97] simulates the evolution of an ice sheet by solving approximate solutions to the Stokes flow equations along with thermodynamic equations and boundary conditions, as resolving the Stokes flow directly would be too computationally expensive. One feature of ice sheets that allow for simplification of their dynamics is their aspect ratio. The thickness of an ice sheet is orders of magnitudes smaller than its horizontal extent. This allows the assumption that the flow is essentially parallel to the base, and vertical shear is negligible [39]. Effectively, the three dimensional flow of the ice sheet can be simplified to two dimensions by integrating the velocities over the depth. For these shallow ice approximations the stresses are dominated in the vertical by the normal (non-deviatoric) stress and in the horizontal by the shear stresses. Then the momentum balance equation 3.2 in the z direction gives

$$\frac{\partial t_{zz}}{\partial z} = -\rho g, \tag{3.22}$$

since $\tau_{xz},\ \tau_{yz} \ll t_{zz}$. This can integrate from the stress-free surface boundary ($z = h$) to give

$$t_{zz} = \rho g(h - z), \tag{3.23}$$

which is the hydrostatic pressure. Using the definition of the deviatoric stress such that $\tau_{zz} = p - t_{zz}$, as well as the traceless quality of the tensor, the pressure is

$$p = \rho g(h - z) - \tau_{xx} - \tau_{yy}, \tag{3.24}$$

which leads to the horizontal normal stresses being given by the shear stresses as

$$t_{xx} = -\rho g(h - z) + 2\tau_{xx} + \tau_{yy}, \tag{3.25}$$
$$t_{yy} = -\rho g(h - z) + \tau_{xx} + 2\tau_{yy}. \tag{3.26}$$

Due to the aspect ratio of the ice sheet, the partial derivatives of the vertical velocity in the horizontal direction are much smaller than the partial derivatives of the horizontal velocity in the vertical direction and are therefore neglected. These equations, along with the flow law relating the velocities to the shear stresses (equations 3.10 and 3.11), give the first-order Blatter-Pattyn

approximation [6, 83],

$$4\frac{\partial}{\partial x}\left(\eta\frac{\partial u_x}{\partial x}\right)+2\frac{\partial}{\partial x}\left(\eta\frac{\partial u_y}{\partial y}\right)+\frac{\partial}{\partial y}\left(\eta\left[\frac{\partial u_x}{\partial y}+\frac{\partial u_y}{\partial x}\right]\right)+\frac{\partial}{\partial z}\left(\eta\frac{\partial u_x}{\partial z}\right)=\rho g\frac{\partial h}{\partial x}, \tag{3.27}$$

$$4\frac{\partial}{\partial y}\left(\eta\frac{\partial u_y}{\partial y}\right)+2\frac{\partial}{\partial y}\left(\eta\frac{\partial u_x}{\partial x}\right)+\frac{\partial}{\partial x}\left(\eta\left[\frac{\partial u_x}{\partial y}+\frac{\partial u_y}{\partial x}\right]\right)+\frac{\partial}{\partial z}\left(\eta\frac{\partial u_y}{\partial z}\right)=\rho g\frac{\partial h}{\partial y}. \tag{3.28}$$

From the conservation of mass (equation 3.1) the partial derivative of the vertical velocity in the vertical direction, $\frac{\partial u_z}{\partial z}$, can be written in terms of the horizontal velocities. This gives the effective strain rate in equation 3.10 as

$$\dot{\varepsilon}^2=\frac{\partial u_x}{\partial x}^2+\frac{\partial u_y}{\partial y}^2+\frac{\partial u_x}{\partial x}\frac{\partial u_y}{\partial y}+\frac{1}{4}\left(\frac{\partial u_x}{\partial y}+\frac{\partial u_y}{\partial x}\right)^2+\frac{1}{4}\frac{\partial u_x}{\partial z}^2+\frac{1}{4}\frac{\partial u_y}{\partial z}^2. \tag{3.29}$$

Further simplifications are required for the above shallow model for efficient computation. The two most typical are the Shallow Ice Approximation (SIA) and the Shallow Shelf Approximation (SSA). They are distinguished by the conditions of the stress at their basal boundary. The SIA is characterized by grounded ice that is frozen at its base, applying a no-slip condition. In this case, the flow is purely shear flow such that all horizontal derivatives may be eliminated. This greatly simplifies equations 3.27 and 3.28 to

$$\frac{\partial}{\partial z}\left(\eta\frac{\partial u_x}{\partial z}\right)=\rho g\frac{\partial h}{\partial x}, \tag{3.30}$$

$$\frac{\partial}{\partial z}\left(\eta\frac{\partial u_y}{\partial z}\right)=\rho g\frac{\partial h}{\partial y}, \tag{3.31}$$

and the effective strain rate in equation 3.29 to

$$\dot{\varepsilon}^2=\frac{1}{4}\frac{\partial u_x}{\partial z}^2+\frac{1}{4}\frac{\partial u_y}{\partial z}^2. \tag{3.32}$$

These equations may then be integrated over the ice thickness to arrive at the horizontal velocities. However, this would require implicit integration, and a more direct integration can be found. Since the shear flow dominates the

momentum balance,

$$\frac{\partial \tau_{xz}}{\partial z} = \frac{\partial p}{\partial x} = \rho g \frac{\partial h}{\partial x} \tag{3.33}$$

$$\frac{\partial \tau_{yz}}{\partial z} = \frac{\partial p}{\partial y} = \rho g \frac{\partial h}{\partial y} \tag{3.34}$$

$$\tag{3.35}$$

it can be integrated, which gives an effective stress of

$$\tau = \sqrt{\frac{1}{2}(\tau_{xz}^2 + \tau_{yz}^2)} = \rho g (h - z)|\nabla h|. \tag{3.36}$$

This can be used in the viscosity equation and substituted into equation 3.31, then integrated from the base ($z = b$) to arrive at

$$u_x = -2(\rho g)^n |\nabla h|^{n-1} \frac{\partial h}{\partial x} \int_b^z A(T,p)(h-s)^n ds \tag{3.37}$$

$$u_y = -2(\rho g)^n |\nabla h|^{n-1} \frac{\partial h}{\partial y} \int_b^z A(T,p)(h-s)^n ds. \tag{3.38}$$

The term $\rho g H |\nabla h|$, which is the negative of the shear stress at the base, is the driving stress $\boldsymbol{\tau}_d$. In the SIA, it is equal to the negative of the basal stress such that the ice sheet flows to an extent there these two are in equilibrium.

On the other hand, the SSA is used to represent fast flow due to low friction at the basal boundary. In this case, the driving stress exceeds the basal stress and the flow is more rapid. This results in a plug flow, where the entire ice column is travelling at the same speed. This is the opposite case of the SIA, where now the shear flow is negligible. As the horizontal velocities are constant over the entire thickness they may be integrated over the vertical coordinate,

$$\bar{v}_x = \frac{1}{H} \int_b^h u_x(z) dz \tag{3.39}$$

$$\bar{v}_y = \frac{1}{H} \int_b^h u_y(z) dz. \tag{3.40}$$

The effective strain rate is

$$\dot{\varepsilon}^2 = \frac{\partial u_x}{\partial x}^2 + \frac{\partial u_y}{\partial y}^2 + \frac{\partial u_x}{\partial x}\frac{\partial u_y}{\partial y} + \frac{1}{4}\left(\frac{\partial u_x}{\partial y} + \frac{\partial u_y}{\partial x}\right)^2. \tag{3.41}$$

due to the independence of velocity on depth. This allows the viscosity to be integrated over the depth,

$$\bar{\eta} = \frac{1}{2}\dot{\varepsilon}^{-(n-1)/n} \int_b^h A(T,p)^{-1/n} dz. \tag{3.42}$$

Then the equations 3.27 and 3.28 become

$$4\frac{\partial}{\partial x}\left(\bar{\eta}\frac{\partial \bar{v}_x}{\partial x}\right) + 2\frac{\partial}{\partial x}\left(\bar{\eta}\frac{\partial \bar{v}_y}{\partial y}\right) + \frac{\partial}{\partial y}\left(\bar{\eta}\left[\frac{\partial \bar{v}_x}{\partial y} + \frac{\partial \bar{v}_y}{\partial x}\right]\right) = \rho g H \frac{\partial h}{\partial x} + \tau_{b,x} \tag{3.43}$$

$$4\frac{\partial}{\partial y}\left(\bar{\eta}\frac{\partial \bar{v}_y}{\partial y}\right) + 2\frac{\partial}{\partial y}\left(\bar{\eta}\frac{\partial \bar{v}_x}{\partial x}\right) + \frac{\partial}{\partial x}\left(\bar{\eta}\left[\frac{\partial \bar{v}_x}{\partial y} + \frac{\partial \bar{v}_y}{\partial x}\right]\right) = \rho g H \frac{\partial h}{\partial y} + \tau_{b,y}, \tag{3.44}$$

where τ_b is the basal stress. These basal stress terms not found in 3.27 and 3.28 appear due to the vertical integration, being related to the boundary conditions.

Often, a hybrid approach combining the SIA and SSA is used to reap the advantages of each. The total horizontal velocity is given as the sum of deformational creep velocity u_d calculated using the SIA and basal sliding velocity u_b calculated using the SSA. Yelmo as described in Robinson et al. [97] is such a hybrid model. However, over its continual development it has changed to replace the hybrid approach with that of a Depth-Integrated Viscosity Approximation (DIVA) [99]. In this scheme, the viscosity is integrated over the depth in the same way as in the SSA but using the entire effective strain rate of equation 3.29. The velocities are also depth averaged. This results in the same form of the stress balance as for the SSA, equation 3.44, but with additional terms in the effective viscosity and a more complete basal stress.

Under the shallow approximation, the horizontal heat conduction terms in the heat flux term in the thermodynamic equation 3.17 are negligible, reducing $\Delta T \approx \frac{\partial^2 T}{\partial z^2}$. Expanding the material derivative, the thermodynamic equation is

$$\frac{\partial T}{\partial t} = \frac{\kappa}{\rho c}\frac{\partial^2 T}{\partial z^2} - \left(u_x\frac{\partial T}{\partial x} + u_y\frac{\partial T}{\partial y} + u_z\frac{\partial T}{\partial z}\right) + \frac{4\eta\dot{\varepsilon}^2}{\rho c}. \tag{3.45}$$

The basal stress $\boldsymbol{\tau}_b$ takes the form of a regularized Coulomb friction law [102],

$$\boldsymbol{\tau}_b = -c_b\left(\frac{|\boldsymbol{u}_b|}{|\boldsymbol{u}_b| + u_0}\right)^q \frac{\boldsymbol{u}_b}{|\boldsymbol{u}_b|}. \tag{3.46}$$

The coefficient c_b is a field that determines the friction properties of the bed itself. It depends linearly on the effective pressure N_{eff} at the base of the ice sheet,

$$c_b = \lambda N_{\text{eff}}, \tag{3.47}$$

with λ in turn describing the relative strength of the till. The exponent q determines the friction regime. It is bounded between 0 and 1, corresponding to plastic friction for $q = 0$ and linear friction for $q = 1$. The variable u_0 is a threshold that sets a maximal value for $|\boldsymbol{\tau}_b/c_b|$. This prevents cases where effective pressure is low from resulting in too large a basal stress [13]. This

effectively allows the model to switch between two modes of basal motion: For $|\boldsymbol{u}_b| < u_0$, the magnitude is

$$|\boldsymbol{\tau}_b/c_b| = \left(\frac{|\boldsymbol{u}_b|}{u_0}\right)^q, \tag{3.48}$$

which corresponds with sliding of hard bedrock. For $|\boldsymbol{u}_b| > u_0$, the magnitude is

$$|\boldsymbol{\tau}_b/c_b| = 1. \tag{3.49}$$

This is the case of deformation of weak till and corresponds to plastic friction, which is independent of the velocity.

The value of λ in the friction coefficient is calculated based on the paleoclimate history of the till. By assuming that areas with bedrock below sea level were previously submerged and thus their till is formed primarily by sediments with a weaker internal friction, a linear relationship with altitude is constructed. The effective pressure is calculated as in Bueler and van Pelt [17],

$$N_{\text{eff}} = \min\left[P_o, N_0\left(\frac{\delta P_o}{N_0}\right)^s 10^{C(1-s)}\right], \tag{3.50}$$

with overburden pressure $P_o = \rho g H$, empirical parameters N_0 and C derived from the conditions of the Siple ice stream in Antarctica [113], and δ setting a lower limit for effective pressure. The till saturation ratio is $s = H_w/H_{w,\max}$. The amount of water in the till H_w increases with basal melt, which is the negative of the basal mass balance,

$$\frac{\partial H_w}{\partial t} = -\frac{\rho}{\rho_w} a_b - C_d, \tag{3.51}$$

where C_d is a constant drainage rate.

The calving rate is determined simply by some threshold thickness for floating ice H_{ref}, along with a characteristic time scale τ_c over which calving occurs,

$$a_c = \frac{H_{\text{ref}} - H}{\tau_c}. \tag{3.52}$$

The ice sheet also interacts with the bedrock below it by compressing it due to its weight. Subsequent removal of the ice sheet will result in the bedrock uplifting, known as isostasy. The rate and extent of this depends on the properties of the solid Earth. The isostatic component in the experiments was handed by an Elastic Lithosphere-Relaxing Asthenosphere (ELRA) model [16]. While on very long timescales the isostasy has been shown in models to cause oscillations in the volume of Greenland [121], the effect of isostasy in the experiments of this paper is relatively minor.

Atmosphere model REMBO

In the experiment, the surface boundary conditions are handled by the regional parameterized atmosphere model REMBO [98]. REMBO stands for *regional energy-moisture balance orographic model* and is a 2D model of temperature and precipitation over the region of Greenland. The temperature component is handled by an energy balance model, where the incoming energy due to solar radiation is balance with the outgoing temperature-dependent outgoing longwave radiation (OLR) [15, 104]. Due to the large spatial and temporal scale of the system, horizontal transport is dominated by diffusion rather than advection. Since the atmosphere is coupled to the ice sheet, there is also energy gained and released via condensation of water (precipitation) and melting of the ice sheet (evaporation). A universal structure of the atmosphere is assumed, meaning the lapse rate of temperature and moisture with altitude is fixed, and the sea-level temperature can be used to derive the temperature at any altitude. Overall, the energy balance is given as

$$\begin{aligned} c_p \rho_a H_a \frac{\partial T_{\text{sl}}}{\partial t} =& D_T \nabla^2 T_{\text{sl}} + (1-\alpha) S - \left[A + B(T_{\text{sl}} - \gamma z) \right] \\ &+ L_w P_w + L_s P_s - L_s M_s, \end{aligned} \tag{3.53}$$

for the sea-level temperature T_{sl}. The diffusion constant D_T decreases with latitude as well as altitude z to represent weaker atmospheric activity. A portion of the incoming solar radiation S is reflected by the albedo α which depends on the snow cover. The functional form of the OLR, $A+B(T_{\text{sl}}-\gamma z)A$, is empirical [15]. The precipitation P is split into water P_w and snowfall P_s, with respective latent heats of condensation L_w and L_s. The final term, M_s, is the melt rate of the surface of the ice sheet.

The precipitation depends on the amount of moisture in the atmosphere Q, which is handled via a moisture balance equation,

$$\rho_a H_e \frac{\partial Q}{\partial t} = D_Q \nabla^2 Q - P. \tag{3.54}$$

The diffusion constant D_Q also decreases with latitude. The precipitation depends not only on the moisture constant, but also on the surface slope: $P = (1 + k|\nabla z|)(Q/\tau)$ [114]. This is what lends the model its orographic nature. The total precipitation is split into water and snow based on the temperature, being all snow below -7°C and all water above 7°C.

As mentioned earlier, the temperature and precipitation determine the surface mass balance a_s of the ice sheet. Precipitation falls as snow with a thickness h_s which then may freeze into ice, which has a thickness h_i. The snow has a maximum thickness $h_{s,\max} = 5$ metres, beyond which it is converted into ice. The snow also freezes into ice depending on the temperature, given by the freezing rate $r_f(T)$. The snow and ice may instead melt, determined by

the temperature-dependent melt rate M_s. Altogether,

$$\frac{dh_s}{dt} = \begin{cases} P_s - M_s(1-r_f) & \text{if } h_s < h_{s,\max} \\ 0 & \text{if } h_s = h_{s,\max} \end{cases}, \tag{3.55}$$

$$\frac{dh_i}{dt} = \begin{cases} P_s - M_s(1-2r_f) & \text{if } h_s = h_{s,\max} \text{ and } \frac{dh_s}{dt} \geq 0 \\ M_s r_f & \text{if } h_s > 0 \\ \min(P_s - M_s, 0) & \text{if } h_s = 0 \end{cases}. \tag{3.56}$$

The melt rate is calculated using an isolation-temperature method (ITM) [114],

$$M_s = \frac{\Delta t}{\rho_w L_m}[\tau_a(1-\alpha)S + c + \lambda T]. \tag{3.57}$$

The ITM explicitly takes albedo into account, such that highly reflective fresh snow will melt less quickly than older, dirtier snow or ice. The transmissivity τ_a represents the amount of shortwave radiation that penetrates through the atmosphere to the surface and increases with altitude. The parameters c and λ are empirical. Many ice sheet models use the positive degree day (PDD) method to compute the melt rates, which depends on temperature only. The inclusion of the altitude-dependent transmissivity in the ITM provides a stronger coupling to the surface elevation than just the constant lapse rate of the temperature [85].

3.3 Ghost attractors and long-lived transients

A dynamical system experiencing a saddle-node bifurcation can manifest a ghost attractor in phase space for a small parameter regime past the bifurcation point [108]. This ghost attractor manifests as a time bottleneck experienced by the system before before leaving the region in phase space where the bifurcation took place. To see this, use the normal form of the saddle-node bifurcation,

$$\dot{x} = \mu + x^2. \tag{3.58}$$

Since the definition of a saddle-node bifurcation guarantees it can be written in this normal form [55], the result is universal to systems experiencing a saddle-node bifurcation. As the ghost exists beyond the bifurcation point $\mu = 0$, equation 3.58 is solved for $\mu > 0$, $x(0) = x_0$

$$\frac{1}{\sqrt{\mu}} \arctan \frac{x(t)}{\sqrt{\mu}} - \frac{1}{\sqrt{\mu}} \arctan \frac{x_0}{\sqrt{\mu}} = t. \tag{3.59}$$

To experience the bottleneck, a trajectory must be pass through the point where the bifurcation took place, in this case $x = 0$. For example, to go from $x_0 = -1$ to $x(t) = 1$, the time spent is

$$2 \arctan \frac{1}{\sqrt{\mu}} = \sqrt{\mu} t, \tag{3.60}$$

which gives

$$t \sim \frac{1}{\sqrt{\mu}} \tag{3.61}$$

in the limit $\mu \to 0$ from the left since $\arctan(x) \to 0$ faster than $\sqrt{x} \to 0$. This bottleneck is a generic feature of the equilibrium system, requiring only a that system is initialized near the bifurcation point on the x axis and must pass through it – the ghost exists even for a fixed parameter value. Simultaneously, it is immediately clear that any transient simulation of a system will not be able to properly capture the bifurcation point, even by a very slow variation of the parameter, since the time a system to tip goes to infinity as the parameter approaches the bifurcation value. This is not problem in climate applications however, as identification of the exact bifurcation value is typically unimportant. Due to the chaotic nature of the climate systems, a probabilistic view of tipping behaviour is more suitable. Additionally, the bottleneck only occurs in very small parameter regimes, as for larger values of $\sqrt{\mu}$ the value of $x(t) - x_0$ dominates.

In the model study of the manuscript of this chapter, an adaptive quasi-equilibrium function (AQEF) is used to attempt to estimate the tipping value. As discussed in the manuscript, this scheme is not be able to capture the bifurcation value but rather give some upper bound depending on the hyperparameters of the AQEF. These hyperparameters are the maximal rate of forcing increase, the temporally averaged ice sheet mass loss for which the system is considered to be in quasi-equilibrium, and the time span over which this mass loss is averaged. The most important is the maximal rate of forcing increase. Since the ghost bottleneck depends only on the value of the parameter above the bifurcation value, so it is entirely independent of its rate of increase. Nevertheless, because the system achieves only a quasi equilibrium, if the rate is too large the bifurcation point will be overshot by a large amount. Interestingly, in transient hysteresis experiments the faster the parameter value is varied, the less abrupt the tipping appears. This is known as rate-dependent hysteresis [2, 49] and occurs because of the inertia of a system rather than the temporal bottleneck. For a large rate, the system is not able to relax to equilibrium before the parameter increases further [14]. Thus a small rate of forcing increase simultaneously ameliorates the issues of both the saddle-node ghost as well as the rate-dependent hysteresis. Nevertheless it can only give an upper bound for the bifurcation value.

Long transients appear as well in chaotic systems. A chaotic transient is a solution trajectory that remains some time around a chaotic nonattracting set [62]. Due to the invertability of the dynamical system, the chaotic nonattracting set has attracting and repelling manifolds such that it is a chaotic saddle. While this nonattracting set can arise for a variety of reasons, focus will be laid on two in particular. The first is a chaotic transient appearing after a boundary crisis. A boundary crisis is a type of bifurcation whereby a chaotic

set collides with some unstable orbit, creating a chaotic non-attracting set [36]. In this way, it has many parallels with the saddle-node bifurcation. Indeed, the nonattracting set that remains after this boundary crisis is also termed a ghost attractor, and also results in a temporal bottleneck before a trajectory may move to another part of phase space. However, where the saddle-node ghost attractor has a transient lifetime that scales as the reciprocal of a square root (equation 3.61), the lifetime of these chaotic transients are exponentially distributed, with a mean that scales as

$$\langle \tau \rangle \sim (p - p_c)^{-\gamma}, \tag{3.62}$$

where p is the parameter, p_c is the parameter value at which the crisis occurs and $\gamma > 0$ is the *critical parameter*, the value of which depends on the system.

Another appearance of a chaotic non-attracting set for systems that experience bistability is as a chaotic saddle in the basin boundary between two stable attractors [18]. Trajectories that start or land near this basin boundary due to a parameter shift spend some time along the stable manifolds of the saddle before eventually escaping to one of the two attractors. In this case, the lifetime of the saddle scales with the fractal dimension of the chaotic saddle,

$$\langle \tau \rangle \sim [(\lambda_1 (D - D_b)]^{-1} \tag{3.63}$$

where D is the phase space dimension, D_b is the dimension of the chaotic saddle (less than D) and λ_1 is the maximum Lyapunov exponent of the saddle. The closer the chaotic saddle is to full dimension, the longer the mean lifetime. The manuscript describes how the scaling of the chaotic transients observed are indicative of a boundary crisis rather than due to crossing a chaotic saddle due to r-tipping.

3.4 The manuscript

Delay of the collapse of the Greenland ice sheet due to ice stream oscillations

Kolja Kypke [1], Marisa Montoya [2,3], Alexander Robinson [4], Jorge Alvarez-Solas [2,3], and Peter Ditlevsen [1]

[1]Physics of Ice, Climate and Earth, Niels Bohr Institute, University of Copenhagen, Copenhagen, Denmark
[2]Department of Earth Physics and Astrophysics, Complutense University of Madrid, Madrid, Spain
[3]Geosciences Institute, CSIC–UCM, Madrid, Spain
[4]Alfred Wegener Institute, Helmholtz Centre for Polar and Marine Research, Potsdam, Germany

Correspondence: Kolja Kypke (kolja.kypke@nbi.ku.dk)

Abstract. Model simulations of the Greenland ice sheet (GrIS) using a state-of-the-art comprehensive ice sheet model coupled to a regional energy-moisture balance atmospheric model under external forcing in the form of temperature increases are performed. These simulations exhibit oscillations in the total ice sheet volume under global temperature increase magnitudes between 1.0 and 2.0 K above pre-industrial temperatures. These oscillations are isolated to the northwestern drainage basin of the GrIS and are due to two ice streams which alternate between fast and slow basal velocities, manifesting in a build-up/surge variability. Further, these ice streams are interacting due to their spatial proximity, resulting in irregular periodicity. The regions these ice streams appear in is also where the large-scale loss (tipping) of the entire GrIS originates, meaning these oscillations affect the tipping behaviour. As a result of these ice streams, the time it takes before the ice sheet collapses can vary by hundreds of thousands of years among simulation ensemble members. These long tipping times are proposed to be due to chaotic transients, implying the ice stream oscillations are a source of internal chaotic variability in ice sheets.

1 Introduction

Due to the existence of positive feedbacks affecting its mass balance, the present-day Greenland ice sheet (GrIS) is thought to experience a sudden loss of mass when an external forcing parameter is increased beyond a critical threshold, known as *tipping point* and causing tipping of the ice sheet to a largely ice-free state (Robinson et al., 2012). The GrIS is therefore one of the principal tipping elements in the Earth's climate system due to its straightforward impact of raising global sea level as well as the relatively uncomplicated dynamics that underlie the tipping. This is principally due to the fact that the feedbacks that determine the equilibrium state, those of the melt elevation and ice-albedo, are positive and dominate over negative feedbacks such as the glacial-isostatic adjustment.

Nevertheless, the GrIS also displays some features of variability that do not have such simple dynamics and are not so well constrained. These are areas of fast flowing ice, which are either topographically-confined outlet glaciers or large ice streams. The discharge of ice through these contributes a large amount to the total ice sheet mass loss despite their relatively small spatial extent (Shepherd et al., 2020). It has also been shown that they may be accelerating due to increased atmospheric and

oceanic forcing (Krabill et al., 2004; Rignot and Kanagaratnam, 2006; Luthcke et al., 2006; Howat et al., 2008; Holland et al., 2008; Khan et al., 2014; Trusel et al., 2018; Larocca et al., 2023).

Due to the magnitude and tempo of anthropogenic forcing on the climate and the resulting accelerating mass loss of the GrIS, it is worth investigating whether the rate of parameter forcing has an effect on the tipping behaviour. The circumstance of a system tipping before the equilibrium bifurcation value of the forcing parameter is reached when it is increased at a large rate is known as *rate-induced tipping* or *r-tipping* (Ritchie et al., 2023) and is expected to occur in non-autonomous systems, especially those with multiple dynamic time scales (Feudel, 2023). In this study, a state-of-the-art ice sheet model coupled to a regional atmospheric energy-moisture balance model is used to simulate the Greenland ice sheet under varying magnitudes and rates of warming to determine whether r-tipping of the Greenland ice sheet is possible.

2 Methods

2.1 Model description

The model used to study the evolution of the ice sheet is the three-dimensional thermomechanical ice-sheet model Yelmo (Robinson et al., 2020) coupled with the regional energy-moisture balance model REMBO (Robinson et al., 2010). This model setup is therefore similar to that of Robinson et al. (2012) but with an alternate ice sheet model. Yelmo is a depth-integrated viscosity approximation (DIVA) model (Robinson et al., 2022). The domain of the ice-sheet model covers the entirety of Greenland at a 16 km horizontal resolution. The surface mass balance is determined by the temperature and precipitation calculated by REMBO. The surface gains mass as precipitation and loses it through a melt rate calculated using an insolation-temperature melt method, whereby insolation and albedo is explicitly taken into account. Additionally, a heuristic 2 m/day melt rate is applied to areas where in the present day there is no ice. The isostatic adjustment is an elastic lithosphere-relaxing asthenosphere (ELRA) model (Bueler et al., 2007) with a relaxation timescale of 3000 years.

Due to the emphasis on regions of fast-flowing ice, the most important processes in this study are those occurring at the base of the ice sheet. The flow of ice in Yelmo is calculated using the Depth Integrated Viscosity Approximation (DIVA) (Robinson et al., 2022) of the first order Blatter-Pattyn shallow ice equations (Blatter, 1995; Pattyn, 2003),

$$4\frac{\partial}{\partial x}\left(\bar{\eta}\frac{\partial \bar{v}_x}{\partial x}\right)+2\frac{\partial}{\partial x}\left(\bar{\eta}\frac{\partial \bar{v}_y}{\partial y}\right)+\frac{\partial}{\partial y}\left(\bar{\eta}\left[\frac{\partial \bar{v}_x}{\partial y}+\frac{\partial \bar{v}_y}{\partial x}\right]\right)=\rho g H\frac{\partial h}{\partial x}+\tau_{b,x} \tag{1}$$

$$4\frac{\partial}{\partial y}\left(\bar{\eta}\frac{\partial \bar{v}_y}{\partial y}\right)+2\frac{\partial}{\partial y}\left(\bar{\eta}\frac{\partial \bar{v}_x}{\partial x}\right)+\frac{\partial}{\partial x}\left(\bar{\eta}\left[\frac{\partial \bar{v}_x}{\partial y}+\frac{\partial \bar{v}_y}{\partial x}\right]\right)=\rho g H\frac{\partial h}{\partial y}+\tau_{b,y}, \tag{2}$$

where x and y are the two horizontal directions and $\bar{u}$ and $\bar{v}$ the vertically integrated flow velocities in these directions, respectively. The parameter $\bar{\eta}$ is the vertically integrated viscosity, which depends on temperature and velocity, H is the ice thickness and $h(x,y)$ is the vertical surface coordinate of the ice sheet. The basal frictional stress $\tau_b=(\tau_{b,x},\tau_{b,y})$ is modelled using a Weertman sliding law,

$$\tau_b=-c_b\left(\frac{|\mathbf{u}_b|}{\mathbf{u}_b+u_0}\right)^q\frac{|\mathbf{u}_b|}{\mathbf{u}_b}, \tag{3}$$

where $\mathbf{u}_b = (u_b, v_b)$ is the basal velocity vector, u_0 and q are empirical parameters, and c_b is a field defining the bed friction coefficient. The threshold speed $u_0 = 100$ m/yr allows the basal stress to saturate at large velocities, where it becomes independent of basal velocity (Schoof, 2005). The coefficient c_b depends linearly on the effective pressure N_{eff} at the base of the ice,

$$c_b = c_0 + \lambda N_{\text{eff}}, \tag{4}$$

where for a lesser effective pressure the bed friction will similarly be lower, decreasing the basal shear stress and increasing basal velocities. The factor λ represents the till strength of the bedrock and depends on the elevation above or below sea level. This due to the past history of the bedrock, with regions being below sea level having weaker till due to previously being submerged. The effective pressure differs from the overburden pressure depending on the basal water content, following the parameterization of Bueler and van Pelt (2015),

$$\hat{N}_{\text{eff}} = N_0 \left(\frac{\delta P_O}{N_0} \right)^s 10^{\frac{e_0}{C_c}(1-s)}, \tag{5}$$

and where $P_O = \rho_i g H$ is the overburden pressure of the ice, N_0 is a reference pressure, and $s = H_{\text{w}}/H_{\text{w,max}}$. The till water thickness H_w cannot exceed this maximum value $H_{\text{w,max}}$, which is set to 2 metres. For a fully saturated till such that $s = 1$, the effective pressure is minimal, and is equal to δP_O, where δ is 0.2. The coefficients e_0 and C_c are till constants taken from (Tulaczyk et al., 2000). Finally, since the overburden pressure is an upper limit for the effective pressure, the minimum of the two is taken,

$$N_{\text{eff}} = \min \left\{ P_O, \hat{N}_{\text{til}} \right\}. \tag{6}$$

The basal water layer thickness H_w changes with the basal melt rate $\dot{b}_g$ and is removed via a constant drainage rate C_d,

$$\frac{\partial H_w}{\partial t} = -\frac{\rho_i}{\rho_w} \dot{b}_g - C_d \tag{7}$$

In turn, the basal melt rate

$$\dot{b}_g = -\frac{1}{\rho_i L} \left(Q_b + k \frac{\partial T}{\partial z}\bigg|_b + Q_{\text{geo}} \right) \tag{8}$$

depends on warming from basal friction due to sliding Q_b as well as geothermal heat flux Q_{geo}, and is reduced by conduction of heat into the ice sheet above through conduction as determined by the ice temperature gradient at the base. Thus an increased basal velocity will induced additional let at the base, further increasing H_w in a positive feedback.

2.2 Experimental setup

The coupled model is first run to equilibrium to arrive at an initial state from which the model is perturbed. To obtain multiple initial states with small differences, a single simulation is run to 400 kiloyears (kyr), with the state of the ice sheet captured at the 100, 200, 300 and 400 kyr marks. This simulation is seen in Fig 1, with the four initial conditions labelled A, B, C and D.

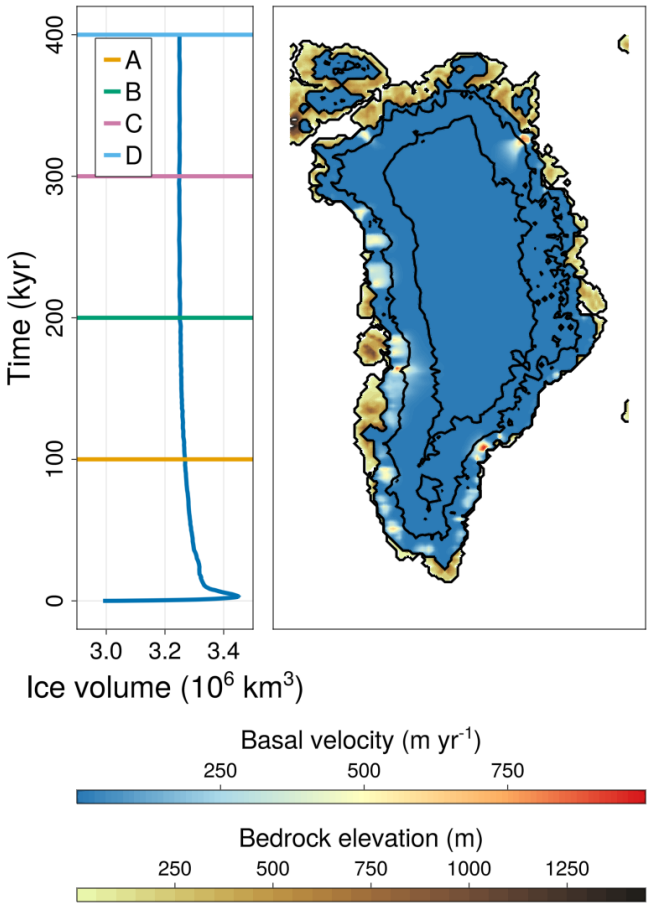

Figure 1. Ice volume time series of the equilibrium simulation for the four initial states A to D (left) and ice sheet extent and ice stream locations of the initial state D (right) with contour lines at 1 km ice thickness.

The forcing in the subsequent experiments is applied as an increase of the summer temperature at seal-level in the atmosphere as well as in the boundary ocean as was done in Robinson et al. (2012). This summer temperature anomaly is approximately equivalent to a global mean temperature increase. To get an estimate of the tipping value, an adaptive quasi-equilibrium function (AQEF) is applied to each of the four initial states. This AQEF increases the forcing small amount, allows the trajectory to relax to near equilibrium, then increases the forcing again. The increase is done in an adaptive way such that the longer it takes the model to equilibrate, the less the forcing is subsequently increased. Using this scheme, the tipping value was found to be around 1.275 K. This will set the range of forcing values investigated, as any forcing at or beyond this value will not be subject to r-tipping.

The values of the forcing parameter thus range from 0.1 to 1.3 K with increments of 0.1K. Additionally, the forcing is applied linearly over some amount of time rather than instantaneously. In this way we examine the effect the rate of increase of the

forcing has on the resultant trajectory. These types of experiments are commonly known as *ramping experiments* as the forcing parameter is ramped up over a period of time. The ramping rates of 0.001, 0.01, and 0.1 K/yr span three orders of magnitude. The ramping experiments are run for 5 kyrs with zero forcing before the ramping is applied, which removes a slight transient. After the forcing has reached its maximum value, it is kept constant and the ice sheet is allowed to evolve to equilibrium.

3 Results

3.1 Tipping of the ice sheet

Figure 2 shows the ice volume in parameter space for the four initial states. There is clear tipping behaviour for a forcing value around 1.3 K. This tipping resembles that of a saddle-node bifurcation. The tipping value for states B, C and D agree quite well, but that of A tips around 1.35 K.

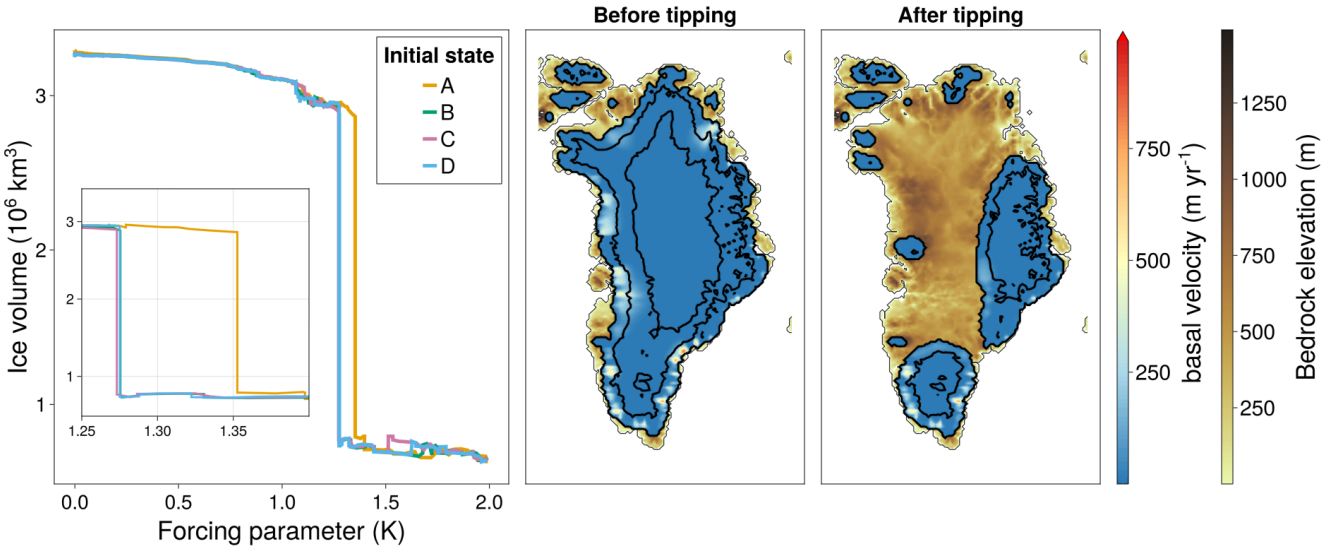

Figure 2. Left: Adaptive quasi-equilibrium function initialised from states A to D in parameter space to estimate the tipping value. Inset: closer look at the parameter range from 1.25 to 1.4 K. Right: ice sheet extent before and after tipping with contour lines at 1 km ice thickness.

3.2 Spatial and temporal behaviour of the oscillations

Figure 3 shows the ice volume time series for the simulations with forcing values of 0.1 to 1.1 K. The simulations with a forcing value of 1.2 K are omitted for visual clarity, but they follow the same variability as the simulations for 1.1 K with eventual tipping to an ice volume of less than 1 million km^3. The colour of the curves for each forcing value represents the rate of forcing, from darkest corresponding to the fastest rate of 0.1 K/yr to the lightest corresponding to the slowest rate of 0.001 K/year. Although the ramping rates vary by a few orders of magnitude, they are still all much faster than the relaxation of the

ice sheet to its equilibrium state and thus there is initially no discernible difference in the trajectories for a given forcing level. Indeed, if the simulation were stopped after 25 kyr, the decrease in ice volume would be very monotonic with respect to the temperature forcing and almost identical for the different forcing rates.

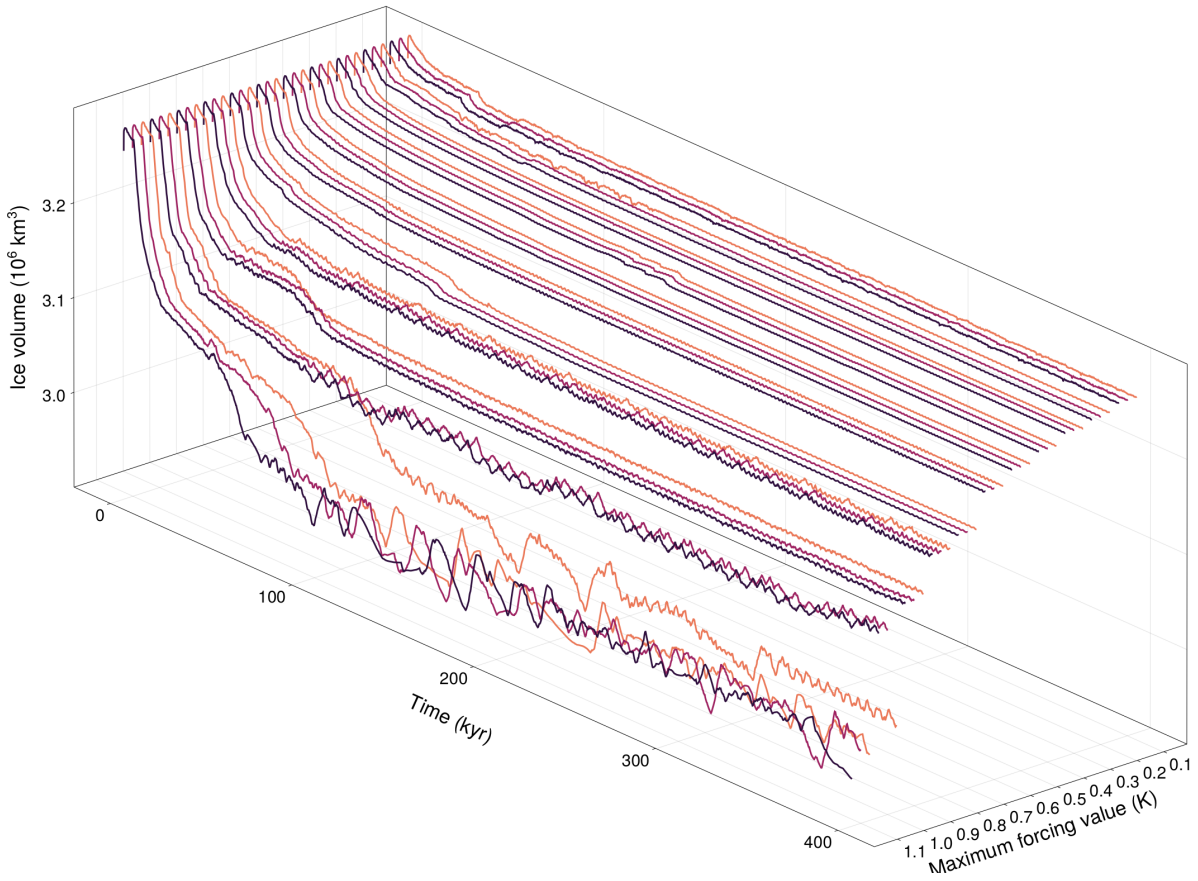

Figure 3. Total ice sheet volumes for forcing from 0.1 to 1.1K for three different rates of forcing: 0.1 K/yr (darkest) to 0.001 K/yr (lightest) for the initial state A.

For warming below 1.0 K there is some slight periodic variability, due to small changes in the volume flux through outlet glaciers. The most striking behaviour appears for the larger values of forcing, 1.0 K and 1.1 K, after about 25 kyr, for which larger amplitude and period oscillations appear. For a forcing of 1.00 K, the oscillations are larger in amplitude and more temporally irregular. Further, for a forcing of 1.05 K, the ice volume is much smaller, and even more variable.

The ice volumes of the individual hydrological drainage basins of Greenland indicate that the source for the variability seen in these large oscillations is primarily in the north-northwest region. The study of the spatial fields is therefore restricted to this area. The spatial extent of the ice sheet in the case of a simulation displaying the larger, irregular oscillations (forcing of 1.05 K) compared to one with the smaller, more regular ones (forcing of 1.00 K) is shown in Fig. 4. The first difference

to be seen is in the extent of the ice sheet in this region. For a forcing of 1.00 K, the ice-sheet margin is such that both areas of large basal velocity, the ice streams, are marine-terminating, termed the 'unretreated' configuration. These ice streams approximately correspond to the Humboldt and Petermann glaciers. The spatial extent of the ice sheet in this case shall be termed the 'unretreated' configuration. In the simulation with a forcing of 1.05 K, the ice sheet extent is much reduced. From the mean ice thickness profiles, the ice margin is almost 100 km further inland. The Humboldt glacier ice stream is no longer connected to the ocean, although the Petermann glacier ice stream still terminates at the Petermann fjord. We refer to this as the 'retreated' configuration.

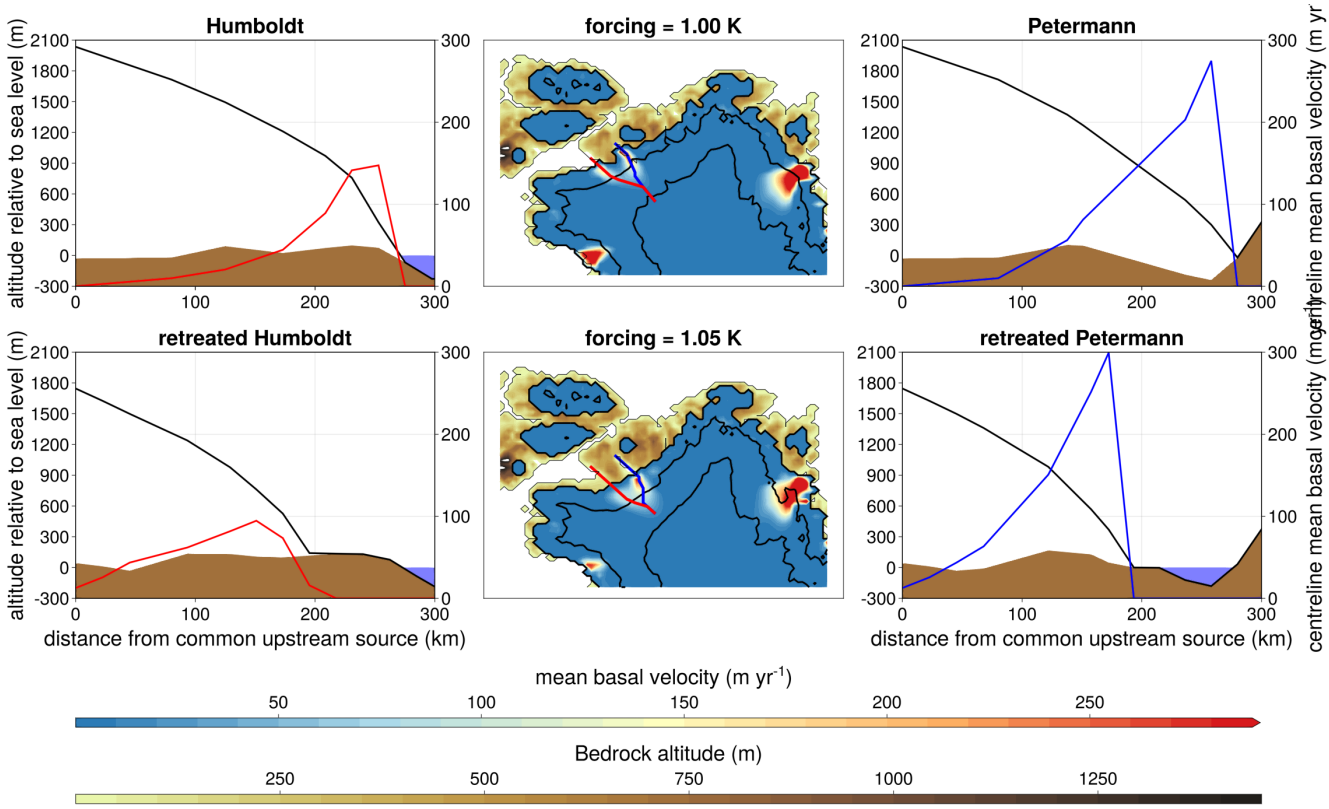

Figure 4. Time-averaged basal velocity field as well as mean ice thickness and basal velocity profiles along the ice stream centreline for the unretreated (top) and retreated (bottom) configurations. The red and blue lines in the middle panels designate the centrelines of the Humboldt and Petermann ice streams respectively.

The temporal behaviour of the two configurations is compared by taking the spatial mean in a small box that contains the Petermann and Humboldt glaciers in the retreated and unretreated configurations and plotted in Fig. 5. For the unretreated case, the basal velocities in the ice streams behave quite differently. The Petermann ice stream is in a state of steady flow of around 100 m/yr. This is facilitated by a till that is close to saturated. The Humboldt alternates between near zero basal movement and sliding velocities of 100 m/yr. The periods of stagnation are due to a refreezing of the till under the ice, evinced by a reduction

in the mean basal water layer thickness. While the basal velocities are minimal, the ice thickness increases, establishing a 'build up' phase. The subsequent loss of mass due to rapid ice streaming is a 'surge' phase. The period of these oscillations switches between approximately 5 and 9 kyr. This steady cycle of mass gain during the build-up phase and loss during the surge results in a change in ice thickness between 300 and 500 metres. The Petermann also shows a change in ice thickness with the temporal same pattern while maintaining constant ice stream flow, suggesting the thickness variations are synchronized with the nearby Humboldt.

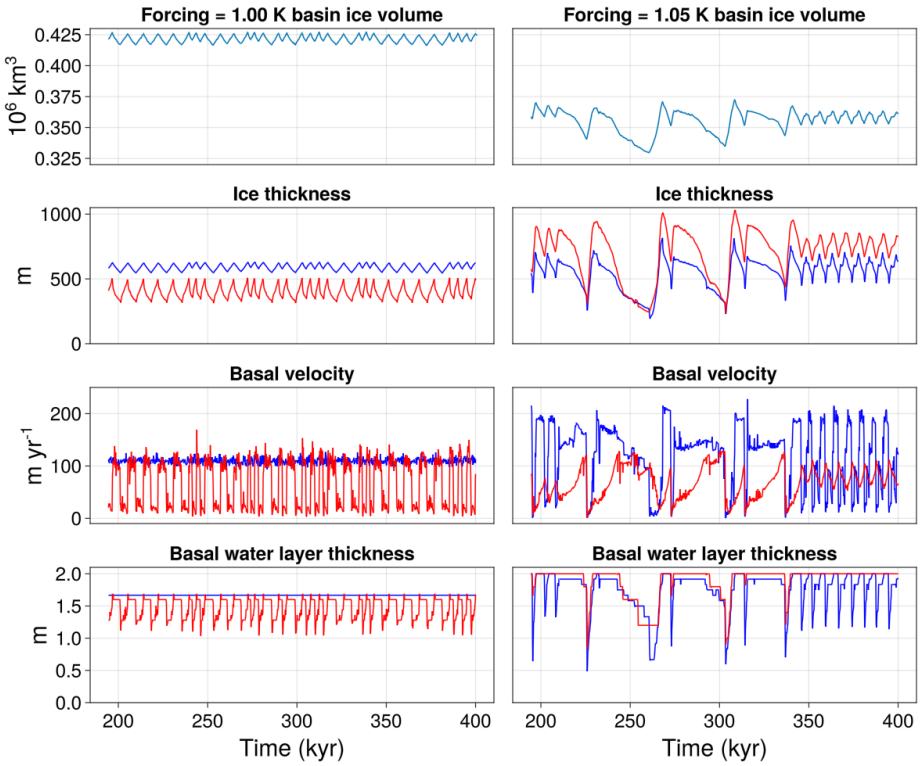

Figure 5. Time series of basin ice volume, mean ice thickness, basal velocity, and basal water content in rP (blue) and rH (red) in the unretreated (left) and retreated (right) configurations.

In the retreated configuration the ice thicknesses and basal velocities are closer in magnitude and the oscillations have larger amplitude and periodicity as mentioned previously. The temporal variables of the remnants of the two ice streams are plotted, here designated the 'retreated Petermann' (rP) and the 'retreated Humboldt' (rH). While the exact location of these points differs slightly for the different simulations, the existence of the two are robust in all the simulations exhibiting the oscillations. In the retreated configuration, the rP is no longer in a steady flow state, with occasional refreezing of the basal till.

Two broad patterns for the oscillations in the retreated configuration emerge. The first is that of short oscillations with a period of around 8 kyr, such as seen at the end of the time series in the left hand side of Fig. 5. The basal velocity in rP abruptly

switches between maximal and minimal, with corresponding drops in basal water layer thickness when the velocity is near zero. In the rH, the till remains saturated, but the flow is not steady. It is increasing during the surge and decreasing during the buildup. The magnitude of this variation is not so large, around10s of m/yr in the spatial mean. This is an order of magnitude less than that of the build-up and surges. In the other pattern, the period is much longer, and the shape of the build-up and surge is asymmetric. While the basal velocity in rP switches abruptly between the build-up and surge phases, the increase in the rH is gradual. This slows the mass loss until a point where the till rapidly refreezes in both ice streams.

Due to the constant saturation of the till in rH during the short oscillations, the changes in basal velocities are rather due to the changes in ice thickness, which are induced by the large build-up and surges in rP. In this manner, the distinguishing factor between the two patterns is that in the short oscillations, rP is in a build-up/surge mode and rH is in a near steady flow mode. In the longer period case, both are in the build-up/surge mode, with more gradual surge in rH. In between the oscillations there is occasionally a period where both rH and rP are in a steady flow state with an associated minimum in the ice volume which may last tens of thousands of years.

3.3 Forcing values beyond 1.05 K

To get a better idea of the tipping behaviour, two slower ramping rates of 1e-4 and 1e-5 K/yr are introduced. The values of the forcing parameter investigated are also increased in resolution, ranging from 1.0K to 1.3 K with increments of 0.05K. For the simulations forced to values above 1.05 K, tipping behaviour is observed. Figure 6 shows time series of simulations for forcing values of 1.05 to 1.30 K. Again, there are three different initial states with four rates of warming for each. The most prominent feature in this case is the seemingly random tipping times, depending neither on the magnitude of the warming nor on the rate.

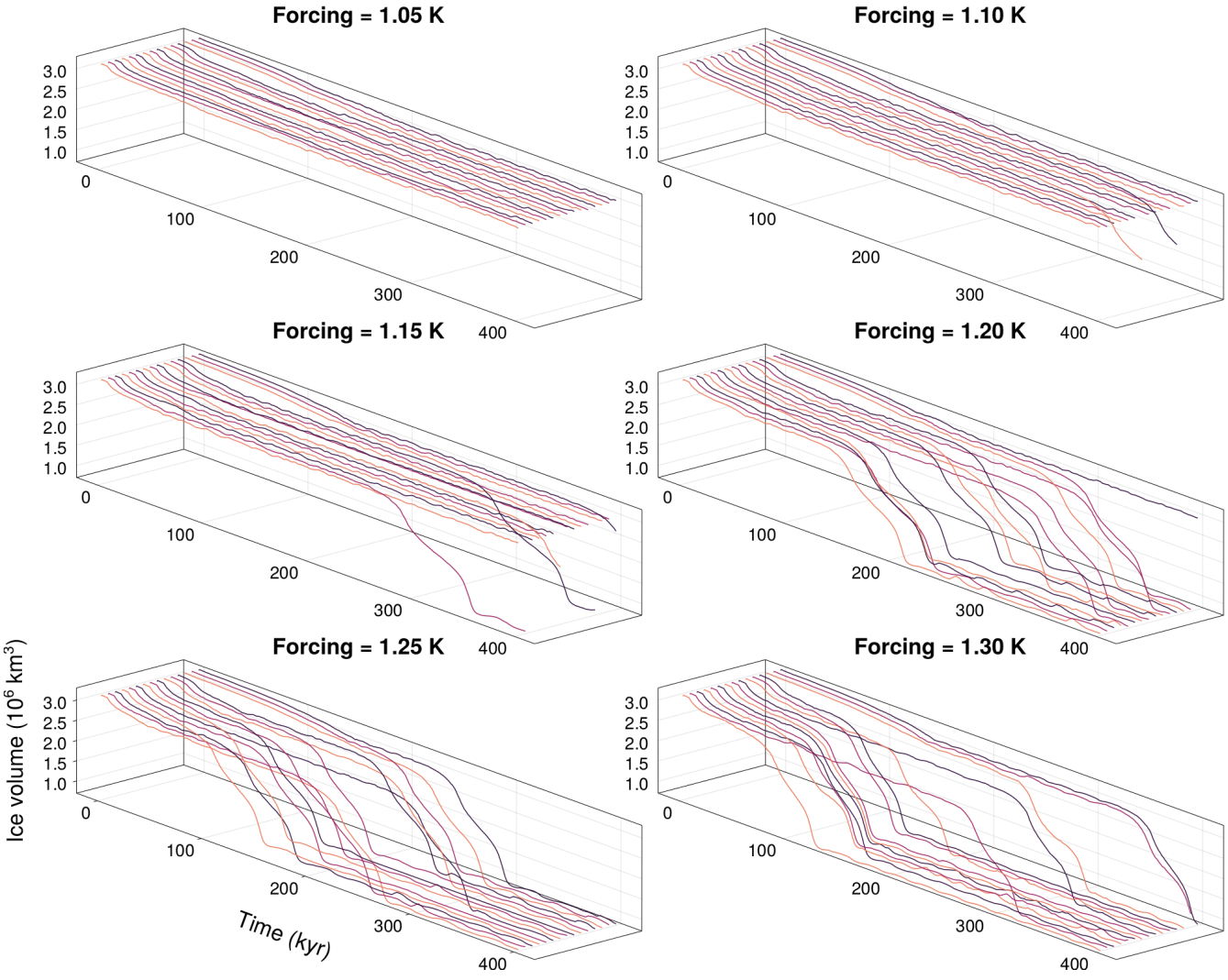

Figure 6. Time series of the ice sheet volume for different forcing values, warming rates, and initial conditions B - D.

Spatially, the retreat of the ice sheet begins primarily in the northern region. This is contrary to ice sheet mass loss patterns of other ice sheet studies, for example Bochow et al. (2023), where mass loss also occurs in the southwest of Greenland. Due to the similarities in the model setups between this study and that of Robinson et al. (2012), the spatial tipping pattern is equivalent. The pattern of ice-sheet loss also looks similar to that of Zeitz et al. (2022) (their Fig. 3a) albeit without the regrowth of the ice sheet. Due to the ice sheet mass loss occurring initially in the region where the oscillations are, they invariably have an effect on the overall tipping behaviour.

3.4 Removal of the unpredictability

As a test to see whether the oscillating ice streams does have an effect on the tipping of the ice sheet, the mechanism responsible is isolated. As described previously, the ice stream oscillations are surges in the basal velocity of the ice stream due to the thermomechanical coupling at the base of the ice sheet. To remove the oscillations but maintain the ice stream, the basal velocities in the region of interest need to be lower but non zero. For lower basal velocities, the mass lost due to streaming is closer to the accumulation rate, bringing the ice stream to a steady flow state (Robel et al., 2013). To achieve this, the value of δ in equation 5 is increased. This raises the minimal effective pressure (Bueler and van Pelt, 2015) which increases the basal frictional stress when the till water layer thickness is maximal. Simulations performed with a value of $\delta = 0.10$ from initial condition B for three forcing values around the tipping point at two rates each are seen in Fig. 7. As this value effects ice streams across the entire ice sheet, the tipping point is different. Specifically, the tipping point is larger as δ increases as the ice sheet loses less mass dynamically due to lower ice stream velocities.

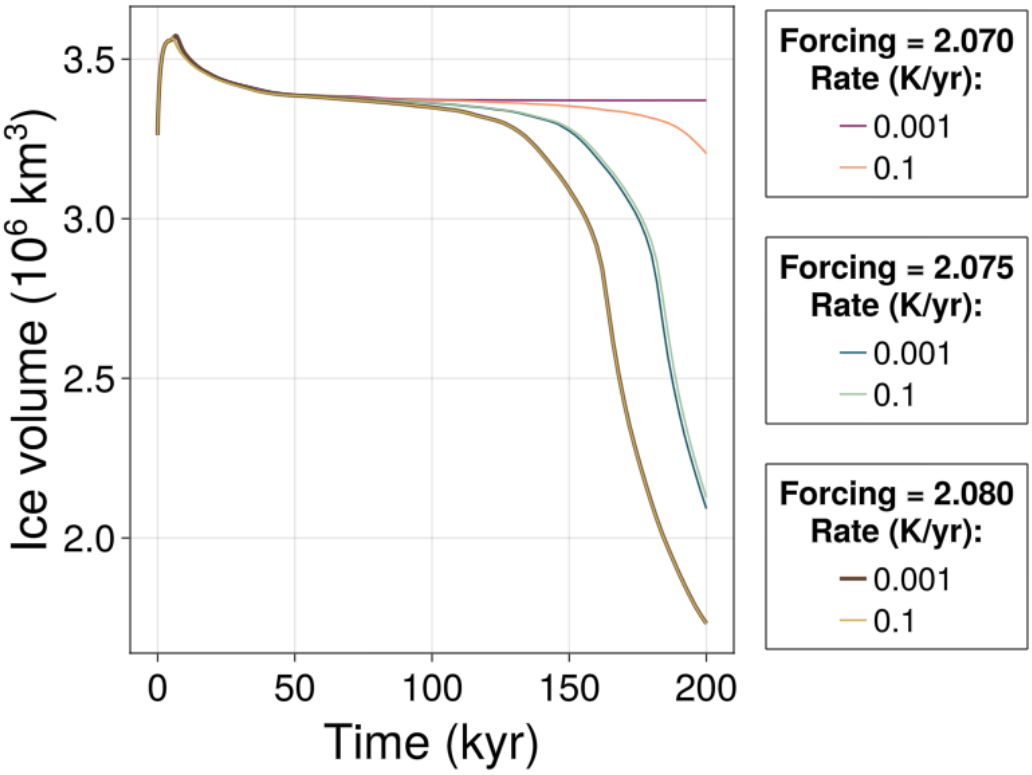

Figure 7. Time series of the ice sheet volume with $\delta = 0.1$.

4 Discussion

4.1 Tipping of the GrIS

The predominant source of mass loss of the GrIS in the present day is still under contention. Accelerating mass loss is typically seen in marine-terminating outlet glaciers due to their sensitivity to oceanic forcing (Krabill et al., 2004; Rignot and Kanagaratnam, 2006; Howat et al., 2008). However, they are topographically confined which might limit their impact under greater forcing ((Joughin et al., 2010). For this reason, future loss due to negative surface mass balance forced by increasing atmospheric temperatures might outweigh that of ice sheet dynamics (Enderlin et al., 2014; Bevis et al., 2019). The ice extent before and after the tipping in Fig. 2 indicates that the mass loss does not start in regions with a lot of marine-terminating outlet glaciers, specifically the southeast Van Den Broeke et al. (2009). In fact, many remain after the tipping has completed. This indicates the importance of oceanic forcing on r-tipping the GrIS is not important.

4.2 Ice stream oscillations

Here we find the appearance of millennial scale periodic oscillations of the ice volume which are unrelated to the isostatic adjustment. Ice streams do not only represent a drain for rapid mass loss in ice sheets, but also are a source of internal periodic variability. Periodic behaviour of ice masses can be seen in glaciers, which are typically confined to some topographical valley and/or have a basal slope, see for example Budd (1975); Kamb et al. (1985); Clarke (1987). Their reduced spatial extent implies that their periodic behaviour is on a much shorter time scale of decades to centuries and thus directly observable. It has been shown in models that ice sheets and ice streams, similar to valley glaciers, can also exhibit oscillatory behaviour under the right conditions. These larger-scale oscillations were first proposed as Heinrich events (HE) during the last glacial period (Heinrich, 1988; Broecker et al., 1992; MacAyeal, 1993) However, HE might be triggered instead to external forcing (Alvarez-Solas et al., 2013).

Studies of oscillatory behaviour in ice sheets include parameterized models (Oerlemans, 1983; Fowler and Johnson, 1995; Payne, 1995; Robel et al., 2013) and comprehensive ice sheet models with both idealized geometries (Calov et al., 2010; Van Pelt and Oerlemans, 2012; Feldmann and Levermann, 2017) and realistic topographies (Papa et al., 2006; Roberts et al., 2016; Schannwell et al., 2023). Additionally, some studies include a coupling to additional components of the climate system (Calov et al., 2002; Ziemen et al., 2019). Common to ice-sheet model simulations of the Laurentide ice sheet are oscillations in ice sheet volume that sometimes show quasiperiodicity or seemingly chaotic behaviour. It would be expected that due to the large spatial extent of the system and the complex basal topography that the oscillations would not have a near-constant period. Even in the idealised geometry of Calov et al. (2010) there is spontaneous spatial asymmetry that leads to inconsistent oscillation frequency. Such irregular variability is of especial importance when studying the tipping behaviour of a system.

4.3 Effect of oscillations on tipping

Figure 6 displays the trajectories of simulations forced close to the tipping point. What is most striking about these simulations is that the time a trajectory takes to begin to tip to the ice-free state can vary by over 100 kyr, and this *tipping time* occurs seemingly randomly. Indeed, there is a marked decrease in the mean tipping time of the ensemble of simulations as the forcing value is increased, but there are trajectories for a forcing of 1.20 K that tip 100 kyr before a trajectory of 1.30 K. Additionally, the tipping time is also independent of the rate of the forcing, so clear there is no critical forcing rate for which r-tipping occurs.

What appears to be occurring is that simulations forced to or beyond 1.10 K enter the retreated spatial configuration, wherein the ice sheet oscillates in volume, before potentially collapsing to an ice-free state. All of the simulations that collapse to so from this oscillatory regime, implying it is inextricably linked to the tipping behaviour. When considering just the final state at the end of the 400 kyr simulation, some trajectories for forcing values of 1.10 and 1.15K tip, whereas virtually all simulations forced beyond these values tip. This might suggest there is a tipping point between 1.15 and 1.20 K, and that some runs which are forced to values below this tip due to rate-induced effects, albeit non-monotonically with rate. However, this r-tipping framework does not explain why almost all of the simulations that do tip do so at drastically different times. Rather, it is important to consider the transient rather than just the asymptotic behaviour.

Long transients occurring before a tipping point are generic to these systems. However, these transients generally have an associated scaling law that relates the transient *lifetime* (i.e. the time before tipping occurs) and the magnitude of the forcing past the bifurcation point (Strogatz, 1994). In this case, it would be expected for all the trajectories for a given forcing value that tip to do so at approximately the same time. There may be some slight differences due to the large dimension of the system, but these would likely not be on the order of tens or even hundred of kiloyears.

Systems where long transients have lifetimes of indeterminate length are ones which experience chaotic variability and are called *chaotic transients* (Lai and Tél, 2011). Specifically, the lifetime of any chaotic transient depends sensitively on its initial condition, but the lifetimes of an ensemble are exponentially distributed. These chaotic transient come about due to the existence of chaotic non-attracting sets, which can appear in one of two ways in our system: Firstly, a chaotic attractor that undergoes a crisis (Grebogi et al., 1982), which is effectively a bifurcation for a chaotic system, can leave behind a *ghost attractor*. A trajectory that is forced beyond this crisis parameter value will remain around the ghost attractor for some time before eventually tipping, causing the chaotic transient. Secondly, the saddle manifold between the ice-free and ice-covered stable states, sometimes called an edge or melancholia state Lucarini and Bódai (2017), might be chaotic itself and a trajectory that experiences an r-tipping through this saddle has a chaotic transient. These two different ways in which chaotic transients can manifest have different scaling laws for their mean lifetimes (Mehling et al., 2024). For chaotic transients after an attractor crisis, the relationship between the mean transient lifetime τ and the forcing parameter value p is (Grebogi et al., 1986)

$$\langle \tau \rangle \sim |p - p_c|^{-\gamma}, \tag{9}$$

where p_c is the parameter value where the attractor crisis occurs, and $\gamma > 0$ is the *critical exponent* that is unique to the system. This scaling is only relevant for forcing values very slightly past the tipping point, as the mean lifetime approaches zero very quickly if $p - p_c$ is large. As the mean transient lifetime for forcing values at or above 1.20 K decreases as the forcing value

is increased, it is expected that the chaotic transients are due to an attractor crisis rather than crossing a chaotic saddle. In the case of forcing values of 1.10 and 1.15 K, the mean lifetime may be longer than the 400 kyr simulation period, explaining why not all of these simulations tip.

4.4 Transient lifetime for a forcing value of 1.05 K

The state of the system at a forcing level of 1.05 K is of interest since it is on the boundary between more predictable patterns and the irregular oscillations of the chaotic transients. None of the simulations at this forcing value tipped to an ice free state after 400 kyr of model time, but their time series look very similar to those that do tip. In this parameter range, the system may either be on a chaotic attractor or otherwise a chaotic transient with a lifetime much longer than 400 kyr. Using the mean lifetime of the simulations that tip to an ice free state and assuming that they are chaotic transients, the critical exponent can be estimated. While there are only 12 simulations at these forcing levels, using a maximum likelihood estimation to fit them to an exponential distribution results in a critical exponent γ in equation 9 of around 9.959. Using this, the mean lifetime for a forcing value is around 511 kyrs, which is indeed larger than the 400 kyr simulation run time. A few additional simulations at this forcing level were done going to 1 myr. None of these simulations tip, suggesting that they are not chaotic transients and the system is on a chaotic attractor at this parameter value. They may be supertransients, which are chaotic transients that have an even longer mean lifetime that scales with system size as well Lai and Tél (2011). Changing, for example, the resolution of the model would increase the system size, increasing the transient lifetimes. Since this does not reflect the physical reality, it is an undesired quality. Roberts et al. (2016) observed that the behaviour of the ice stream oscillations of the Laurentide ice sheet in a comprehensive ice sheet model do not qualitatively change as the resolution is increased, supporting the idea that they are not supertransients due to the spatial dimension of the numerical model.

Lohmann and Ditlevsen (2021) use similar methodology to this study, wherein the Atlantic meridional overturning circulation (AMOC) was forced at different rates in an ocean model. While there is a clear rate of forcing below which tipping does not occur, at rates faster than 150 years there is irregular behaviour in the tipping probabilities and tipping times. Due to the understanding that this is rate-induced behaviour as the tipping parameter value is not being crossed, the fact that some runs tip and some do not is due to the basin of attraction of the stable 'AMOC on' state is riddled with the fractal basin boundary of the chaotic saddle. What is clear for the simulations of this study is that all of the trajectories beyond a forcing value of 1.20 K eventually tip. This suggests not only that partial tipping does not occur, but also that there is no riddled basin boundary in this parameter regime. Further, the scaling of the tipping times of the tipping simulations for parameter values less than this is on a similar order of magnitude. As demonstrated in Mehling et al. (2024), the transient lifetime associated with a ghost attractor can be magnitudes larger than that associated with the lifetime of the chaotic saddle. While this indeed only describes the lifetime when starting on the saddle and not crossing it, the spatial and temporal similarities of the trajectories displaying oscillations implies that those with forcing between 1.05 and 1.20 K share a chaotic non-attracting set with those of forcing equal to and greater than 1.20 K. Similarly, we see that the scaling of the transient lifetime suggests the bifurcation point has been crossed. Mehling et al. (2024) show the lifetime of the chaotic saddle increases as the bifurcation point is neared from

the left. This is the reverse of the scaling due to a boundary crisis, where the lifetime increases as the bifurcation point is approached from the right.

4.5 Removal of the unpredictability

Removing the oscillatory mode by increasing δ makes the tipping more predictable. For forcing values of 2.075 and 2.080 K, the tipping occurs at approximately the same time for both the fast and slow rates of forcing increase. This is in contrast to the simulations with the oscillations, where the tipping at a given forcing value can vary by tens to hundreds of millennia, and corroborates the hypothesis that the oscillations cause the delay in tipping. For a forcing value of 2.070, the simulation forced at a fast rate of 0.1 K/year tips, whereas it does not for a slow rate of 0.001 K/year, suggesting rate-induced tipping.

Increasing δ also reveals some interesting interplay between the parameterization that allows for the oscillations and the tipping. As increasing δ decreases the ice stream velocity, the ice sheet loses less mass dynamically and thus the tipping value increases. For a slowly increasing external forcing, the tipping now may occur much later, depending on the rate. However, the tipping is now no longer delayed by the oscillations. Since the lifetime of the transients can be upwards of 100 kyrs, it may be the case that the tipping occurs later for a lower forcing value. Thus the oscillations simultaneously serve to lower the value of the tipping point as well as increase the time before tipping occurs.

4.6 Intermediate tipping

Within the simulation ensemble, there are a few anomalous runs that do not behave as expected. There are two such types: for a forcing level of 1.00 K, which is generally in the unretreated configuration, some simulations end up in the retreated configuration with ice volume variability similar to but slightly smaller in magnitude than those of larger forcing values as seen in Fig. 8. This might suggest the chaotic attractor associated with the ice stream oscillations also exists for lesser forcing values, albeit with a smaller basin of attraction. Secondly, there is a simulation with a forcing value of 1.15 K which remains in the unretreated configuration. That is, for larger forcing values the less chaotic attractor remains at a diminished size. This represents a complication in the analysis, since this parameter value is assumed to be already in the monostable, ice-free state. In this case, the structure of the attractors may be that there is intermediate tipping (Lohmann et al., 2024). The picture would be that around a forcing value of 1.00 K, there are two attractors for the ice-covered state, corresponding to the retreated and unretreated configurations. The attractor for the retreated configuration experiences a boundary crisis between 1.05 and 1.10 K, with corresponding chaotic transients remaining on the associated ghost attractor. On the other hand, the attractor of the unretreated configuration experiences a bifurcation at a forcing value slightly larger than 1.15 K. This scenario could then have r-tipping onto either the unretreated or retreated configurations, the latter of which experiences an earlier tipping to an ice-free state, resulting in an indirect r-tipping to the ice-free state. The basin boundary between the two ice-covered attractors could be fractal which leads to nearby initial conditions approaching one or the other (McDonald et al., 1985).

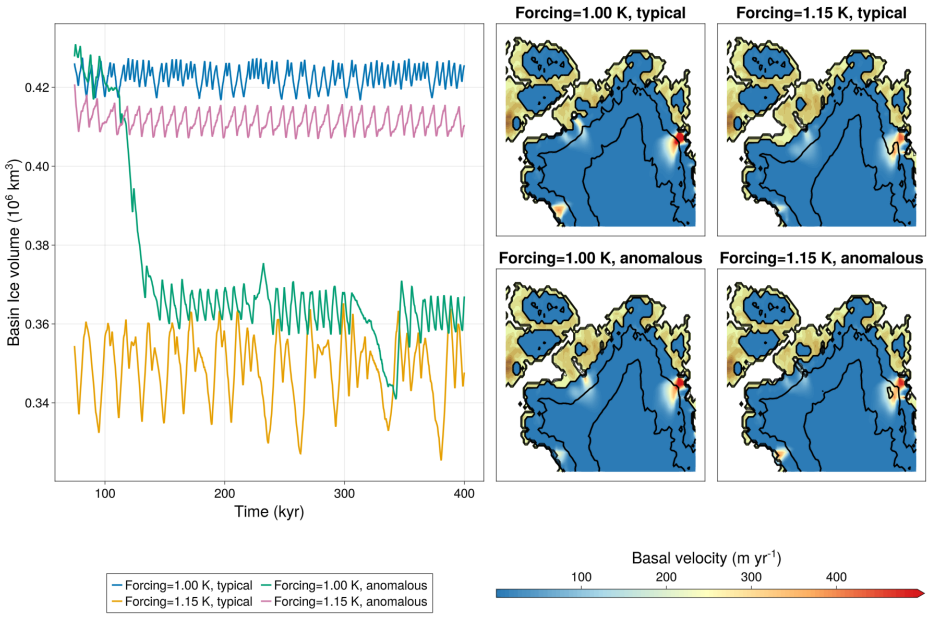

Figure 8. Time series (left) and mean ice thickness and basal velocity fields (right) for typical and anomalous model trajectories.

5 Conclusion

We have demonstrated the existence of oscillations of ice streams in the present-day GrIS under moderate seal-level temperature forcing in a comprehensive ice sheet model, which occur due to thermomechanical coupling at the base of the ice. These oscillations appear for a retreated configuration of the Petermann and Humboldt glaciers. As the tipping of the ice sheet is in the region where these ice streams are found, they delay the tipping of the ice sheet to an ice-free state, with a longer delay for smaller forcing values past a threshold. That is, the chaotic attractor corresponding to the oscillations is generated between a forcing value of 1.0 and 1.05 K. It then experiences a boundary crisis between 1.05 and 1.1K, whereafter the ghost of this attractor is a chaotic non-attracting set generating chaotic transients that tip after some indeterminate amount of time. This delay in the tipping obscures whether the GrIS is susceptible to r-tipping, since chaotic transients can also occur as a result of crossing a chaotic saddle. However, scaling of their lifetimes as well as removal of the oscillatory mechanism indicates they are rather due to a bifurcation-induced tipping.

The conclusions are limited by the amounts and types of simulations conducted. A full investigation of the phase space and the basins of attraction in the parameter range around the tipping would give a much clearer picture on when the tipping may occur, or if there are multiple, closer steady states before a larger tipping. Additionally, an edge-tracking algorithm (Lucarini and Bódai, 2017; Mehling et al., 2024) can be used to approximate the chaotic non-attracting set, even for a ghost attractor. This can be used to identify whether it is such a ghost attractor or else a chaotic saddle. In connection with other elements of the climate system, the oscillations themselves on a shorter time scale are worth studying. For example, they may represent a peri-

odic freshwater forcing condition on the Atlantic Meridional Overturning Circulation. Considering the retreated configuration where oscillations occur as a different state, r-tipping onto this attractor may be investigated.

The implications of chaotic transients on anthropogenic climate change in this context is phenomenological rather than directly relevant due to the long time scales. The chaotic transients demonstrate that a system, in this case the GrIS, may appear to be on a stable ice-covered attractor. However, the tipping to an ice-free state does eventually happen even if the forcing parameter is kept constant, as the tipping point had been crossed a long time ago - the 'safe' parameter space to prevent tipping is actually smaller than originally believed. On the other hand, these long transients allow for overshooting of the tipping point, after which the forcing parameter may still be reduced to prevent the tipping (Bochow et al., 2023).

References

Alvarez-Solas, J., Robinson, A., Montoya, M., and Ritz, C.: Iceberg discharges of the last glacial period driven by oceanic circulation changes, Proceedings of the National Academy of Sciences, 110, 16 350–16 354, https://doi.org/10.1073/pnas.1306622110, 2013.

Bevis, M., Harig, C., Khan, S. A., Brown, A., Simons, F. J., Willis, M., Fettweis, X., Van Den Broeke, M. R., Madsen, F. B., Kendrick, E., Caccamise, D. J., Van Dam, T., Knudsen, P., and Nylen, T.: Accelerating changes in ice mass within Greenland, and the ice sheet's sensitivity to atmospheric forcing, Proceedings of the National Academy of Sciences, 116, 1934–1939, https://doi.org/10.1073/pnas.1806562116, 2019.

Blatter, H.: Velocity and stress fields in grounded glaciers: a simple algorithm for including deviatoric stress gradients, Journal of Glaciology, 41, 333–344, https://doi.org/10.3189/S002214300001621X, 1995.

Bochow, N., Poltronieri, A., Robinson, A., Montoya, M., Rypdal, M., and Boers, N.: Overshooting the critical threshold for the Greenland ice sheet, Nature, 622, 528–536, https://doi.org/10.1038/s41586-023-06503-9, number: 7983 Publisher: Nature Publishing Group, 2023.

Broecker, W., Bond, G., Klas, M., Clark, E., and McManus, J.: Origin of the northern Atlantic's Heinrich events, Climate Dynamics, 6, 265–273, https://doi.org/10.1007/BF00193540, 1992.

Budd, W. F.: A First Simple Model for Periodically Self-Surging Glaciers, Journal of Glaciology, 14, 3–21, https://doi.org/10.3189/S0022143000013344, 1975.

Bueler, E. and van Pelt, W.: Mass-conserving subglacial hydrology in the Parallel Ice Sheet Model version 0.6, Geoscientific Model Development, 8, 1613–1635, https://doi.org/10.5194/gmd-8-1613-2015, publisher: Copernicus GmbH, 2015.

Bueler, E., Lingle, C. S., and Brown, J.: Fast computation of a viscoelastic deformable Earth model for ice-sheet simulations, Annals of Glaciology, 46, 97–105, https://doi.org/10.3189/172756407782871567, 2007.

Calov, R., Ganopolski, A., Petoukhov, V., Claussen, M., and Greve, R.: Large-scale instabilities of the Laurentide ice sheet simulated in a fully coupled climate-system model, Geophysical Research Letters, 29, https://doi.org/10.1029/2002GL016078, 2002.

Calov, R., Greve, R., Abe-Ouchi, A., Bueler, E., Huybrechts, P., Johnson, J. V., Pattyn, F., Pollard, D., Ritz, C., Saito, F., and Tarasov, L.: Results from the Ice-Sheet Model Intercomparison Project–Heinrich Event Intercomparison (ISMIP HEINO), Journal of Glaciology, 56, 371–383, https://doi.org/10.3189/002214310792447789, 2010.

Clarke, G. K. C.: Fast glacier flow: Ice streams, surging, and tidewater glaciers, Journal of Geophysical Research: Solid Earth, 92, 8835–8841, https://doi.org/10.1029/JB092iB09p08835, 1987.

Enderlin, E. M., Howat, I. M., Jeong, S., Noh, M.-J., van Angelen, J. H., and van den Broeke, M. R.: An improved mass budget for the Greenland ice sheet, Geophysical Research Letters, 41, 866–872, https://doi.org/10.1002/2013GL059010, _eprint: https://onlinelibrary.wiley.com/doi/pdf/10.1002/2013GL059010, 2014.

Feldmann, J. and Levermann, A.: From cyclic ice streaming to Heinrich-like events: the grow-and-surge instability in the Parallel Ice Sheet Model, The Cryosphere, 11, 1913–1932, https://doi.org/10.5194/tc-11-1913-2017, publisher: Copernicus GmbH, 2017.

Feudel, U.: Rate-induced tipping in ecosystems and climate: the role of unstable states, basin boundaries and transient dynamics, Nonlinear Processes in Geophysics, 30, 481–502, https://doi.org/10.5194/npg-30-481-2023, publisher: Copernicus GmbH, 2023.

Fowler, A. C. and Johnson, C.: Hydraulic run-away: a mechanism for thermally regulated surges of ice sheets, Journal of Glaciology, 41, 554–561, https://doi.org/10.3189/S002214300003478X, 1995.

Grebogi, C., Ott, E., and Yorke, J. A.: Chaotic Attractors in Crisis, Physical Review Letters, 48, 1507–1510, https://doi.org/10.1103/PhysRevLett.48.1507, publisher: American Physical Society, 1982.

Grebogi, C., Ott, E., and Yorke, J. A.: Critical Exponent of Chaotic Transients in Nonlinear Dynamical Systems, Physical Review Letters, 57, 1284–1287, https://doi.org/10.1103/PhysRevLett.57.1284, publisher: American Physical Society, 1986.

Heinrich, H.: Origin and Consequences of Cyclic Ice Rafting in the Northeast Atlantic Ocean During the Past 130,000 Years, Quaternary Research, 29, 142–152, https://doi.org/10.1016/0033-5894(88)90057-9, 1988.

Holland, D. M., Thomas, R. H., de Young, B., Ribergaard, M. H., and Lyberth, B.: Acceleration of Jakobshavn Isbræ triggered by warm subsurface ocean waters, Nature Geoscience, 1, 659–664, https://doi.org/10.1038/ngeo316, publisher: Nature Publishing Group, 2008.

Howat, I. M., Joughin, I., Fahnestock, M., Smith, B. E., and Scambos, T. A.: Synchronous retreat and acceleration of southeast Greenland outlet glaciers 2000–06: ice dynamics and coupling to climate, Journal of Glaciology, 54, 646–660, https://doi.org/10.3189/002214308786570908, 2008.

Joughin, I., Smith, B. E., Howat, I. M., Scambos, T., and Moon, T.: Greenland flow variability from ice-sheet-wide velocity mapping, Journal of Glaciology, 56, 415–430, https://doi.org/10.3189/002214310792447734, 2010.

Kamb, B., Raymond, C. F., Harrison, W. D., Engelhardt, H., Echelmeyer, K. A., Humphrey, N., Brugman, M. M., and Pfeffer, T.: Glacier Surge Mechanism: 1982-1983 Surge of Variegated Glacier, Alaska, Science, New Series, 227, 469–479, http://www.jstor.org/stable/1694144, 1985.

Khan, S. A., Kjær, K. H., Bevis, M., Bamber, J. L., Wahr, J., Kjeldsen, K. K., Bjørk, A. A., Korsgaard, N. J., Stearns, L. A., Van Den Broeke, M. R., Liu, L., Larsen, N. K., and Muresan, I. S.: Sustained mass loss of the northeast Greenland ice sheet triggered by regional warming, Nature Climate Change, 4, 292–299, https://doi.org/10.1038/nclimate2161, 2014.

Krabill, W., Hanna, E., Huybrechts, P., Abdalati, W., Cappelen, J., Csatho, B., Frederick, E., Manizade, S., Martin, C., Sonntag, J., Swift, R., Thomas, R., and Yungel, J.: Greenland Ice Sheet: Increased coastal thinning, Geophysical Research Letters, 31, https://doi.org/10.1029/2004GL021533, _eprint: https://onlinelibrary.wiley.com/doi/pdf/10.1029/2004GL021533, 2004.

Lai, Y.-C. and Tél, T.: Transient Chaos, vol. 173 of *Applied Mathematical Sciences*, Springer New York, New York, NY, ISBN 978-1-4419-6986-6 978-1-4419-6987-3, https://doi.org/10.1007/978-1-4419-6987-3, 2011.

Larocca, L. J., Twining–Ward, M., Axford, Y., Schweinsberg, A. D., Larsen, S. H., Westergaard–Nielsen, A., Luetzenburg, G., Briner, J. P., Kjeldsen, K. K., and Bjørk, A. A.: Greenland-wide accelerated retreat of peripheral glaciers in the twenty-first century, Nature Climate Change, pp. 1–5, https://doi.org/10.1038/s41558-023-01855-6, publisher: Nature Publishing Group, 2023.

Lohmann, J. and Ditlevsen, P. D.: Risk of tipping the overturning circulation due to increasing rates of ice melt, Proceedings of the National Academy of Sciences, 118, e2017989 118, https://doi.org/10.1073/pnas.2017989118, 2021.

Lohmann, J., Dijkstra, H. A., Jochum, M., Lucarini, V., and Ditlevsen, P. D.: Multistability and intermediate tipping of the Atlantic Ocean circulation, Science Advances, 10, eadi4253, https://doi.org/10.1126/sciadv.adi4253, publisher: American Association for the Advancement of Science, 2024.

Lucarini, V. and Bódai, T.: Edge states in the climate system: exploring global instabilities and critical transitions, Nonlinearity, 30, R32–R66, https://doi.org/10.1088/1361-6544/aa6b11, 2017.

Luthcke, S. B., Zwally, H. J., Abdalati, W., Rowlands, D. D., Ray, R. D., Nerem, R. S., Lemoine, F. G., McCarthy, J. J., and Chinn, D. S.: Recent Greenland Ice Mass Loss by Drainage System from Satellite Gravity Observations, Science, 314, 1286–1289, https://doi.org/10.1126/science.1130776, 2006.

MacAyeal, D. R.: Binge/purge oscillations of the Laurentide Ice Sheet as a cause of the North Atlantic's Heinrich events, Paleoceanography, 8, 775–784, https://doi.org/10.1029/93PA02200, 1993.

McDonald, S. W., Grebogi, C., Ott, E., and Yorke, J. A.: Fractal basin boundaries, Physica D: Nonlinear Phenomena, 17, 125–153, https://doi.org/10.1016/0167-2789(85)90001-6, 1985.

Mehling, O., Börner, R., and Lucarini, V.: Limits to predictability of the asymptotic state of the Atlantic Meridional Overturning Circulation in a conceptual climate model, Physica D: Nonlinear Phenomena, 459, 134 043, https://doi.org/10.1016/j.physd.2023.134043, 2024.

Oerlemans, J.: A numerical study on cyclic behaviour of polar ice sheets, Tellus A, 35A, 81–87, https://doi.org/10.1111/j.1600-0870.1983.tb00187.x, 1983.

Papa, B. D., Mysak, L. A., and Wang, Z.: Intermittent ice sheet discharge events in northeastern North America during the last glacial period, Climate Dynamics, 26, 201–216, https://doi.org/10.1007/s00382-005-0078-4, 2006.

Pattyn, F.: A new three-dimensional higher-order thermomechanical ice sheet model: Basic sensitivity, ice stream development, and ice flow across subglacial lakes, Journal of Geophysical Research: Solid Earth, 108, https://doi.org/10.1029/2002JB002329, _eprint: https://onlinelibrary.wiley.com/doi/pdf/10.1029/2002JB002329, 2003.

Payne, A. J.: Limit cycles in the basal thermal regime of ice sheets, Journal of Geophysical Research: Solid Earth, 100, 4249–4263, https://doi.org/10.1029/94JB02778, 1995.

Rignot, E. and Kanagaratnam, P.: Changes in the Velocity Structure of the Greenland Ice Sheet, Science, 311, 986–990, https://doi.org/10.1126/science.1121381, 2006.

Ritchie, P. D. L., Alkhayuon, H., Cox, P. M., and Wieczorek, S.: Rate-induced tipping in natural and human systems, Earth System Dynamics, 14, 669–683, https://doi.org/10.5194/esd-14-669-2023, 2023.

Robel, A. A., DeGiuli, E., Schoof, C., and Tziperman, E.: Dynamics of ice stream temporal variability: Modes, scales, and hysteresis, Journal of Geophysical Research: Earth Surface, 118, 925–936, https://doi.org/10.1002/jgrf.20072, 2013.

Roberts, W. H. G., Payne, A. J., and Valdes, P. J.: The role of basal hydrology in the surging of the Laurentide Ice Sheet, Climate of the Past, 12, 1601–1617, https://doi.org/10.5194/cp-12-1601-2016, publisher: Copernicus GmbH, 2016.

Robinson, A., Calov, R., and Ganopolski, A.: An efficient regional energy-moisture balance model for simulation of the Greenland Ice Sheet response to climate change, The Cryosphere, 2010.

Robinson, A., Calov, R., and Ganopolski, A.: Multistability and critical thresholds of the Greenland ice sheet, Nature Climate Change, 2, 429–432, https://doi.org/10.1038/nclimate1449, 2012.

Robinson, A., Alvarez-Solas, J., Montoya, M., Goelzer, H., Greve, R., and Ritz, C.: Description and validation of the ice-sheet model Yelmo (version 1.0), Geoscientific Model Development, 13, 2805–2823, https://doi.org/10.5194/gmd-13-2805-2020, 2020.

Robinson, A., Goldberg, D., and Lipscomb, W. H.: A comparison of the stability and performance of depth-integrated ice-dynamics solvers, The Cryosphere, 16, 689–709, https://doi.org/10.5194/tc-16-689-2022, 2022.

Schannwell, C., Mikolajewicz, U., Ziemen, F., and Kapsch, M.-L.: Sensitivity of Heinrich-type ice-sheet surge characteristics to boundary forcing perturbations, Climate of the Past, 19, 179–198, https://doi.org/10.5194/cp-19-179-2023, publisher: Copernicus GmbH, 2023.

Schoof, C.: The Effect of Cavitation on Glacier Sliding, Proceedings: Mathematical, Physical and Engineering Sciences, 461, 609–627, https://www.jstor.org/stable/30046308, publisher: The Royal Society, 2005.

Shepherd, A., Ivins, E., Rignot, E., Smith, B., van den Broeke, M., Velicogna, I., Whitehouse, P., Briggs, K., Joughin, I., Krinner, G., Nowicki, S., Payne, T., Scambos, T., Schlegel, N., A, G., Agosta, C., Ahlstrøm, A., Babonis, G., Barletta, V. R., Bjørk, A. A., Blazquez, A., Bonin, J., Colgan, W., Csatho, B., Cullather, R., Engdahl, M. E., Felikson, D., Fettweis, X., Forsberg, R., Hogg, A. E., Gallee, H., Gardner, A., Gilbert, L., Gourmelen, N., Groh, A., Gunter, B., Hanna, E., Harig, C., Helm, V., Horvath, A., Horwath, M., Khan, S., Kjeldsen, K. K., Konrad, H., Langen, P. L., Lecavalier, B., Loomis, B., Luthcke, S., McMillan, M., Melini, D., Mernild, S., Mohajerani, Y., Moore, P.,

Mottram, R., Mouginot, J., Moyano, G., Muir, A., Nagler, T., Nield, G., Nilsson, J., Noël, B., Otosaka, I., Pattle, M. E., Peltier, W. R., Pie, N., Rietbroek, R., Rott, H., Sandberg Sørensen, L., Sasgen, I., Save, H., Scheuchl, B., Schrama, E., Schröder, L., Seo, K.-W., Simonsen, S. B., Slater, T., Spada, G., Sutterley, T., Talpe, M., Tarasov, L., van de Berg, W. J., van der Wal, W., van Wessem, M., Vishwakarma, B. D., Wiese, D., Wilton, D., Wagner, T., Wouters, B., Wuite, J., and The IMBIE Team: Mass balance of the Greenland Ice Sheet from 1992 to 2018, Nature, 579, 233–239, https://doi.org/10.1038/s41586-019-1855-2, 2020.

Strogatz, S. H.: Nonlinear dynamics and chaos: with applications to physics, biology, chemistry, and engineering, Studies in nonlinearity, Westview Press, Cambridge (Mass.), ISBN 978-0-7382-0453-6, 1994.

Trusel, L. D., Das, S. B., Osman, M. B., Evans, M. J., Smith, B. E., Fettweis, X., McConnell, J. R., Noël, B. P. Y., and Van Den Broeke, M. R.: Nonlinear rise in Greenland runoff in response to post-industrial Arctic warming, Nature, 564, 104–108, https://doi.org/10.1038/s41586-018-0752-4, 2018.

Tulaczyk, S., Kamb, W. B., and Engelhardt, H. F.: Basal mechanics of Ice Stream B, west Antarctica: 1. Till mechanics, Journal of Geophysical Research: Solid Earth, 105, 463–481, https://doi.org/10.1029/1999JB900329, _eprint: https://onlinelibrary.wiley.com/doi/pdf/10.1029/1999JB900329, 2000.

Van Den Broeke, M., Bamber, J., Ettema, J., Rignot, E., Schrama, E., Van De Berg, W. J., Van Meijgaard, E., Velicogna, I., and Wouters, B.: Partitioning Recent Greenland Mass Loss, Science, 326, 984–986, https://doi.org/10.1126/science.1178176, 2009.

Van Pelt, W. J. and Oerlemans, J.: Numerical simulations of cyclic behaviour in the Parallel Ice Sheet Model (PISM), Journal of Glaciology, 58, 347–360, https://doi.org/10.3189/2012JoG11J217, 2012.

Zeitz, M., Haacker, J. M., Donges, J. F., Albrecht, T., and Winkelmann, R.: Dynamic regimes of the Greenland Ice Sheet emerging from interacting melt–elevation and glacial isostatic adjustment feedbacks, Earth System Dynamics, 13, 1077–1096, https://doi.org/10.5194/esd-13-1077-2022, 2022.

Ziemen, F. A., Kapsch, M.-L., Klockmann, M., and Mikolajewicz, U.: Heinrich events show two-stage climate response in transient glacial simulations, Climate of the Past, 15, 153–168, https://doi.org/10.5194/cp-15-153-2019, publisher: Copernicus GmbH, 2019.

Chapter 4

Chaos and crises in a physically-derived conceptual model of coupled ice streams

4.1 Introduction

The manuscript that is the topic of this chapter is an extension of the study of the behaviour seen in the comprehensive ice sheet model simulations of the previous chapter, specifically their chaotic behaviour. Since the primary candidate of the unpredictability of the tipping are the oscillations of the ice stream, it is desirable to construct a conceptual model of these such that parameters analogous to those in the ice sheet model may be altered and it can be studied:

1. what parameter changes cause the model to exhibit chaos,
2. what characteristics of the chaotic mode change as parameters are further changed,
3. how robust this chaos is in the parameter space.

Since the oscillations are believed to behave chaotically, there must be some manner of nonlinearity. Obviously, the oscillations themselves are a product of some nonlinear behaviour, but if the ice sheet system were such that multiple ice streams were oscillating at different frequencies, this would not amount to a chaotic system. There must be some sort of interaction between certain oscillating ice streams. As seen in the manuscript of the previous chapter, the northwestern basin was the primary contributor to the irregular behaviour preceding the tipping of the ice sheet, and in that region was what looked like an ice stream that is bisected such that it has two termini that oscillate aperiodically. This motivates the construction of a conceptual model that consists of the coupling of multiple ice streams in a nonlinear way. What

follows in this chapter is a derivation of the equations used in the model from the general equations of ice sheet evolution form the previous chapter. Thereafter, the various transitions from periodic to chaotic variability are introduced, whereafter the manuscript is presented.

4.2 Ice stream velocity

Firstly, a conceptual model with zero spatial dimensions that is based on the 2D flow field as described in the previous chapter is required. Raymond [89] derived a reduced-order model of the basal velocity of an ice stream with a horizontal bed, i.e. a pure ice stream and not one in a topographic valley. This results in a uniform ice thickness along the width of the ice stream. The deviatoric stress and effective strain rate are defined as in the previous chapter, giving the viscosity from the flow law

$$\eta = \frac{1}{2A\tau^{n-1}}. \tag{4.1}$$

In this case, the rate factor A is assumed to be constant. The assumptions on the flow are thus: the horizontal flow is unidirectional, taken to be in the x direction, such that $u_y = 0$. The horizontal flow is also plug flow, such that it is constant along the z direction. There is no normal stress beyond the hydrostatic stress. Thus, the remaining components of the shear stress tensor are τ_{xy} and τ_{xz}. The result is that the B-P equations 3.27, 3.28 become

$$\frac{\partial}{\partial y}\left(\eta\frac{\partial u_x}{\partial y}\right) + \frac{\partial}{\partial z}\left(\eta\frac{\partial u_x}{\partial z}\right) = \rho g\frac{\partial h}{\partial x}, \tag{4.2}$$

and the effective stress is

$$\tau = \frac{1}{2}\sqrt{\left(\tau_{xy}^2 + \tau_{xz}^2\right)}. \tag{4.3}$$

A useful relationship for solving for the velocity is derived from the relationship between the strain rate and the shear stress,

$$\frac{\partial u_x}{\partial y} = \frac{\tau_{xy}}{\eta} = 2A\tau^{n-1}\tau_{xy}, \tag{4.4}$$

$$\frac{\partial u_x}{\partial z} = \frac{\tau_{xz}}{\eta} = 2A\tau^{n-1}\tau_{xz}. \tag{4.5}$$

Since the boundary condition for the base is not known when it is not frozen to the bedrock, an empirical *sliding law* must be used. Such sliding laws are well known in ice sheet models, appearing even in comprehensive SIA models [19, 81, 96] to represent ice streams or glacier surges. These multi-valued sliding laws are piecewise functions that switch from zero basal velocity to basal shear stress-dependent velocity when some condition is met. This condition

may simply be that the base has reached pressure melting point and is temperate, or that basal melting has produced a sufficient amount of subglacial water to induce sliding. As described in the previous chapter, the relationship between the basal velocity and the basal stress has a different functional from depending on the condition of the base. In the case of deformation of a weak till, the basal shear stress saturates and is independent of velocity [46]. In this case, the basal shear stress at the base of the ice sheet $z = H$ is prescribed,

$$\tau_{xz}(y, H) = \tau_f, \tag{4.6}$$

and will be derived later. The boundary at the surface $z = 0$ is again stress-free,

$$\tau_{xz}(y, 0) = 0. \tag{4.7}$$

To derive a zero-dimensional equation for the basal velocity, the system described by equations 4.1 - 4.7 is integrated over the entire thickness and width then evaluated at the centreline, where the velocity is the greatest. Evaluating at the centreline allows the assumption $\frac{\partial u_x}{\partial y} \gg \frac{\partial u_x}{\partial z}$ as away from the shear margins, the horizontal gradients in velocity are stronger than vertical gradients. This means the effective shear stress is simply $\frac{1}{2}\tau_{xy}$. Using this, the integral of equation 4.2 at $z = H$ is

$$\frac{\partial}{\partial y}\left(\eta \frac{\partial u_b}{\partial y}\right) H - \tau_0 = \rho g H \frac{\partial h}{\partial x}, \tag{4.8}$$

using the stress boundary conditions. From the flow law, we have

$$\eta \frac{\partial u_x}{\partial y} = \left(\frac{1}{2A}\frac{\partial u_x}{\partial y}\right)^{1/n}. \tag{4.9}$$

The first integral over the width from some point y to the centreline at the half-width $W/2$ gives

$$-\frac{1}{2A}\frac{\partial u_b}{\partial y} H^n = \left[-\rho g H \frac{\partial h}{\partial x} + \tau_0 \right]^n [W/2 - y]^n, \tag{4.10}$$

where the boundary condition $\frac{\partial u_b}{\partial y}|_{(W/2,z)} = 0$ is used. The final integral gives

$$u_b(W/2) = \frac{A W^{n+1}}{2^n (n+1) H^n} \left[\rho g H \frac{\partial h}{\partial x} - \tau_0\right]^n, \tag{4.11}$$

which is the basal velocity at the centreline.

This equation 4.11 differs from equation 5 of Robel et al. [95] by a factor of 2^n. This is because that paper assumed the relation between the rate factor A and the associated rate factor B used in Raymond [89] to be of the usual form $A = B^{-n}$. However, comparing equation 1b in Raymond to equation 4.22 in Greve and Blatter [39], the actual form of B used in the former reads

$A = (2B)^{-n}$. This is supported by the calculation in Tulaczyk et al. [113] of $2^{1-n}(n+1)^{-1}B^{-n} = 1.45 \times 10^{-25}$ s^{-1} Pa^{-3} for an ice temperature of -15 degrees Celsius, which matches a value of $A/2$ from table 5.2 in Paterson [82] for the typical value of $n = 3$. As a result, the basal velocity as given in equation 5 of Robel et al. is too small by a factor of 2^n. However, the rate factor varies by orders of magnitude with ice temperature, so this factor can be corrected by assuming the ice is warmer which allows a larger rate factor to be used that is equal to that of Robel et al. after the correction. To remain consistent with Robel et al., their equation for the basal velocity as well as their value of A is used.

The sliding law also requires the aforementioned dynamic variable that determines whether the ice is streaming or stagnant with zero velocity. Since the streaming is assumed to be due to deformation of subglacial till rather than sliding over hard bedrock, the switch should be related to the till water content rather than just the basal temperature being at pressure melting point. This has been formulated using concepts from soil mechanics in Tulaczyk et al. [112, 113]. Effectively, the till has some internal failure stress τ_f below which it remains consolidated and above which it can deform. This failure stress depends on the normal stress applied, meaning that as water enters the till and the effective normal stress σ_n is lowered, the failure stress also decreases,

$$\tau_f = c + \sigma_n \tan(\phi), \tag{4.12}$$

where ϕ is the internal friction angle of the soil, which is larger for more dense (i.e. lower void ratio) till [109]. A driving stress greater than this failure stress induces shear deformation of the soil and sliding of the ice stream.

The amount of water the till can contain is represented by the void ratio $e = V_V/V_T$, which is the ratio of the volume of liquid V_v, or rather *void* that the liquid can occupy, to the volume of solid V_s in a soil sample. As the total soil volume is $V = V_v + V_S$, the void ratio has a limit of infinity in the case of $V_s \to 0$. The lower bound of e is 0. This void ratio depends also on the effective normal stress σ_n,

$$e = e_0 - C \log[\sigma_n/\sigma_{n,0}], \tag{4.13}$$

where e_0 and $\sigma_{n,0}$ are empirical parameters [113]. The greater the applied stress, the more compact the soil will be and the less liquid can enter. This equation is inverted to solve for the effective normal stress $\sigma_n(e)$. Since the void ratio represents the water content of the till, its change in time can be described by the basal melt rate. As mentioned in the previous chapter, basal melting can occur when the sum of the thermodynamic sources and sinks including geothermal heat flux, heat generated by friction due to sliding, and heat lost by conduction into the ice sheet above are overall positive.

The failure stress τ_f is equivalent to the basal friction stress and a sliding law is thereby constructed. When the till water content is low, the basal

friction is larger than the driving stress and the basal velocity is zero. When the driving stress exceeds the friction, the term $\tau_d - \tau_f > 0$ and the streaming velocity is nonzero. If this induces further basal melt, the frictional stress will continue to decrease until it is near zero, and the basal velocity will reach an upper limit based on the driving stress. This increased velocity will serve to reduce the ice thickness (equation 3.21) which reduces the driving stress. This is a negative feedback to ensure solutions do not blow up.

4.3 Routes to chaos and attractor crises

In this section, the different ways chaotic behaviour in dynamical systems arises is qualitatively described. While quantitative theoretical results exist for one or two dimensional maps [35, 37, 38, 80], for systems of higher dimension most useful equations are for calculating the dimensions of chaotic saddles or escape rates from chaotic non-attracting sets, or even supertransients in spatiotemporal systems [62]. For this project, the goal was to describe a model that can qualitatively reproduce the chaotic variability of ice streams, with less focus on the calculation of these quantities. Perhaps more relevant is the fact that scaling laws exist for many of of these phenomena, due to the notion that chaotic variability is actually a universal phenomenon [41, 55, 79, 108]. That is, all systems displaying chaotic behaviour do so in very similar ways. This is a remarkable feature, as commonly chaotic systems are thought of to behave unpredictably. It is these qualities of universality that make studying lower-dimensional systems relevant to understanding chaos in higher-dimensional ones.

The change in dynamics from periodic to chaotic in a system is termed the *route to chaos* and can occur in a variety of ways [41, 79]. Firstly, a periodic attractor may undergo local bifurcations that cause it to transform into a chaotic attractor. There are three such types:

1. Cascade of period doubling bifurcations,
2. Quasiperiodic (Ruelle-Takens) route to chaos,
3. Intermittent (Poumeau-Manneville) route to chaos.

The first one is the most classical example. A limit cycle experiences a a period-doubling or flip bifurcation when looking at a discrete mapping. This period doubling then repeats as the parameter is increased, generating an infinite number of periodic orbits. In the limit, the motion between all of these periodic orbits becomes chaotic. The cascade of period doubling bifurcations is associated with Feigenbaum universality – the ratio of the differences between parameter values of successive period doubling bifurcations is constant in the limit as the chaotic regime is approached *regardless of the system in which it occurs* [55, 108].

In the quasiperiodic route to chaos, a limit cycle becomes quasiperiodic after experiencing a Hopf bifurcation. This introduces a second oscillatory frequency to the motion, which will be quasiperiodic if it is incommensurate with that of the original limit cycle. If this occurs a second time, the resulting orbit is chaotic. Unlike in the case with the cascade of period doubling occurring an infinite number of times, only three incommensurate frequencies are required for chaos [77, 100].

Finally, the intermittent route to chaos can occur in a variety of ways. A periodic attractor can experience one of three bifurcations that will remove its attracting nature: it may be destroyed via a saddle-node bifurcation of limit cycles (also known as a tangent bifurcation in the discrete mapping), or else become unstable through a Hopf bifurcation or the inverse of a period doubling bifurcation. As a result, the system spends time in a part of phase space that experiences regular periodic behaviour before intermittently *bursting* with chaotic variability. The case of the tangent bifurcation in the case of an iterative map is the most illuminating. Before such a tangent bifurcation, there is a stable periodic orbit. After the tangent bifurcation, locally the stable orbit has disappeared, but any trajectory in the area will be caught in the area of phase space where the tangent bifurcation occurred – in this way, it is similar to the ghost of the saddle-node bifurcation discussed in the previous chapter.

The three types of intermittent routes to chaos as given by Poumeau and Manneville [88] correspond to the three bifurcations listed above, and can be recognized by qualities of the intermittently periodic motion as well as scaling laws for the mean time in between intermittent bursts. In the case of a type I intermittency which arises due to a tangent bifurcation, the periodic motion of of the intermittent trajectory will look similar to that of the periodic orbit before the route to chaos. The mean time between intermittent bursts scales as a reciprocal square root [79],

$$\langle \tau \rangle \sim |p - p_c|^{-1/2}, \tag{4.14}$$

where p is the value of the parameter past the critical value p_c where the intermittency begins. Much like the quasiperiodic route to chaos begins with a Hopf bifurcation, type II intermittency will see the appearance of a second frequency in the intermittently periodic behaviour. The scaling law is similar to that of type I in equation 4.14, with the exponent instead being -1. Finally, type III occurs due to a period doubling bifurcation, and as such the regular oscillations of the intermittency will have double the period of that of the pre-chaotic limit cycle. The scaling is the same as for type II. Parameter regimes where the chaotic attractors exists are also dense with periodic windows. Periodic windows are the result of a tangent bifurcation which creates a stable periodic orbit that replaces the chaotic one. These tangent bifurcations are the reverse of those that lead to type I intermittency, explaining why chaotic orbits before a periodic window are strongly intermittent.

Alternative to a local bifurcation, there may be some global bifurcation that causes the appearance of a chaotic attractor or for a chaotic attractor to suddenly grow in size. These are called *crises* and come in two flavours: *boundary* and *interior* [36], the former of which was introduced in the previous chapter. A boundary crisis results in the collision and annihilation of a chaotic attractor with an unstable periodic orbit as a parameter is varied. Similar to a saddle-node bifurcation, it can also result in the spontaneous appearance of a chaotic attractor when the parameter changes in the opposite direction. It is termed a boundary crisis as it occurs when a chaotic attractor collides with an unstable orbit in its own basin boundary. As mentioned in the previous chapter, the annihilation of the chaotic attractor leaves a ghost of the chaotic attractor, a non-attracting chaotic set that causes chaotic transients.

An interior crisis results in the sudden enlargement of a chaotic attractor. Similarly to a boundary crisis, it is the result of a collision between a chaotic attractor and an unstable orbit, which in this case is in the *interior* of the basin of attraction. Interior crises are associated with periodic windows. Near the end of a periodic window, a cascade of period-doubling bifurcations recreates a chaotic attractor. As the tangent bifurcation that initiated the periodic window creates an unstable periodic orbit as well, the eventual collision of this with the chaotic attractor during the interior crisis causes it to increase in size. Additionally, chaotic non-attracting sets are present in these periodic windows, being the ghost of the former chaotic attractor that existed before the saddle-node bifurcation. Thus even in a periodic window, chaotic transients can occur. Interior crises also causes *crisis-induced intermittency*, which is similar to the intermittent route to chaos albeit with the non-intermittent motion being chaotic as well. Just as for Pomeau-Manneville intermittency, the mean lifetime between intermittent bursts scales with the parameter value beyond the crisis. However, the scaling law is that same as that of a boundary crisis, with a critical exponent γ that depends on the system under consideration.

4.4 The manuscript

Chaotic variability in a model of coupled ice streams

Kolja Kypke,[1] Peter Ashwin,[2] and Peter Ditlevsen[1]

[1] *Physics of Ice, Climate and Earth,*

Niels Bohr Institute, University of Copenhagen

[2] *Department of Mathematics and Statistics, University of Exeter*

(Dated: September 23, 2024)

Abstract

Regions of fast-flowing ice in ice sheets, known as ice streams, have been theorized to be able to exhibit build-up/surge oscillatory variability due to thermomechanical coupling at the base of the ice. A simple model of three coupled ice streams is constructed to replicate the spatial configuration of a single ice stream being bisected into two termini. This model is shown to exhibit both steady-flow and build-up/surge oscillations. Further, the variability can be chaotic due to the nonlinear coupling of three incommensurate frequencies. This provides a mode of chaotic internal variability for ice sheets that contain these ice streams, which evolve via purely laminar flow.

I. INTRODUCTION

Fast variations in ice sheet volumes are most commonly thought to occur due to variability in other components of the climate externally forcing the ice sheet. This is because the dynamics of ice sheets are dominated by the slow deformational creep of an extremely viscous fluid. However, ice sheets possess an internal mode of variability that manifests as a cyclic variation of the volume of the ice sheet driven by the thermomechanical coupling of the ice sheet at its base. Due to the immense overburden pressure of the ice, the base can find itself at the pressure melting point such that the base of the ice is liquid. The water under the ice sheet can promote very rapid movement of the ice, generally in topographically confined channels, known as ice streams. Important to this process is the characteristics of the bedrock under the ice. The water can either lubricate the ice sheet base causing it to slide on top of hard bedrock (basal sliding), or saturate a weak till enough to cause it to shear (subglacial deformation) [1].

In comprehensive ice sheet model simulations of the Laurentide ice sheet (LIS) covering parts of North America during the Last Glacial Period (LGP), such ice streams have been shown to transport large quantities of ice over relatively short periods of time [2–6]. These have been theorized to result in what are known as Heinrich events (HE), which are large amounts of ice-rafted debris found in the marine sediment records of the LGP [7, 8]. These HE are marked for their abrupt nature and are sometimes synchronous with the Dansgaard-Oeschger events seen in the ice-core record of Greenland [9]. Due to their rapid onset, HE are most commonly thought to have occurred due to rapid ice streams. Whether they are externally forced or occur spontaneously due to the internal variability of the ice sheet is

still under contention [10].

The aforementioned model studies of the LIS display these oscillations in ice sheet volume even under constant external forcing conditions. These oscillations are irregular in period, also described as quasiperiodic [11], as to be expected due to the size and complexity of the ice sheet. Non-chaotic oscillations have also been suggested in a zero-dimensional conceptual model of Robel et al. [12] (hereafter R13), where a subcritical Hopf bifurcation between steady-streaming and oscillations of the ice stream thickness results in hysteresis behaviour and bistability for a range of ice surface temperatures. This model has also been expanded with a stochastic component [13]. In this case, the noise represents fast, small-scale processes, such as atmospheric variability in surface temperature and accumulation rates. The resulting model is able to randomly alternate between steady streaming and oscillations due to noise-induced tipping from one mode to the other. This is an example of the Hasselmann paradigm [14], where small amplitude variations of the mean climate state are modelled using stochastic forcing.

Recently, a comprehensive model study of the present-day Greenland ice sheet has displayed oscillations similar to those of R13 [12] under mild temperature forcing [15] However, the period and amplitude of these oscillations are highly irregular despite the external forcing containing no stochastic or chaotic component. These oscillations are evidenced to delay the tipping of the ice sheet and are theorized to be chaotic transients [16]. In this study, a conceptual model of ice streams displaying chaotic variability is constructed. Building upon the model of R13 [12], it is modified to include nonlinear coupling. The coupling is inspired by the oscillating ice stream seen in Kypke et al. [15]. What is originally two individual ice streams, that behave independently, retreat inland under an external temperature perturbation such that they are much closer and seemingly coupled. Since they are fed by a common upstream section of the ice stream the system of ODEs is able to display chaos when two 'downstream' terminating ice stream boxes are coupled to a single 'upstream' ice stream box with unidirectional flow with three incommensurate frequencies [17]. Using this model, it is demonstrated how certain parameters affect the overall variability, and how chaotic modes and chaotic transients can arise solely from ice stream dynamics. While the setup of this conceptual model does not exactly match the conditions and configuration of the comprehensive ice sheet model simulations on which it is based, there is a suitable similarity to be able to explore the situations that can lead the system to exhibit chaotic variability.

II. R13 MODEL FOR ICE STREAM TEMPORAL VARIABILITY

The R13 [12] conceptual model of ice stream temporal variability assumes an idealized geometry of an ice stream with constant width and length. The variables are "spatially lumped" such that they are described by average values and reduced to zero spatial dimensions. The upper panel of Fig. 1 shows a cross section of the ice stream displaying the mass and energy fluxes. The prognostic variables of the model are ice stream ice thickness H, ice sheet basal temperature T_b, the thickness of the solids in the unfrozen section of till $h_{\text{till},s}$, and till void ratio e. The void ratio is the fraction $e = \frac{V_w}{V_s}$, where V_w is the volume of water and V_s is the volume of solids in the till such that the total till volume is $V_T = V_w + V_s$. It can take on any value greater than zero is related to the porosity $\phi \in [0, 1)$ by the relationship

$$\phi = \frac{e}{1+e}. \tag{1}$$

The thickness of the water in the till is given as $h_{\text{till},w} = \phi h_{\text{till, max}}$ and is related to the void ratio and thickness of the solids in the unfrozen till by $h_{\text{till},w} = e h_{\text{till},s}$. The basal velocity is a diagnostic variable determined by the driving stress and the basal frictional stress, which depends on the till water content. The till water content depends on the unfrozen till height and the void ratio via $h_{\text{water}} = e h_{\text{till},s}$. The model has three cases for the state of the basal till, seen in the lower panel of Fig. 1 and described below.

A. Frozen till

The first state is completely frozen till: the unfrozen till height $h_{\text{till},s} = 0$ and either $T_b \geq 0$ (T_b is positive for negative temperatures) or it is 0 and the basal melt rate is negative. In this case, there is no basal sliding,

$$u = 0, \tag{2}$$

the void ratio does not change, i.e. no water in the till is melting or freezing,

$$\frac{de}{dt} = 0, \tag{3}$$

the unfrozen till thickness stays at 0,

$$\frac{dh_{\text{till},s}}{dt} = 0, \tag{4}$$

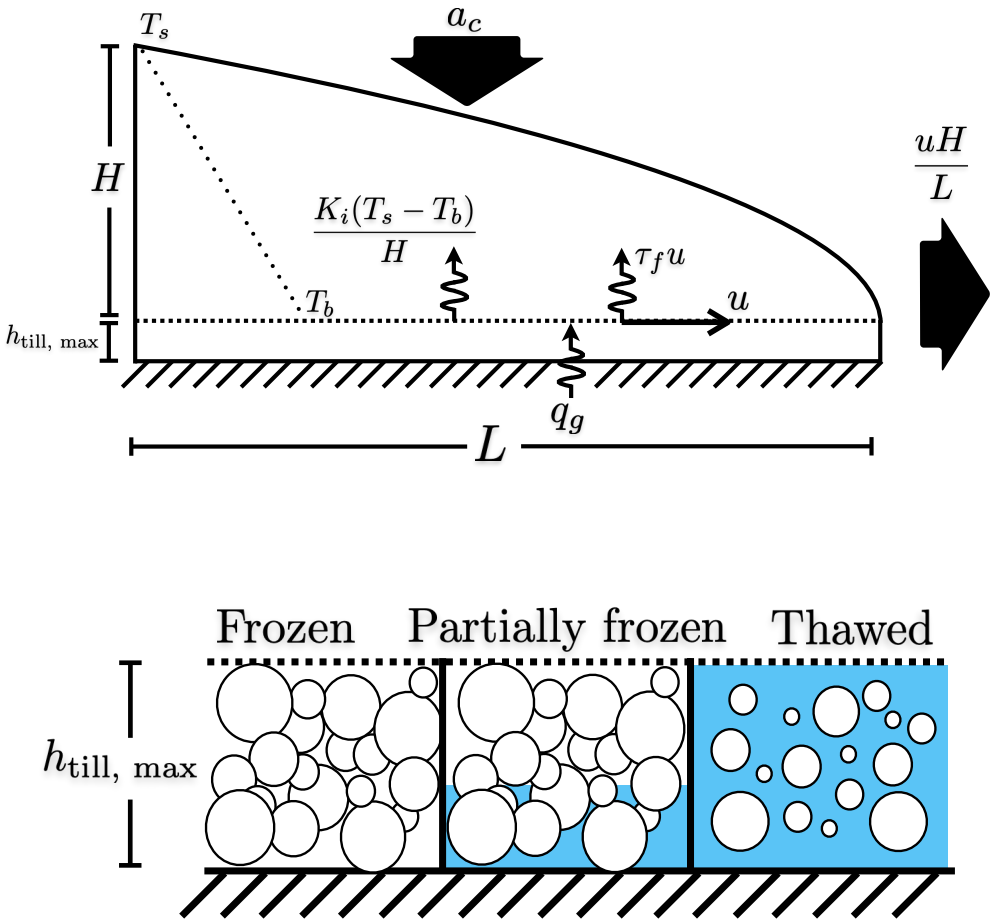

FIG. 1. (Top) Schematic of the fluxes of the R13 model. Broad arrows represent mass fluxes and wiggly arrows represent energy fluxes. (Bottom) Schematic of the three till cases.

and the temperature of the basal ice layer increases or decreases,

$$\frac{dT_b}{dt} = -\frac{1}{C_i h_b}\left(\tau_f u + q_g - \frac{K_i(T_s - T_b)}{H}\right), \tag{5}$$

depending on the difference between the geothermal heat flux q_g and the energy diffusing to the surface of the ice as determined by the gradient between the surface and basal temperatures, T_s and T_b respectively. The prefactor C_i is the heat capacity of ice and h_b is the thickness of the base of the ice that is being warmed.

B. Partially frozen till

The second case is partially frozen till. In this case, the basal temperature is 0°C, and the void ratio is at a minimum value, $e = e_c$, known as the 'till consolidation void ratio'. Additionally, the unfrozen till thickness is greater than zero but must be either less than its maximum value, or it is at its maximum value and with a negative melt rate. In this case, there is again no basal sliding since it is still partially frozen,

$$u = 0, \tag{6}$$

the void ratio does not change,

$$\frac{de}{dt} = 0, \tag{7}$$

the unfrozen till thickness changes depending on the melt rate,

$$\frac{dh_{\text{till},s}}{dt} = \frac{\tau_f u + q_g - \frac{K_i(T_s - T_b)}{H}}{L_f \rho_i}, \tag{8}$$

where L_f is the latent heat of fusion of ice and ρ_i is the density of ice. As all the energy is being used to melt or refreeze the till, so the basal temperature stays at 0°C

$$\frac{dT_b}{dt} = 0. \tag{9}$$

C. Thawed till

The final case is where the till is thawed. The unfrozen till thickness will be maximum, and an additional energy budget is used to increase the void ratio. The basal velocity in nonzero and is given as

$$u = \frac{A_f W^{n+1}}{4^n (n+1) H^n} \max\left[\tau_d - \tau_f, 0\right]^n, \tag{10}$$

where the driving stress τ_d depends on the ice thickness and surface slope and the basal stress τ_f depends on the water content: it is equal to ∞ for fully or partially frozen till (resulting in $u = 0$ in sections 2.1 and 2.2) and decreases to zero with increasing till water content: $\tau_f = \tau_0 \exp\left[-ce\right]$. The parameter A_g is the rate factor and n the exponent of Glen's Flow law [18].

The void ratio changes depending on the melt rate,

$$\frac{de}{dt} = \frac{\tau_f u + q_g - \frac{K_i(T_s - T_b)}{H}}{h_{\text{till},s} L_f \rho_i}, \tag{11}$$

the unfrozen till thickness does not change and stays maximal,

$$\frac{dh_{\text{till},s}}{dt} = 0, \tag{12}$$

and the basal temperature stays at 0°C,

$$\frac{dT_b}{dt} = 0. \tag{13}$$

A large, increasing void ratio for a fixed total till thickness represents the solids gradually being replaced until the entire till is just a layer of water. Physically, a maximum void ratio that depends on the till properties would be expected, and any water beyond this is somehow drained from the system. A large void ratio is not an issue in this simplified model however, as the only component that depends on the void ratio is the basal friction τ_f which saturates to near zero very quickly as the void ratio increases.

D. Ice thickness

In all three of the cases, the change in ice thickness is

$$\frac{dH}{dt} = a_c - \frac{Hu_b}{L}, \tag{14}$$

i.e. a balance between the mass gained via accumulation due to precipitation a_c and the mass lost due to sliding, assuming ice thickness goes to 0 at the end of the ice stream. This gives a mean surface slope of h/L.

III. SPLIT ICE STREAM MODEL

In Kypke et al. [15], a single large ice stream is split by a topographical ridge into two termini. These ice stream sections have differing basal properties and geometries, the subsequent oscillations will have different amplitudes and potentially different periods. This is modelled as a coupling between three ice streams, each described by the conceptual R13 model [12]. The coupling in the model is achieved by designating the three box models and coupling them by conserving volume between one 'upstream' box (box 1) and two smaller 'downstream' boxes (boxes 2 and 3), as in Fig. 2 This figure is not to scale: the lengths are on the order of 100s of kilometres and the widths on the order of 10s of kilometres, while the height is on the order of a kilometre.

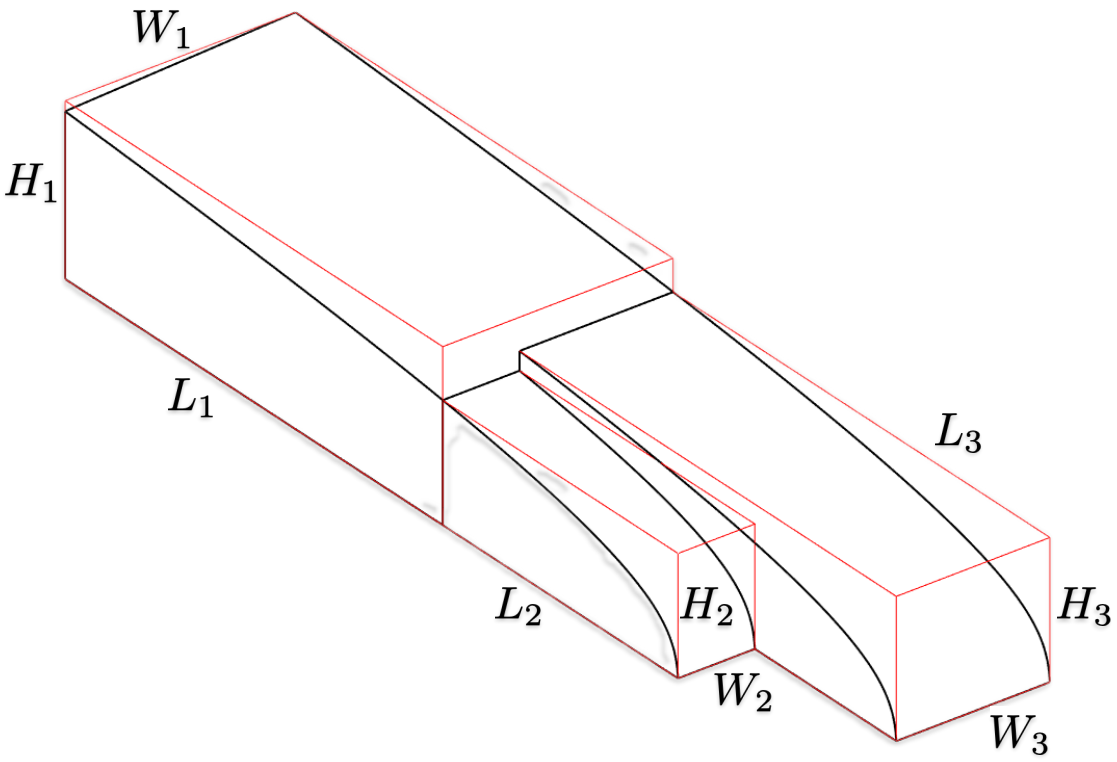

FIG. 2. Schematic of the three-box split ice stream mode. Box 1 gains volume from accumulation and loses volume to boxes 2 and 3 due to streaming flow. Boxes 2 and 3 gain volume from accumulation and as volume flux from box 1, and lose volume due to streaming flow.

For the upstream box, the ice thickness lost due to basal sliding depends on the difference between the height of box 1 and the heights of boxes 2 and 3. This difference is a linear combination of the heights of boxes 2 and 3, weighted by their relative widths.

$$\frac{dH_1}{dt} = a_c - \frac{(H_1 - \frac{W_2}{W_1}H_2 - \frac{W_3}{W_1}H_3)u_{b,1}}{L_1} \tag{15}$$

This can cause a scenario where the height of box 2 or 3 is larger than that of box 1, since H_1 represents the mean height for box 1. The widths of box 2 and box 3 sum up to the width of box 1 ($W_1 = W_2 + W_3$), but otherwise the rest of the parameters are unconstrained. Coupling between the boxes also occurs via modulation of the driving stress. Since the driving stress depends on the surface slope, the driving stress of the upstream box 1 is modified to depend on the difference between its height and the height of the downstream boxes in the same

manner as described above,

$$\tau_{d1} = \rho_i g \frac{H_1}{L_1}\left(H_1 - \frac{W_2}{W_1}H_2 - \frac{W_3}{W_1}H_3\right). \tag{16}$$

There is also a coupling through a volume flux when box 1 is losing volume. Since boxes 2 and 3 are downstream from box 1, and volume loss occurs via basal sliding, this volume must enter boxes 2 and 3. with each getting a fraction determined by $W_{2,3}/W_1$. To keep the coupling unidirectional, the condition is set that the volume flux is only nonzero if the change in volume of box 1 is negative. This prevents the case where boxes 2 and 3 lose volume while box 1 is gaining volume. Explicitly, this means

$$\frac{dV_i}{dt} = \begin{cases} L_i W_i a_c - W_i H_i u_{b,i} - \frac{W_i}{W_1}\frac{dV_1}{dt} & \text{if} \quad \frac{dV_1}{dt} < 0 \\ L_i W_i a_c - W_i H_i u_{b,i} & \text{otherwise} \end{cases} \tag{17}$$

for $i = 2, 3$.

The basal velocity depends largely on three parameters: the box width, the box length via the driving stress, and the rate factor A_g. The rate factor is a parameter that depends largely on the temperature of the ice. This factor can vary by multiple orders of magnitude, from 6.8×10^{-24} Pa^{-3} s^{-1} at 0 degrees to 3.6×10^{-27} Pa^{-3} s^{-1} at -50 degrees [18]. The larger the rate factor, the 'softer' the ice, and the faster it will to flow. Since the temperature of the ice is not specified, a constant value of 5×10^{-16} as in R13 [12] is used, which corresponds to a temperature of around -10 °C. The basal velocity depends very strongly on box width, being raised to the fourth power of this parameter. Otherwise, the only other appearance of the box widths are in determining the relative strength of the coupling of the driving stress of box 1 to boxes 2 and 3. While the basal velocity does scale as $\sim L^{-3}$, the primary effect that the length of the box has on the basal velocity is to determine the flow regime. The equilibrium ice thickness in the steady flow regime, derived from equation (14), depends on the length and the basal velocity such that it ultimately scales linearly with length. A larger L means a larger ice thickness, which increases the basal melt rate and brings any configuration closer to the steady-flow regime.

As in R13 [12], the geothermal heat flux and surface temperature also determine the flow regime in opposite ways. A large geothermal heat flux increases the basal melt rate, and a larger (more negative) surface temperature increases the conduction of heat from the base upwards through the ice sheet, decreasing the basal melt rate. Depending on the size of

the ice stream boxes we may expect a smaller geothermal heat flux in the upstream box, which is closer to the centre of the ice sheet. This is due to the properties of the crust and mantle of Greenland. However, the difference would not be more than a few $\mathrm{mW/m^2}$, so a constant value across the boxes can also be assumed The surface temperature is also assumed to be larger in the upstream box, primarily to represent a lower temperature due to a higher altitude as a result of a larger ice sheet thickness. Similarly, the accumulation rate in the upstream box is larger to represent a larger surface mass balance due to lower runoff at lower temperatures.

IV. CHAOTIC VARIABILITY AND ROUTES TO CHAOS

The split ice stream model displays all the same modes of variability as in R13 [12]: steady flow as well as weak and strong build-up/surge (stick-slip) oscillations. Further, it is able to exhibit chaotic variability, an example of which is presented in this section. Figure 3 shows a simulation for a set of parameters where the tree boxes are in the three different modes: Box 1 is in the steady-flow mode, characterized by the arbitrarily large void ratio (not pictured) and small but nonzero basal velocity. Spikes in this basal velocity occur due to the coupling to box two, where strong surging occurs. This build-up/surging mode in box 2 is due to occasional refreezing of the till, identified by a basal velocity that becomes zero when the void ratio becomes minimal and the unfrozen till thickness becomes less than maximal. Box 3, on the other hand, is in the regime of weaker build-up/surge oscillations. The unfrozen till thickness is maximal, but the void ratio varies along with the basal velocity. Altogether, their coupling results in a chaotic state.

To investigate how chaos arises under parameter variation, we restrict ourselves to only changing one parameter. Figure 4 shows a bifurcation diagram, given by the peaks in the total ice volume in all three boxes, as a function of the surface temperature in box 2. It should be noted that the steady-streaming mode does not appear as the surface temperatures of box 3 is such that it are fixed in the oscillatory mode. There are three regimes, characterized by the rate of change of the void ratios in boxes 1 and 2 and determined by the value of $T_{s,2}$. These three regimes represent different dominant sources of variability. In the first one, for $T_{s,2} <$, box 2 has a large and increasing void ratio and box 1 has a minimal void ratio. The oscillations are subsequently paced by the variability in box 1. For a large enough

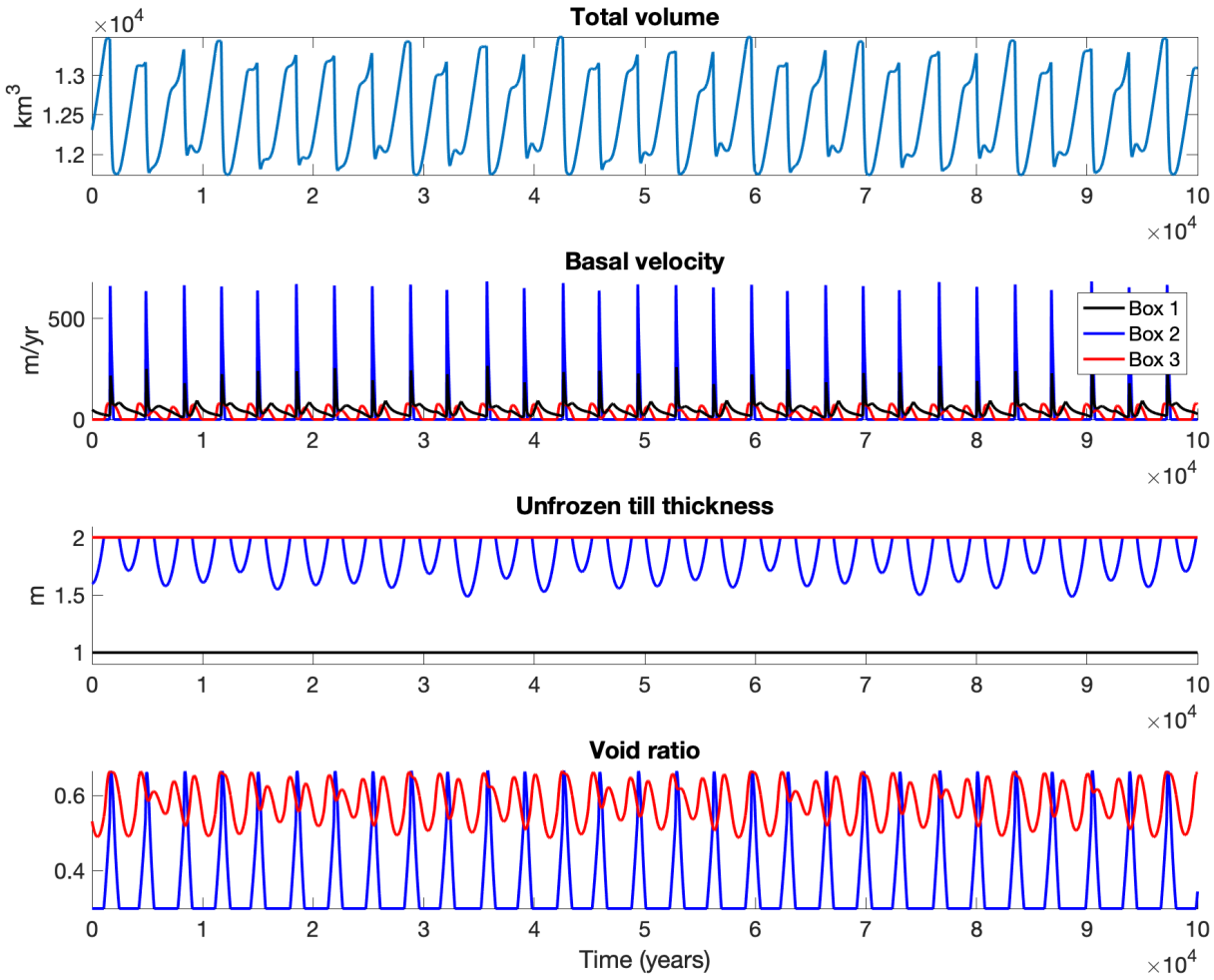

FIG. 3. Variables for the individual boxes in the chaotic regime. The void ratio of box 1 is arbitrarily large, so it is omitted for readability.

$T_{s,2} > 6.65$, box 2 is now in the weak build-up/surge mode. For even larger $T_{s,2} > 9.05$, the less frequent surging events allows the thickness of box 1 to grow to the point where it has a positive basal melt rate and e_1 is increasing. That is, box 2 is in the build-up/surge mode and box 1 is in the steady-streaming mode meaning box 2 dominates the variability. These regimes describe the asymptotic state, but as the void ratio can increase without bound, transitions from one regime to another can take a very long time to equilibrate depending on the initial values of these variables which may introduce long transients in the non-equilibrium setting.

The bifurcation diagram reveals a few chaotic windows. In the parameter window between 14.9 and 15.4 (lower part of Fig. 4), the transition from periodic to chaotic as $T_{s,2}$ is reduced

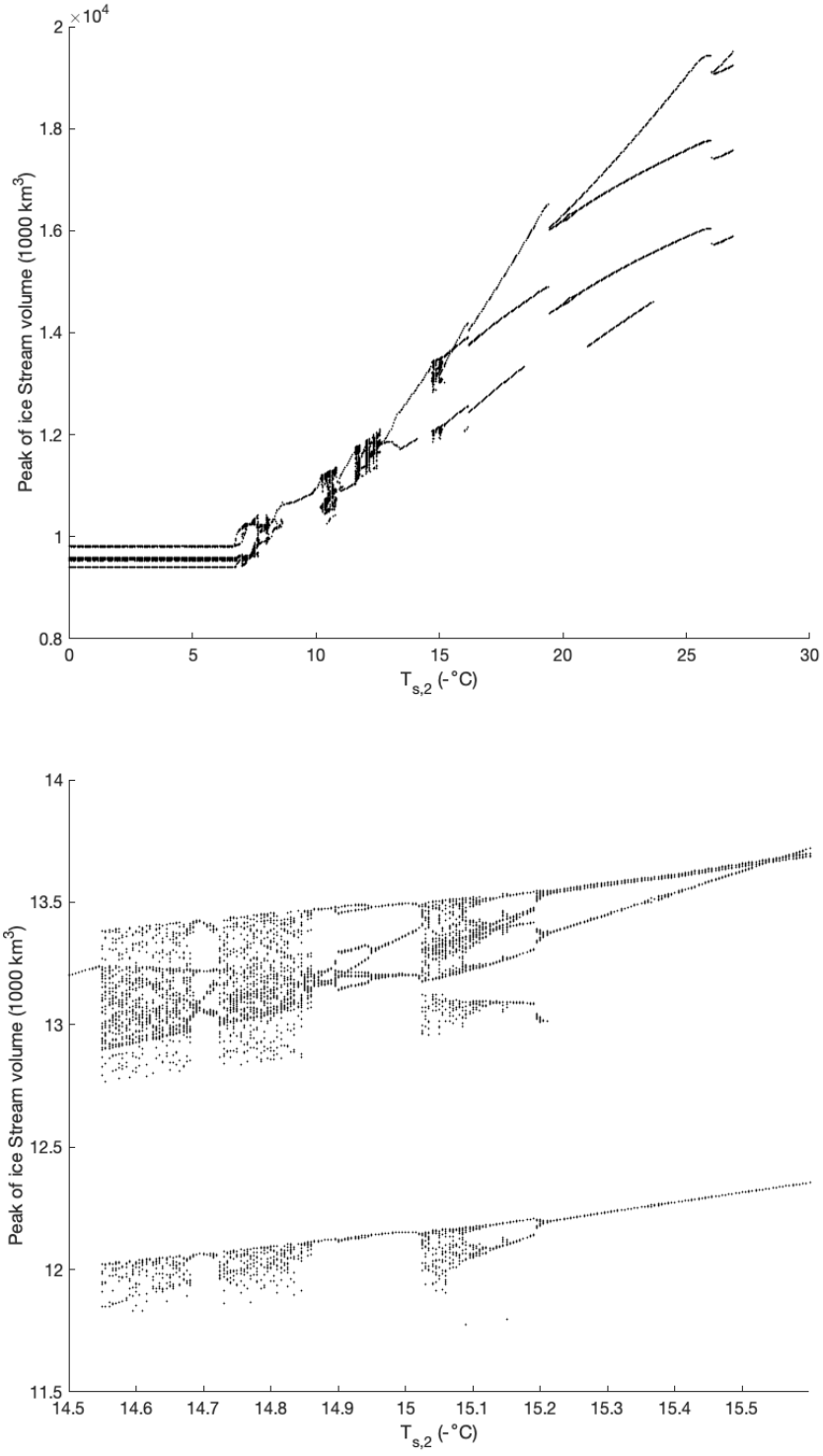

FIG. 4. Bifurcation diagram for $T_{s,2}$ from 0 to 27 (top) and a zoomed view of the chaotic window between 14.6 and 15.6 (bottom).

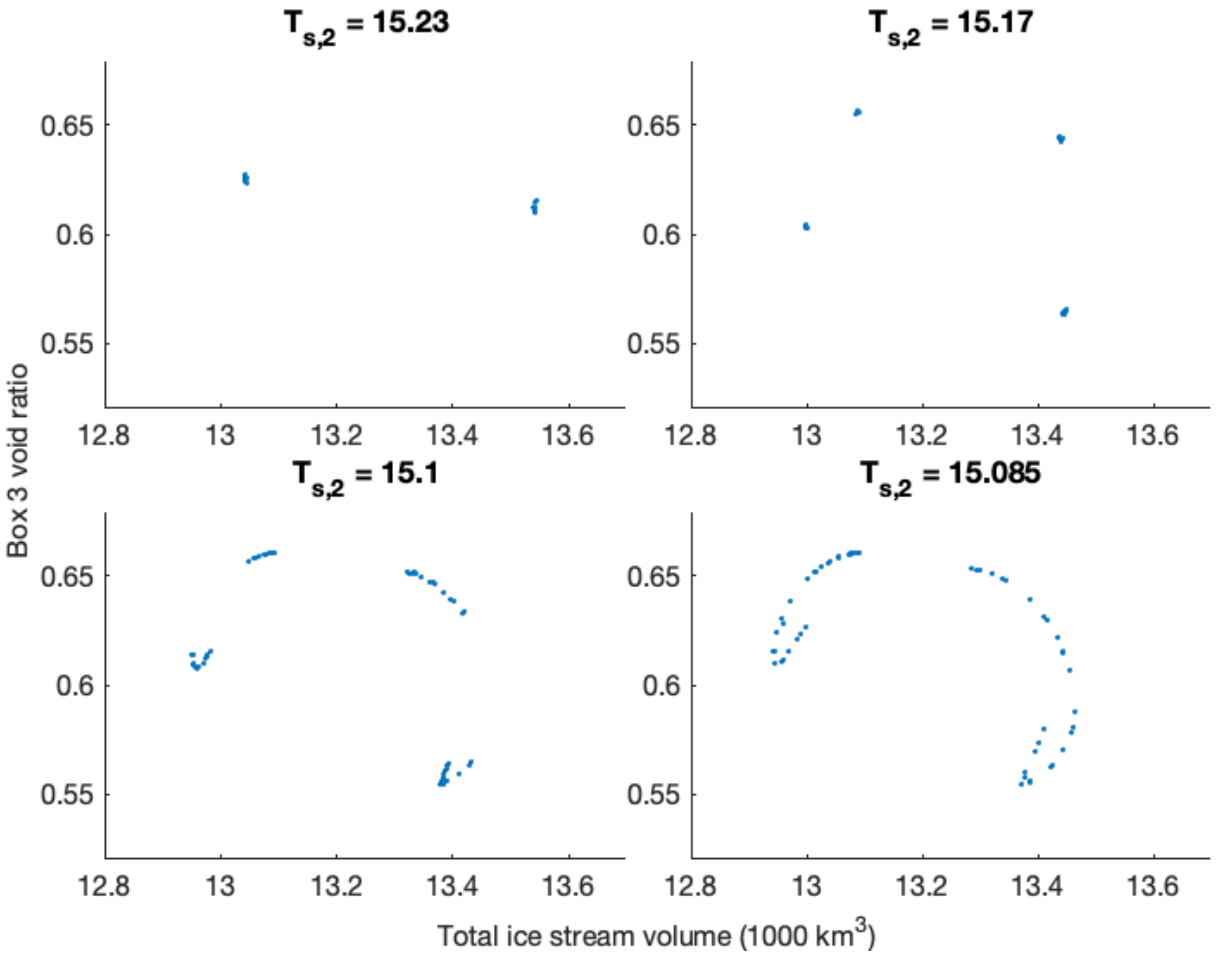

FIG. 5. Poincaré map of the period-doubling route to chaos at the beginning of the chaotic window of Fig.3.

occurs as a cascade of period-doubling bifurcations. Figure 5 shows a sequence of a return map of a Poincaré-like map at the onset of the chaotic window. What begins as a 2-cycle experiences a period-doubling bifurcation into a 4-cycle. The return map then begins to appear as a strange attractor by $T_{s,2} = 15.10$.

The transition back to a periodic orbit occurs as the orbits become increasingly more intermittent, with bursts of chaotic behaviour in between regular periodic motion. This can be seen in Fig. 6, which shows the same Poincaré-like maps as Fig. 5. As $T_{s,2}$ continues to decrease, these intermittent bursts become more and more rare, as shown by the clustering of points around one part of the attractor around $(12.6, 0.48)$. This continues until the motion is purely periodic. Hence this route to chaos, or rather route from chaos, occurs as

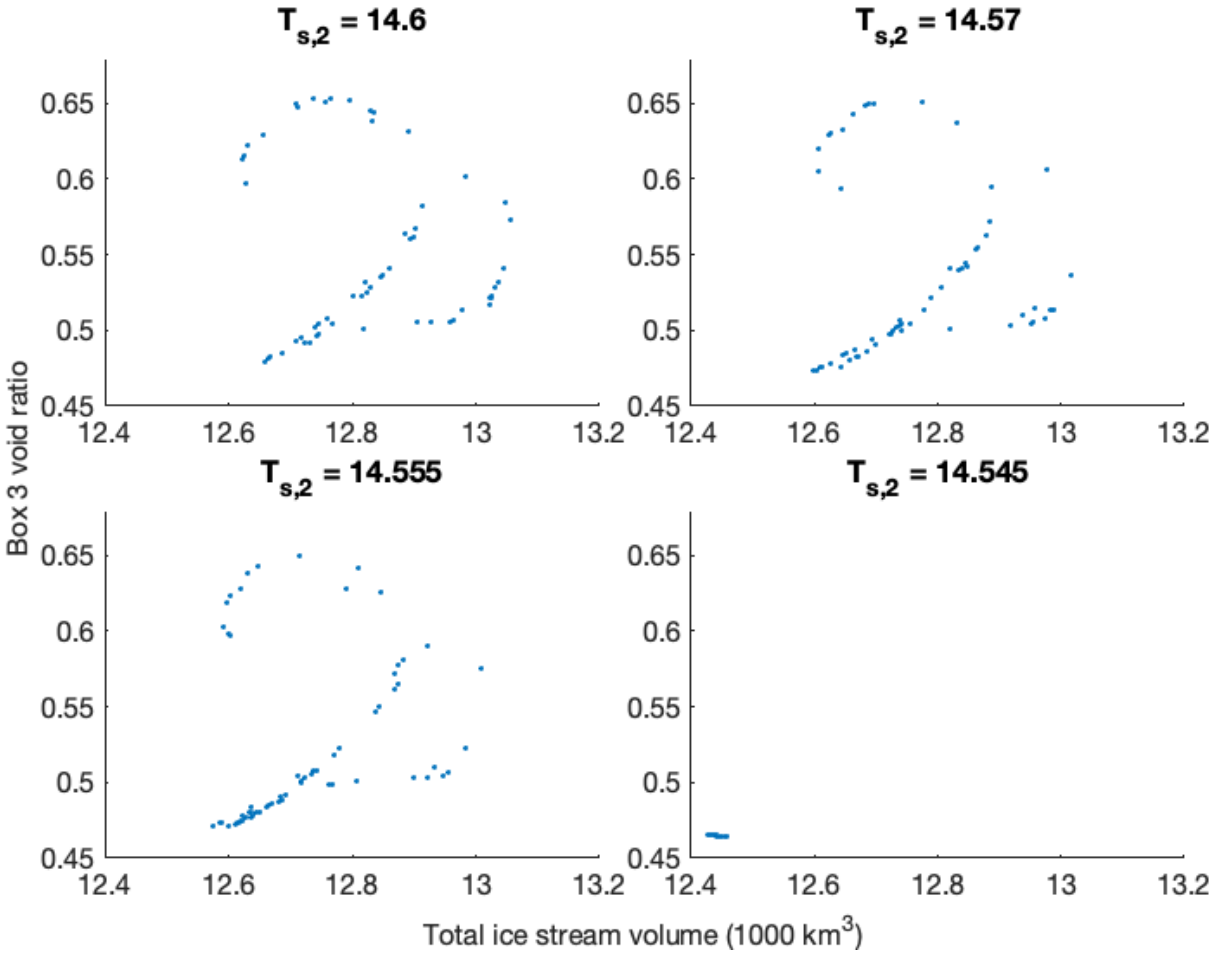

FIG. 6. Poincaré map of the intermittency route to chaos at the end of the chaotic window Fig. 3.

the Pomeau-Manneville intermittency type [19].

V. BISTABILITY, CRISES AND CHAOTIC TRANSIENTS

In this section, the model is applied to replicate the behaviour seen in Kypke et al. [15]. In that study, there are two configurations of the ice sheet in the northwestern drainage basin with two distinct ice sheet extents. In the 'unretreated' case with a larger ice sheet extent, the ice streams oscillate in a more regular manner. Under moderate warming of about 1°C, the ice sheet in that region retreats and the ice streams now oscillate in a more irregular pattern. As has been shown in the previous section, the model can shift from regularly periodic to chaotic under very small surface temperature perturbations. We also demonstrate the transition from oscillatory to chaotic under variation of the length of

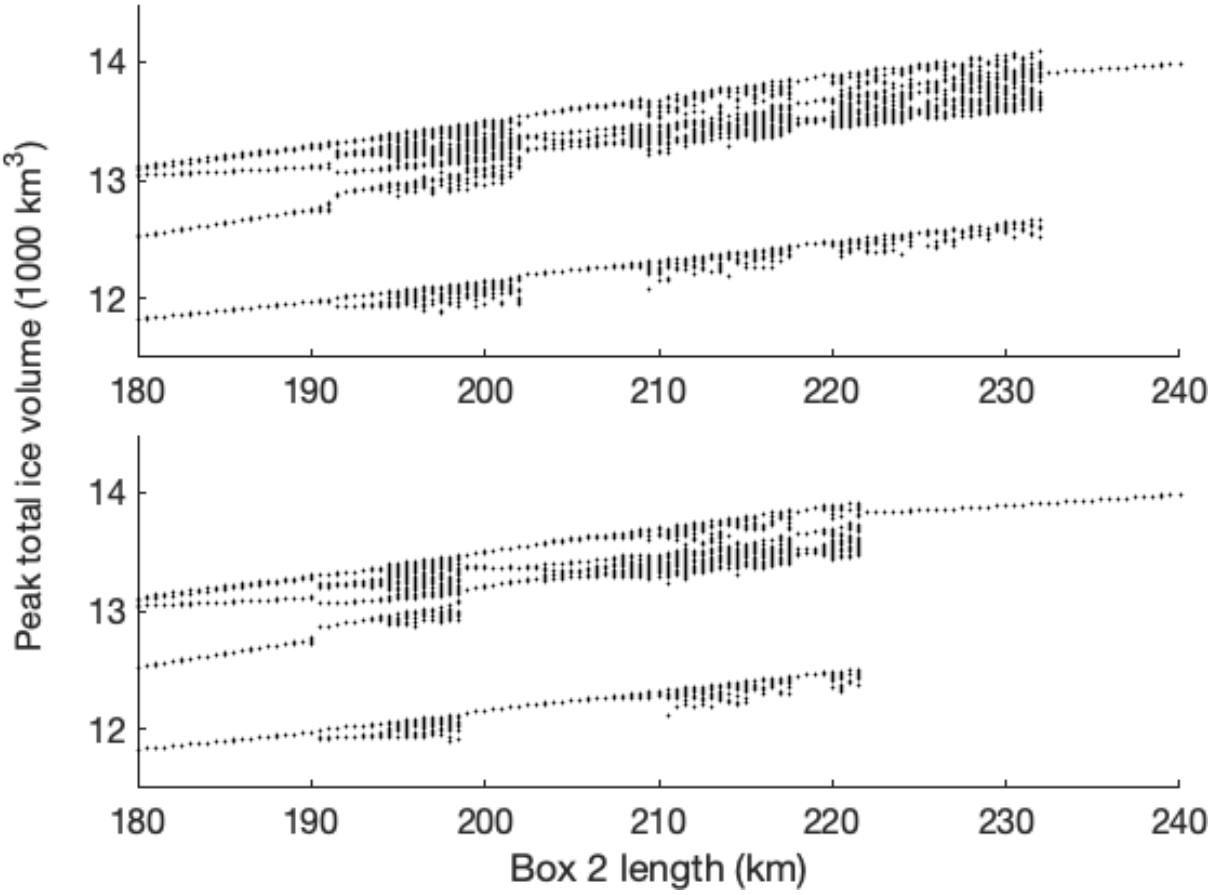

FIG. 7. Bifurcation diagram for varying L_2 displaying hysteresis of chaotic and regular periodicity. The top figure shows increasing L_2, bottom figure is decreasing L_2. Observe the region of bistability in $222 < L_2 < 231.5$.

one of the downstream boxes in this section to represent the retreat of the ice sheet under temperature forcing. This comes with the caveat that the conceptual model parameters have not been altered to match those of the comprehensive ice sheet model, so the similarities are purely qualitative.

Figure 7 shows the bifurcation diagram under variation of the length of box 2. The region between 222 and 232 km is bistable, displaying both periodic and chaotic variability. At $L_2 = 231.5$ km, the chaotic attractor experiences a boundary crisis [20]. At $L_2 = 222$ km, the periodic attractor disappears and only the chaotic attractor remains, implying a saddle-node bifurcation of limit cycles. The periodic motion occurs when the unfrozen till thickness of box 2 $h_{\text{till},2}$ is constant and maximal. On the chaotic attractor, the till periodically partially

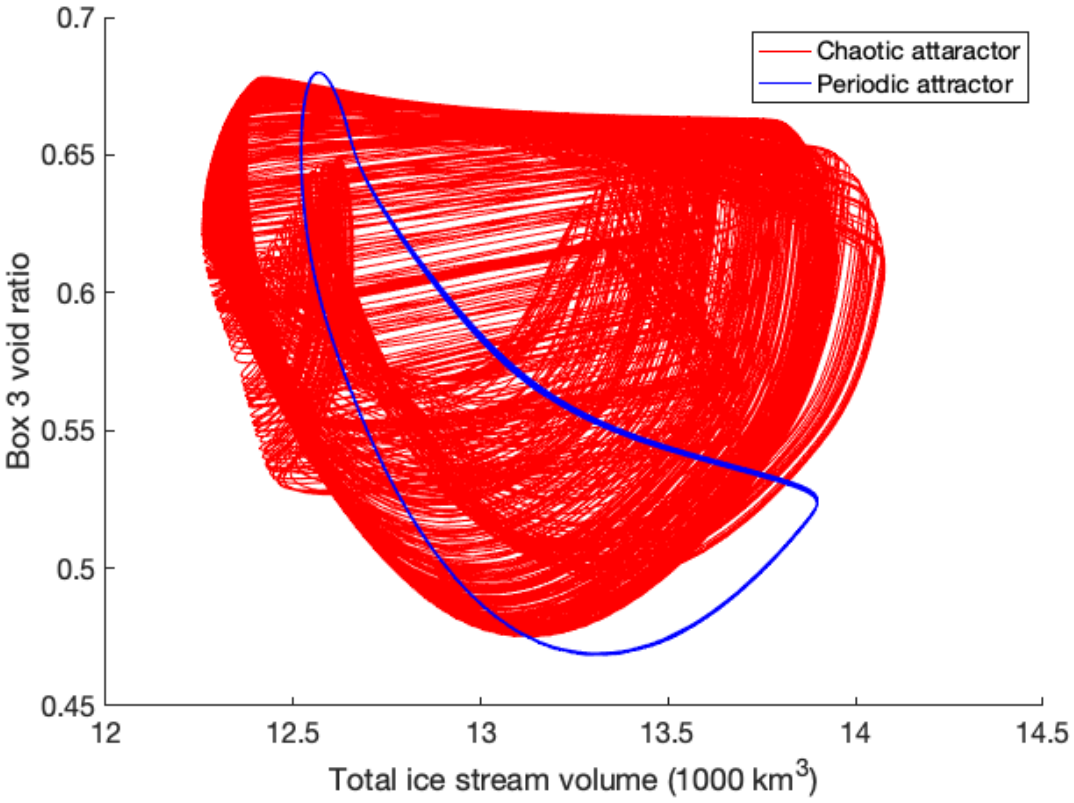

FIG. 8. Projection of the attractor in the ice stream volume and box 3 void ratio plane for $L_2 = 231.5$ km, displaying the existence of bistable chaotic and periodic attractors.

refreezes. This explains the direction of the hysteresis: for larger ice stream lengths the ice thickness will be larger, decreasing the heat lost to conduction and maintaining a larger basal melt rate which in turn keeps the till unfrozen. The bistability in this region also results in a fractal boundary between the basins of attraction of the chaotic and periodic attractors [21]. This results in neighbouring initial conditions near the basin boundary approaching one attractor or the other, and can explain the appearance of the 'anomalous' simulations in Kypke et al. [15], where trajectories forced to parameter values expected to be in the retreated configuration are in the unretreated configuration, and vice versa.

The split-stream model also displays a chaotic transient in the transition between chaotic to periodic after the boundary crisis at $L_2 = 232$ km. Figure 9 shows a time series for a trajectory initialized on the chaotic attractor for $L_2 = 231.5$ km. After 100 kyr of simulation time (orange line in Fig. 9), the value of L_2 is slowly increased to 232.5 km over 50 kyr and

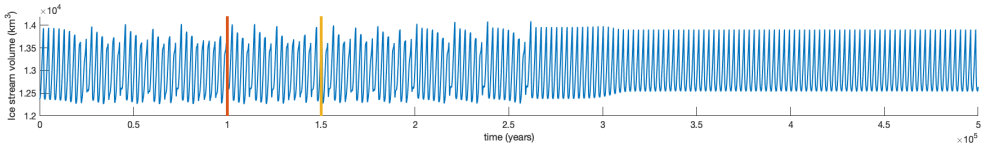

FIG. 9. Transient transition from chaotic to periodic for a slow parameter shift of L_2 from 231.5 km to 232.5 km. The orange line indicates where the parameter shift begins, and the yellow line is where it ends. The system does not transition to periodic until more than 100 kyr after the parameter has changed.

kept constant at that value thereafter (yellow line in Fig. 9). The trajectory remains chaotic for a while although the system only has a periodic attractor at this parameter value. The periodic motion then begins around 260 kyrs of simulation time, more than 100 kyr after the parameter shift is finished. A similar chaotic transient is proposed to occur in Kypke et al. [15], albeit with a collapse to a state where the ice stream no longer exists rather than to a periodic orbit.

VI. CONCLUSIONS

A model of split ice streams based on the simple model of R13 [12] has been proposed. Our model displays all of the same modes of variability due to thermomechanical coupling at the base of the ice sheet: steady flow, oscillations, and build-up/surge (or stick-slip) oscillations. Using this split ice stream model it has been demonstrated that ice streams can exhibit purely temporally chaotic variability over a range of parameter values. Chaotic windows arise in a variety of ways, including period doubling, type I intermittency, and boundary crises. While the coupling geometry implemented in this paper is inspired by a scenario seen in model simulations of the Greenland ice sheet, a simple reversing of the coupling direction could allow for the model to represent ice streams which converge into a common terminus. This scenario could also be applicable to regions such as the Siple ice stream in the West Antarctic ice sheet [1].

An important process not accounted for is the positive melt-elevation feedback which would decrease the accumulation rate at smaller ice thicknesses. This feature is vital if one wishes to extend the model to be able to include the effects of 'tipping' of the ice streams as seen in Kypke et al. [15]. That is, if the ice thickness is brought low enough to decrease the

accumulation rate a suitable amount, the ice stream could lose all of its mass and not recover. The first question is whether this feedback would dominate over the feedbacks that allow for the oscillations. If the surface temperature is allowed to decrease as H decreases, the conductive term in the basal melt rate would be less sensitive to changes in ice thickness. As mentioned in R13 [12] there is no timescale associated with the vertical temperature gradient through the ice, which can occur on a timescale of thousands of years. The inclusion of such a propagation timescale might alleviate the complications associated with introducing an altitude-dependent accumulation rate.

Appendix A: Model parameters

TABLE I. Shared parameter values

Constant	Description	Value	Units
ρ_i	Density of ice	917	kg m^{-3}
L_f	Latent heat of fusion of ice	3.335×10^5	J kg^{-1}
K_i	Thermal conductivity of ice	2.1	J s^{-1} m^{-1} K^{-1}
h_b	Basal ice layer thickness	10	m
C_i	Specific heat capacity of ice	1.94×10^6	J K^{-1} m^{-3}
A_f	Glen's flow law rate factor	5×10^{-25}	Pa^{-3} s^{-1}
e_c	Till consolidation void ratio	0.3	—
τ_0	Empirical till coefficient	9.44×10^8	Pa
c	Empirical till exponent	21.7	—
q_g	Geothermal heat flux	0.07	W m^{-2}

TABLE II. Specific parameter values for boxes 1,2 and 3 respectively

Constant	Description	Value	Units
$h_{\text{till, max}}$	Maximal till thickness	1	m
		2	
		2	
a_c	Accumulation rate	0.05	m yr^{-1}
		0.0455	
		0.0417	
T_s	Surface Temperature	15	°C
		0-30 [a]	
		15	
L	Ice stream length	200	km
		200-300 [b]	
		250	
W	Ice stream width	60	km
		35	
		25	

[a] Parameter range in section IV. Fixed at 15 in section V

[b] Parameter range in section V. Fixed at 200 in section IV

[1] M. R. Bennett, Ice streams as the arteries of an ice sheet: their mechanics, stability and significance, Earth-Science Reviews **61**, 309 (2003).

[2] R. Calov, A. Ganopolski, V. Petoukhov, M. Claussen, and R. Greve, Large-scale instabilities of the Laurentide ice sheet simulated in a fully coupled climate-system model, Geophysical Research Letters **29**, 10.1029/2002GL016078 (2002).

[3] B. D. Papa, L. A. Mysak, and Z. Wang, Intermittent ice sheet discharge events in northeastern North America during the last glacial period, Climate Dynamics **26**, 201 (2006).

[4] R. Calov, R. Greve, A. Abe-Ouchi, E. Bueler, P. Huybrechts, J. V. Johnson, F. Pattyn,

D. Pollard, C. Ritz, F. Saito, and L. Tarasov, Results from the Ice-Sheet Model Intercomparison Project–Heinrich Event Intercomparison (ISMIP HEINO), Journal of Glaciology **56**, 371 (2010).

[5] W. H. G. Roberts, A. J. Payne, and P. J. Valdes, The role of basal hydrology in the surging of the Laurentide Ice Sheet, Climate of the Past **12**, 1601 (2016), publisher: Copernicus GmbH.

[6] C. Schannwell, U. Mikolajewicz, F. Ziemen, and M.-L. Kapsch, Sensitivity of Heinrich-type ice-sheet surge characteristics to boundary forcing perturbations, Climate of the Past **19**, 179 (2023), publisher: Copernicus GmbH.

[7] H. Heinrich, Origin and Consequences of Cyclic Ice Rafting in the Northeast Atlantic Ocean During the Past 130,000 Years, Quaternary Research **29**, 142 (1988).

[8] W. Broecker, G. Bond, M. Klas, E. Clark, and J. McManus, Origin of the northern Atlantic's Heinrich events, Climate Dynamics **6**, 265 (1992).

[9] W. Dansgaard, S. J. Johnsen, H. B. Clausen, D. Dahl-Jensen, N. S. Gundestrup, C. U. Hammer, C. S. Hvidberg, J. P. Steffensen, A. E. Sveinbjörnsdottir, J. Jouzel, and G. Bond, Evidence for general instability of past climate from a 250-kyr ice-core record, Nature **364**, 218 (1993).

[10] J. Alvarez-Solas, A. Robinson, M. Montoya, and C. Ritz, Iceberg discharges of the last glacial period driven by oceanic circulation changes, Proceedings of the National Academy of Sciences **110**, 16350 (2013).

[11] A. J. Payne, Limit cycles in the basal thermal regime of ice sheets, Journal of Geophysical Research: Solid Earth **100**, 4249 (1995).

[12] A. A. Robel, E. DeGiuli, C. Schoof, and E. Tziperman, Dynamics of ice stream temporal variability: Modes, scales, and hysteresis, Journal of Geophysical Research: Earth Surface **118**, 925 (2013).

[13] E. Mantelli, M. B. Bertagni, and L. Ridolfi, Stochastic ice stream dynamics, Proceedings of the National Academy of Sciences **113**, 10.1073/pnas.1600362113 (2016).

[14] K. Hasselmann, Stochastic climate models Part I. Theory, Tellus **28**, 473 (1976), _eprint: https://onlinelibrary.wiley.com/doi/pdf/10.1111/j.2153-3490.1976.tb00696.x.

[15] K. Kypke, M. Montoya, A. Robinson, J. Alvarez-Sola, and P. Ditlevsen, Delay of collapse of the greenland ice sheet due to ice stream oscillations, in preparation.

[16] Y.-C. Lai and T. Tél, *Transient Chaos*, Applied Mathematical Sciences, Vol. 173 (Springer

New York, New York, NY, 2011).

[17] R. C. Hilborn, Quasi-Periodicity and Chaos, in *Chaos and Nonlinear Dynamics* (Oxford University PressOxford, 2000) 2nd ed., pp. 210–249.

[18] W. Paterson, Structure and Deformation of Ice, in *The Physics of Glaciers* (Elsevier, 1994) pp. 78–102.

[19] Y. Pomeau and P. Manneville, Intermittent transition to turbulence in dissipative dynamical systems, Communications in Mathematical Physics **74**, 189 (1980).

[20] C. Grebogi, E. Ott, and J. A. Yorke, Chaotic Attractors in Crisis, Physical Review Letters **48**, 1507 (1982), publisher: American Physical Society.

[21] S. W. McDonald, C. Grebogi, E. Ott, and J. A. Yorke, Fractal basin boundaries, Physica D: Nonlinear Phenomena **17**, 125 (1985).

Chapter 5

Outlook

The concepts explored in the studies contained in this thesis are simultaneously vast and nuanced, requiring further work to fully flesh out their understanding. The modelling study of chapter 3 presents the most opportunity for further study. The question of whether the chaotic transients are caused by a chaotic saddle or a boundary crisis, which in turn provides an answer whether the system is in a bistable or monostable regime when the tipping occurs and thus if r-tipping is possible, still requires a concrete answer. The application of an edge-tracking algorithm [72] to approximate the chaotic non-attracting set that delays the ice sheet mass loss allows for more focused study of its patterns of variability. In the context of the spatially extended system that is the GrIS, understanding of the edge state could hint at which regions of the ice sheet are most sensitive to changes that may bring them towards this edge state form which tipping may occur. Most interestingly would be if this edge state was in a part of phase space that is distinct from either the ice-covered of ice-free attractors, indicating that arriving at such a state by any means would facilitate tipping. Specifically, the study of chapter 3 only explored one path of trajectories in parameter space, beginning at a cluster of very similar initial states. This line of investigation could be buttressed with many additional equilibrium simulations starting from very different initial conditions to get a better idea of the parameter space. This would also help to shed light on the possibility of multistability of the ice-covered state that was suggested in the the article.

Another relevant study is using the same methodology as in the paper of chapter 3 but restricting the analysis to a shorter time scale. The question to be answered is whether there could be r-tipping into the oscillatory state. As the ice stream oscillations themselves have a non negligible amplitude vis-a-vis global seal level rise and are quite rapid when compared to the typical evolution of the ice sheet, the local and global impact caused by entering this configuration may be relevant on the order of kiloyears.

As the goal of the paper of chapter 4 is primarily to introduce the coupled

conceptual ice stream model, the analysis can naturally be extended in future works. Most relevant is a more focused application to the ice streams seen in the comprehensive model – this includes more direct parameterization to fit the ice stream configuration seen in the Greenland ice sheet. Another step could be the more rigorous exploration of the chaotic attractors, routes to chaos, and crises present in the model. For example, an explicit calculation of the critical parameter of the chaotic transients introduced in section VI of that paper can be done, along with identification of the types of intermittency routes to chaos.

More interestingly, this model may allow for the investigation of the interaction between r-tipping and chaotic transients. A primary issue in the comprehensive model study was the inability to distinguish whether r-tipping was actually occurring, owing to the random tipping times and long transients before tipping. The question in particular is whether there exists some empirical scaling of the tipping times for a system that tips through a chaotic saddle due to rate-induced effects. While the lifetime (which is the inverse of the escape rate from) of the saddle, which depends on its fractal dimension [34], determines some part of this chaotic transient, whether the rate at which the parameter is change also plays a role is unknown. Applying the aforementioned edge tracking algorithm can be used to approximate this chaotic saddle, allowing estimation of the escape rate. Such concepts have been explored before with regards to tipping probabilities in Kaczas et al. [47], which focuses on predictability of a final system based on how well the initial state is known rather than the mean time it may take a trajectory to tip in this scenario. Of course, it might be preferable to use an even simpler, purely conceptual system in such a study instead.

Bibliography

[1] H. M. Alkhayuon and P. Ashwin. Rate-induced tipping from periodic attractors: Partial tipping and connecting orbits. *Chaos: An Interdisciplinary Journal of Nonlinear Science*, 28(3):033608, 2018.

[2] S.-I. An, H.-J. Kim, and S.-K. Kim. Rate-Dependent Hysteresis of the Atlantic Meridional Overturning Circulation System and Its Asymmetric Loop. *Geophysical Research Letters*, 48(1):e2020GL090132, 2021.

[3] D. I. Armstrong McKay, A. Staal, J. F. Abrams, R. Winkelmann, B. Sakschewski, S. Loriani, I. Fetzer, S. E. Cornell, J. Rockström, and T. M. Lenton. Exceeding 1.5°C global warming could trigger multiple climate tipping points. *Science*, 377(6611):eabn7950, 2022.

[4] P. Ashwin, S. Wieczorek, R. Vitolo, and P. Cox. Tipping points in open systems: bifurcation, noise-induced and rate-dependent examples in the climate system. *Philosophical Transactions of the Royal Society A: Mathematical, Physical and Engineering Sciences*, 370(1962):1166–1184, 2012.

[5] A. Berger and M. Loutre. Insolation values for the climate of the last 10 million years. *Quaternary Science Reviews*, 10(4):297–317, 1991.

[6] H. Blatter. Velocity and stress fields in grounded glaciers: a simple algorithm for including deviatoric stress gradients. *Journal of Glaciology*, 41(138):333–344, 1995.

[7] N. Boers. Observation-based early-warning signals for a collapse of the Atlantic Meridional Overturning Circulation. *Nature Climate Change*, 11(8):680–688, 2021.

[8] N. Boers, M. D. Chekroun, H. Liu, D. Kondrashov, D.-D. Rousseau, A. Svensson, M. Bigler, and M. Ghil. Inverse stochastic–dynamic models for high-resolution Greenland ice core records. *Earth System Dynamics*, 8(4):1171–1190, 2017.

[9] N. Boers, M. Ghil, and D.-D. Rousseau. Ocean circulation, ice shelf, and sea ice interactions explain Dansgaard-Oeschger cycles. *Proceedings*

of the National Academy of Sciences of the United States of America, 115(47):E11005–E11014, 2018.

[10] N. Boers and M. Rypdal. Critical slowing down suggests that the western Greenland Ice Sheet is close to a tipping point. *Proceedings of the National Academy of Sciences*, 118(21):e2024192118, 2021.

[11] C. A. Boulton, T. M. Lenton, and N. Boers. Pronounced loss of Amazon rainforest resilience since the early 2000s. *Nature Climate Change*, 12(3):271–278, 2022.

[12] W. S. Broecker, D. M. Peteet, and D. Rind. Does the ocean-atmosphere system have more than one stable mode of operation? *Nature*, 315(6014):21–26, 1985.

[13] J. Brondex, F. Gillet-Chaulet, and O. Gagliardini. Sensitivity of centennial mass loss projections of the Amundsen basin to the friction law. *The Cryosphere*, 13(1):177–195, 2019.

[14] F. Broner, G. H. Goldsztein, and S. H. Strogatz. Dynamical Hysteresis without Static Hysteresis: Scaling Laws and Asymptotic Expansions. *SIAM Journal on Applied Mathematics*, 57(4):1163–1187, 1997.

[15] M. I. Budyko. The effect of solar radiation variations on the climate of the Earth. *Tellus*, 21(5):611–619, 1969.

[16] E. Bueler, C. S. Lingle, and J. Brown. Fast computation of a viscoelastic deformable Earth model for ice-sheet simulations. *Annals of Glaciology*, 46:97–105, 2007.

[17] E. Bueler and W. van Pelt. Mass-conserving subglacial hydrology in the Parallel Ice Sheet Model version 0.6. *Geoscientific Model Development*, 8(6):1613–1635, 2015.

[18] T. Bódai and V. Lucarini. Rough basin boundaries in high dimension: Can we classify them experimentally? *Chaos: An Interdisciplinary Journal of Nonlinear Science*, 30(10):103105, 2020.

[19] R. Calov, R. Greve, A. Abe-Ouchi, E. Bueler, P. Huybrechts, J. V. Johnson, F. Pattyn, D. Pollard, C. Ritz, F. Saito, and L. Tarasov. Results from the Ice-Sheet Model Intercomparison Project–Heinrich Event Intercomparison (ISMIP HEINO). *Journal of Glaciology*, 56(197):371–383, 2010.

[20] W. Dansgaard. The Abundance of O18 in Atmospheric Water and Water Vapour. *Tellus*, 5(4):461–469, 1953.

[21] W. Dansgaard, S. J. Johnsen, H. B. Clausen, D. Dahl-Jensen, N. S. Gundestrup, C. U. Hammer, C. S. Hvidberg, J. P. Steffensen, A. E. Sveinbjörnsdottir, J. Jouzel, and G. Bond. Evidence for general instability of past climate from a 250-kyr ice-core record. *Nature*, 364(6434):218–220, 1993.

[22] H. A. Dijkstra. *Nonlinear Climate Dynamics*. Cambridge University Press, Cambridge, 2013.

[23] P. Ditlevsen and S. Ditlevsen. Warning of a forthcoming collapse of the Atlantic meridional overturning circulation. *Nature Communications*, 14(1):4254, 2023.

[24] P. D. Ditlevsen. Observation of α-stable noise induced millennial climate changes from an ice-core record. *Geophysical Research Letters*, 26(10):1441–1444, 1999.

[25] P. D. Ditlevsen, S. Ditlevsen, and K. K. Andersen. The fast climate fluctuations during the stadial and interstadial climate states. *Annals of Glaciology*, 35:457–462, 2002.

[26] P. D. Ditlevsen and S. J. Johnsen. Tipping points: Early warning and wishful thinking. *Geophysical Research Letters*, 37(19), 2010.

[27] T. M. Dokken, K. H. Nisancioglu, C. Li, D. S. Battisti, and C. Kissel. Dansgaard-Oeschger cycles: Interactions between ocean and sea ice intrinsic to the Nordic seas. *Paleoceanography*, 28(3):491–502, 2013.

[28] J. Feldmann and A. Levermann. Collapse of the West Antarctic Ice Sheet after local destabilization of the Amundsen Basin. *Proceedings of the National Academy of Sciences*, 112(46):14191–14196, 2015.

[29] U. Feudel. Rate-induced tipping in ecosystems and climate: the role of unstable states, basin boundaries and transient dynamics. *Nonlinear Processes in Geophysics*, 30(4):481–502, 2023.

[30] R. FitzHugh. Impulses and Physiological States in Theoretical Models of Nerve Membrane. *Biophysical Journal*, 1(6):445–466, 1961.

[31] A. D. Fokker. Die mittlere Energie rotierender elektrischer Dipole im Strahlungsfeld. *Annalen der Physik*, 348(5):810–820, 1914.

[32] Gardiner CW. *Handbook of stochastic methods: for physics, chemistry and natural sciences*. Number 15 in Springer Series in Synergetics. Springer, Berlin, 2nd ed. edition, 1997.

[33] J. W. Glen. The Creep of Polycrystalline Ice. *Proceedings of the Royal Society of London. Series A, Mathematical and Physical Sciences*, 228(1175):519–538, 1955.

[34] C. Grebogi, S. W. McDonald, E. Ott, and J. A. Yorke. Final state sensitivity: An obstruction to predictability. *Physics Letters A*, 99(9):415–418, 1983.

[35] C. Grebogi, E. Ott, F. Romeiras, and J. A. Yorke. Critical exponents for crisis-induced intermittency. *Physical Review A*, 36(11):5365–5380, 1987.

[36] C. Grebogi, E. Ott, and J. A. Yorke. Chaotic Attractors in Crisis. *Physical Review Letters*, 48(22):1507–1510, 1982.

[37] C. Grebogi, E. Ott, and J. A. Yorke. Fractal Basin Boundaries, Long-Lived Chaotic Transients, and Unstable-Unstable Pair Bifurcation. *Physical Review Letters*, 50(13):935–938, 1983.

[38] C. Grebogi, E. Ott, and J. A. Yorke. Critical Exponent of Chaotic Transients in Nonlinear Dynamical Systems. *Physical Review Letters*, 57(11):1284–1287, 1986.

[39] R. Greve and H. Blatter. *Dynamics of Ice Sheets and Glaciers*. Advances in Geophysical and Environmental Mechanics and Mathematics. Springer Berlin Heidelberg, Berlin, Heidelberg, 2009.

[40] K. Hasselmann. Stochastic climate models Part I. Theory. *Tellus*, 28(6):473–485, 1976.

[41] R. C. Hilborn. *Chaos and Nonlinear Dynamics: An Introduction for Scientists and Engineers*. Oxford University Press, 2000.

[42] D. M. Holland, R. H. Thomas, B. de Young, M. H. Ribergaard, and B. Lyberth. Acceleration of Jakobshavn Isbræ triggered by warm subsurface ocean waters. *Nature Geoscience*, 1(10):659–664, 2008.

[43] Horsthemke W and Lefever R. *Noise-induced transitions: theory and applications in physics, chemistry, and biology*. Number 15 in Springer Series in Synergetics. Springer-Verlag, Berlin, 1984.

[44] I. M. Howat, I. Joughin, M. Fahnestock, B. E. Smith, and T. A. Scambos. Synchronous retreat and acceleration of southeast Greenland outlet glaciers 2000–06: ice dynamics and coupling to climate. *Journal of Glaciology*, 54(187):646–660, 2008.

[45] I. Joughin, B. E. Smith, I. M. Howat, T. Scambos, and T. Moon. Greenland flow variability from ice-sheet-wide velocity mapping. *Journal of Glaciology*, 56(197):415–430, 2010.

[46] I. Joughin, B. E. Smith, and C. G. Schoof. Regularized Coulomb Friction Laws for Ice Sheet Sliding: Application to Pine Island Glacier, Antarctica. *Geophysical Research Letters*, 46(9):4764–4771, 2019.

[47] B. Kaszás, U. Feudel, and T. Tél. Tipping phenomena in typical dynamical systems subjected to parameter drift. *Scientific Reports*, 9(1):8654, 2019.

[48] S. A. Khan, K. H. Kjær, M. Bevis, J. L. Bamber, J. Wahr, K. K. Kjeldsen, A. A. Bjørk, N. J. Korsgaard, L. A. Stearns, M. R. Van Den Broeke, L. Liu, N. K. Larsen, and I. S. Muresan. Sustained mass loss of the northeast Greenland ice sheet triggered by regional warming. *Nature Climate Change*, 4(4):292–299, 2014.

[49] H.-J. Kim, S.-I. An, S.-K. Kim, and J.-H. Park. Feedback Processes Modulating the Sensitivity of Atlantic Thermohaline Circulation to Freshwater Forcing Timescales. *Journal of Climate*, 34(12):5081–5092, 2021.

[50] P. Kindler, M. Guillevic, M. Baumgartner, J. Schwander, A. Landais, and M. Leuenberger. Temperature reconstruction from 10 to 120 kyr b2k from the NGRIP ice core. *Climate of the Past*, 10(2):887–902, 2014.

[51] A. Kolmogoroff. Über die analytischen Methoden in der Wahrscheinlichkeitsrechnung. *Mathematische Annalen*, 104(1):415–458, 1931.

[52] W. Krabill, E. Hanna, P. Huybrechts, W. Abdalati, J. Cappelen, B. Csatho, E. Frederick, S. Manizade, C. Martin, J. Sonntag, R. Swift, R. Thomas, and J. Yungel. Greenland Ice Sheet: Increased coastal thinning. *Geophysical Research Letters*, 31(24), 2004.

[53] S. Krumscheid, M. Pradas, G. A. Pavliotis, and S. Kalliadasis. Data-driven coarse graining in action: Modeling and prediction of complex systems. *Physical Review E*, 92(4):042139, 2015.

[54] C. Kuehn. *Multiple Time Scale Dynamics*. Applied Mathematical Sciences, 191. Springer International Publishing, Cham, Switzerland, 1st ed. 2015. edition, 2015.

[55] Y. A. Kuznetsov. *Elements of Applied Bifurcation Theory*. Number 112 in Applied Mathematical Sciences Series. Springer, Cham, Switzerland, 4th edition, 2023 - 2004.

[56] F. Kwasniok. Analysis and modelling of glacial climate transitions using simple dynamical systems. *Philosophical transactions of the Royal Society of London. Series A: Mathematical, physical, and engineering sciences*, 371(1991):20110472–20110472, 2013.

[57] F. Kwasniok and G. Lohmann. Deriving dynamical models from paleoclimatic records: Application to glacial millennial-scale climate variability. *Physical Review E*, 80(6):066104, 2009.

[58] F. Kwasniok and G. Lohmann. A stochastic nonlinear oscillator model for glacial millennial-scale climate transitions derived from ice-core data. *Nonlinear Processes in Geophysics*, 19(6):595–603, 2012.

[59] K. Kypke, P. Ashwin, and P. Ditlevsen. Chaotic variability in a model of coupled ice streams. Prepared for submission.

[60] K. Kypke and P. Ditlevsen. On the representation of multiplicative noise in modeling Dansgaard–Oeschger events. *Physica D: Nonlinear Phenomena*, 466:134215, 2024.

[61] K. Kypke, M. Montoya, A. Robinson, J. Alvarez-Solas, and P. Ditlevsen. Delay of collapse of the Greenland ice sheet due to ice stream oscillations. Prepared for submission.

[62] Y.-C. Lai and T. Tél. *Transient Chaos*, volume 173 of *Applied Mathematical Sciences*. Springer New York, New York, NY, 2011.

[63] L. J. Larocca, M. Twining–Ward, Y. Axford, A. D. Schweinsberg, S. H. Larsen, A. Westergaard–Nielsen, G. Luetzenburg, J. P. Briner, K. K. Kjeldsen, and A. A. Bjørk. Greenland-wide accelerated retreat of peripheral glaciers in the twenty-first century. *Nature Climate Change*, pages 1–5, 2023.

[64] D. S. Lemons and A. Gythiel. Paul Langevin's 1908 paper "On the Theory of Brownian Motion" ["Sur la théorie du mouvement brownien," C. R. Acad. Sci. (Paris) 146, 530–533 (1908)]. *American Journal of Physics*, 65(11):1079–1081, 1997.

[65] A. Levermann and R. Winkelmann. A simple equation for the melt elevation feedback of ice sheets. *The Cryosphere*, 10(4):1799–1807, 2016.

[66] C. Li and A. Born. Coupled atmosphere-ice-ocean dynamics in Dansgaard-Oeschger events. *Quaternary Science Reviews*, 203:1–20, 2019.

[67] V. N. Livina, F. Kwasniok, and T. M. Lenton. Potential analysis reveals changing number of climate states during the last 60 kyr. *Climate of the Past*, 6(1):77–82, 2010.

[68] J. Lohmann and P. D. Ditlevsen. A consistent statistical model selection for abrupt glacial climate changes. *Climate Dynamics*, 52(11):6411–6426, 2019.

[69] J. Lohmann and P. D. Ditlevsen. Objective extraction and analysis of statistical features of Dansgaard–Oeschger events. *Climate of the Past*, 15(5):1771–1792, 2019.

[70] J. Lohmann and A. Svensson. Ice core evidence for major volcanic eruptions at the onset of Dansgaard–Oeschger warming events. *Climate of the Past*, 18(9):2021–2043, 2022.

[71] E. N. Lorenz. Deterministic Nonperiodic Flow. *Journal of the Atmospheric Sciences*, 20(2):130–141, 1963.

[72] V. Lucarini and T. Bódai. Edge states in the climate system: exploring global instabilities and critical transitions. *Nonlinearity*, 30(7):R32–R66, 2017.

[73] S. B. Luthcke, H. J. Zwally, W. Abdalati, D. D. Rowlands, R. D. Ray, R. S. Nerem, F. G. Lemoine, J. J. McCarthy, and D. S. Chinn. Recent Greenland Ice Mass Loss by Drainage System from Satellite Gravity Observations. *Science*, 314(5803):1286–1289, 2006.

[74] I. Malmierca-Vallet, L. C. Sime, and the D–O community members. Dansgaard–Oeschger events in climate models: review and baseline Marine Isotope Stage 3 (MIS3) protocol. *Climate of the Past*, 19(5):915–942, 2023.

[75] T. Mitsui and M. Crucifix. Influence of external forcings on abrupt millennial-scale climate changes: a statistical modelling study. *Climate Dynamics*, 48(7):2729–2749, 2017.

[76] A. H. Monahan, A. Timmermann, and G. Lohmann. Comments on "Noise-Induced Transitions in a Simplified Model of the Thermohaline Circulation". *Journal of Physical Oceanography*, 32(3):1112–1116, 2002.

[77] S. Newhouse, D. Ruelle, and F. Takens. Occurrence of strange AxiomA attractors near quasi periodic flows on T^m, m$\geq$3. *Communications in Mathematical Physics*, 64(1):35–40, 1978.

[78] J. F. Nye. The Distribution of Stress and Velocity in Glaciers and Ice-Sheets. *Proceedings of the Royal Society of London. Series A, Mathematical and Physical Sciences*, 239(1216):113–133, 1957.

[79] E. Ott. *Chaos in dynamical systems*. Cambridge University Press, Cambridge, U.K. ; New York, 2nd ed edition, 2002.

[80] E. Ott, J. C. Sommerer, J. C. Alexander, I. Kan, and J. A. Yorke. Scaling behavior of chaotic systems with riddled basins. *Physical Review Letters*, 71(25):4134–4137, 1993.

[81] B. D. Papa, L. A. Mysak, and Z. Wang. Intermittent ice sheet discharge events in northeastern North America during the last glacial period. *Climate Dynamics*, 26(2-3):201–216, 2006.

[82] W. S. B. Paterson. *The physics of glaciers*. Pergamon, Oxford, OX, England, 3rd edition, 1994.

[83] F. Pattyn. A new three-dimensional higher-order thermomechanical ice sheet model: Basic sensitivity, ice stream development, and ice flow across subglacial lakes. *Journal of Geophysical Research: Solid Earth*, 108(B8), 2003.

[84] J. B. Pedro, M. Jochum, C. Buizert, F. He, S. Barker, and S. O. Rasmussen. Beyond the bipolar seesaw: Toward a process understanding of interhemispheric coupling. *Quaternary Science Reviews*, 192:27–46, 2018.

[85] F. Pellicciotti, B. Brock, U. Strasser, P. Burlando, M. Funk, and J. Corripio. An enhanced temperature-index glacier melt model including the shortwave radiation balance: development and testing for Haut Glacier d'Arolla, Switzerland. *Journal of Glaciology*, 51(175):573–587, 2005.

[86] S. V. Petersen, D. P. Schrag, and P. U. Clark. A new mechanism for Dansgaard-Oeschger cycles. *Paleoceanography*, 28(1):24–30, 2013.

[87] M. Planck. Über einen satz der statistischen dynamik und seine erweiterung in der quantentheorie. *Sitzungsberichte der Königlich Preussischen Akademie der Wissenschaften zu Berlin*, 24:324–341, 1917.

[88] Y. Pomeau and P. Manneville. Intermittent transition to turbulence in dissipative dynamical systems. *Communications in Mathematical Physics*, 74(2):189–197, 1980.

[89] C. Raymond. Shear margins in glaciers and ice sheets. *Journal of Glaciology*, 42(140):90–102, 1996.

[90] J. A. Rial and R. Saha. Modeling Abrupt Climate Change as the Interaction Between Sea Ice Extent and Mean Ocean Temperature Under Orbital Insolation Forcing. In *Abrupt Climate Change: Mechanisms, Patterns, and Impacts*, pages 57–74. American Geophysical Union (AGU), 2011.

[91] K. Riechers, G. Gottwald, and N. Boers. Glacial abrupt climate change as a multiscale phenomenon resulting from monostable excitable dynamics. *Journal of Climate*, 37(8):2741 – 2763, 2024.

[92] K. Riechers, L. Rydin Gorjão, F. Hassanibesheli, P. G. Lind, D. Witthaut, and N. Boers. Stable stadial and interstadial states of the last glacial's climate identified in a combined stable water isotope and dust record from Greenland. *Earth System Dynamics*, 14(3):593–607, 2023.

[93] E. Rignot and P. Kanagaratnam. Changes in the Velocity Structure of the Greenland Ice Sheet. *Science*, 311(5763):986–990, 2006.

[94] P. D. L. Ritchie, H. Alkhayuon, P. M. Cox, and S. Wieczorek. Rate-induced tipping in natural and human systems. *Earth System Dynamics*, 14(3):669–683, 2023.

[95] A. A. Robel, E. DeGiuli, C. Schoof, and E. Tziperman. Dynamics of ice stream temporal variability: Modes, scales, and hysteresis. *Journal of Geophysical Research: Earth Surface*, 118(2):925–936, 2013.

[96] W. H. G. Roberts, A. J. Payne, and P. J. Valdes. The role of basal hydrology in the surging of the Laurentide Ice Sheet. *Climate of the Past*, 12(8):1601–1617, 2016.

[97] A. Robinson, J. Alvarez-Solas, M. Montoya, H. Goelzer, R. Greve, and C. Ritz. Description and validation of the ice-sheet model Yelmo (version 1.0). *Geoscientific Model Development*, 13(6):2805–2823, 2020.

[98] A. Robinson, R. Calov, and A. Ganopolski. An efficient regional energy-moisture balance model for simulation of the Greenland Ice Sheet response to climate change. *The Cryosphere*, 2010.

[99] A. Robinson, D. Goldberg, and W. H. Lipscomb. A comparison of the stability and performance of depth-integrated ice-dynamics solvers. *The Cryosphere*, 16(2):689–709, 2022.

[100] D. Ruelle and F. Takens. On the nature of turbulence. *Communications in Mathematical Physics*, 20(3):167–192, 1971.

[101] K. Sakai and W. R. Peltier. Dansgaard–Oeschger Oscillations in a Coupled Atmosphere–Ocean Climate Model. *Journal of Climate*, 10(5):949–970, 1997.

[102] C. Schoof. The Effect of Cavitation on Glacier Sliding. *Proceedings: Mathematical, Physical and Engineering Sciences*, 461(2055):609–627, 2005.

[103] C. Schoof. Ice sheet grounding line dynamics: Steady states, stability, and hysteresis. *Journal of Geophysical Research: Earth Surface*, 112(F3), 2007.

[104] W. D. Sellers. A Global Climatic Model Based on the Energy Balance of the Earth-Atmosphere System. *Journal of Applied Meteorology and Climatology*, 8(3):392–400, 1969.

[105] W. Steffen, J. Rockström, K. Richardson, T. M. Lenton, C. Folke, D. Liverman, C. P. Summerhayes, A. D. Barnosky, S. E. Cornell, M. Crucifix, J. F. Donges, I. Fetzer, S. J. Lade, M. Scheffer, R. Winkelmann, and H. J. Schellnhuber. Trajectories of the Earth System in the Anthropocene. *Proceedings of the National Academy of Sciences*, 115(33):8252–8259, 2018.

[106] T. F. Stocker and S. J. Johnsen. A minimum thermodynamic model for the bipolar seesaw. *Paleoceanography*, 18(4):2003PA000920, 2003.

[107] H. Stommel. Thermohaline Convection with Two Stable Regimes of Flow. *Tellus*, 13(2):224–230, 1961.

[108] S. H. Strogatz. *Nonlinear dynamics and chaos: with applications to physics, biology, chemistry, and engineering*. Studies in Nonlinearity. Westview Press, Cambridge, 1994.

[109] K. Terzaghi, R. B. Peck, G. Mesri, and R. B. Peck. *Soil mechanics in engineering practice*. Wiley, New York, 3rd edition, 1996.

[110] A. Timmermann and G. Lohmann. Noise-Induced Transitions in a Simplified Model of the Thermohaline Circulation. *Journal of Physical Oceanography*, 30(8):1891–1900, 2000.

[111] L. D. Trusel, S. B. Das, M. B. Osman, M. J. Evans, B. E. Smith, X. Fettweis, J. R. McConnell, B. P. Y. Noël, and M. R. Van Den Broeke. Nonlinear rise in Greenland runoff in response to post-industrial Arctic warming. *Nature*, 564(7734):104–108, 2018.

[112] S. Tulaczyk, W. B. Kamb, and H. F. Engelhardt. Basal mechanics of Ice Stream B, west Antarctica: 1. Till mechanics. *Journal of Geophysical Research: Solid Earth*, 105(B1):463–481, 2000.

[113] S. Tulaczyk, W. B. Kamb, and H. F. Engelhardt. Basal mechanics of Ice Stream B, west Antarctica: 2. Undrained plastic bed model. *Journal of Geophysical Research: Solid Earth*, 105(B1):483–494, 2000.

[114] J. Van Den Berg, R. Van De Wal, and H. Oerlemans. A mass balance model for the Eurasian Ice Sheet for the last 120,000 years. *Global and Planetary Change*, 61(3-4):194–208, 2008.

[115] B. van der Pol Jun. LXXXVIII. On "relaxation-oscillations". *The London, Edinburgh, and Dublin Philosophical Magazine and Journal of Science*, 2(11):978–992, 1926.

[116] G. Vettoretti, P. Ditlevsen, M. Jochum, and S. O. Rasmussen. Atmospheric CO2 control of spontaneous millennial-scale ice age climate oscillations. *Nature Geoscience*, 15(4):300–306, 2022.

[117] A. S. Von Der Heydt, P. Ashwin, C. D. Camp, M. Crucifix, H. A. Dijkstra, P. Ditlevsen, and T. M. Lenton. Quantification and interpretation of the climate variability record. *Global and Planetary Change*, 197:103399, 2021.

[118] J. Weertman. Stability of the Junction of an Ice Sheet and an Ice Shelf. *Journal of Glaciology*, 13(67):3–11, 1974.

[119] S. Wieczorek, P. Ashwin, C. M. Luke, and P. M. Cox. Excitability in ramped systems: the compost-bomb instability. *Proceedings of the Royal Society A: Mathematical, Physical and Engineering Sciences*, 467(2129):1243–1269, 2011.

[120] E. Wolff, J. Chappellaz, T. Blunier, S. Rasmussen, and A. Svensson. Millennial-scale variability during the last glacial: The ice core record. *Quaternary Science Reviews*, 29(21-22):2828–2838, 2010.

[121] M. Zeitz, J. M. Haacker, J. F. Donges, T. Albrecht, and R. Winkelmann. Dynamic regimes of the Greenland Ice Sheet emerging from interacting melt–elevation and glacial isostatic adjustment feedbacks. *Earth System Dynamics*, 13(3):1077–1096, 2022.